CRAPS, MATTHEW, Ph.D. Reaction kinetics in the synthesis of highly Nitrogen doped Carbon Nanotubes. (2020)
Directed by Dr. Dan Herr. 132 pp.

Nitrogen doped carbon nanotubes (NCNTs) consist of bamboo structure CNTs with nitrogen atoms in situ doped into the CNT lattice. In this research, NCNTs were synthesized via CVD using ferrocene and pyridine precursors in a pure NH_3 environment. To understand the kinetics of nitrogen incorporation in carbon nanotubes, I performed time and temperature evolution studies and logged the mass of NCNT product collected from each run. SEM and TEM visualized the structural changes to the NCNTs, and helped to quantify lengths and diameters. We used XPS to detect the atomic percent nitrogen changes in the nanotubes during growth. The data helped to determine the kinetics of the NCNT growth process. Unexpectedly, two competing mechanisms became apparent at temperatures above 775°C. The percent nitrogen detected by XPS shows a significant drop at 825°C and 850°C relative to the syntheses at 800°C and below. The total mass of NCNT product started decreasing at 800°C and continued decreasing at an increasingly faster rate as temperatures increased. This result caused us to reevaluate our hypotheses and develop some new hypotheses and tests. We proposed a de-doping mechanism, created a de-doping test, and evaluated the percent nitrogen removed at different temperatures, and the types of nitrogen species lost from the lattice. We considered several rate limiting processes and observed specific nitrogen species from the in situ synthesis of NCNTs, as detected by XPS.

REACTION KINETICS IN THE SYNTHESIS OF HIGHLY NITROGEN DOPED CARBON NANOTUBES

by

Matthew Craps

A Dissertation Submitted to
the Faculty of the Graduate School at
The University of North Carolina at Greensboro
in Partial Fulfillment
of the Requirements for the Degree
Doctor of Philosophy

Greensboro
2020

Approved by

__Dr. Dan Herr_____
Committee Chair

APPROVAL PAGE

This dissertation has been approved by the following committee of the Faculty of the Graduate School at the University of North Carolina at Greensboro.

Committee Chair _____

Committee Members _____

_____

_____

_____

Date of Acceptance by Committee

_____

Date of Final Oral Examination

ACKNOWLEDGEMENTS

Thanks to my wife, Becca, and my son, Vance for supporting me through all of this work.

TABLE OF CONTENTS

Page

LIST OF TABLES

Page

LIST OF FIGURES

Page

CHAPTER I

LITERATURE REVIEW

Carbon nanotubes (CNT) first appeared in the literature in 1991 by Iijima[1]. However, hollow tubules of carbon appeared in the literature several times as early as 1952[2,3]. CNTs consist of carbon atoms arranged in six-membered rings in their pure form, but some atoms of other elements can be substituted for a carbon atom in the CNT lattice. Nitrogen doping in CNTs was first reported in 1994[4] via the arc discharge method. Arc discharge utilizes a welding supply to apply a DC voltage between two graphite electrodes. One or both electrodes are impregnated with a source of nitrogen and metal powder, and a welding supply in a vacuum. An arc is struck between the anode and cathode, creating a plasma of catalyst particles, carbon, and nitrogen vapor, where the nitrogen doped carbon nanotubes (NCNTs) are formed. The incorporation of nitrogen as a dopant causes a shift of the Fermi level, making the CNTs more electrically conductive, due to the introduction of electron donor states near the Fermi level.[5] Nitrogen atoms included in the lattice compromise the crystallinity of NCNTs. More dopant atoms create more disorder and physical bonds get distorted. There are many reports on NCNT synthesis and applications. However, few studies consider the kinetics and rates of formation of nitrogen doping in carbon nanotubes, especially in a pure NH3 environment. This work investigates the mechanism of incorporation of nitrogen in the

NCNT lattice and determines the rate of formation and kinetics involved in the polymerization of the NCNT.

1.1 Background

Soon after Iijima's publication of transmission electron micrographs (TEM) of CNTs, Yi[6] provided the first ab initio calculations regarding nitrogen doping in CNTs with direct substitution of a nitrogen atom for a carbon atom. This bond is substitutional or graphitic nitrogen doping as seen in Figure 1.1A.

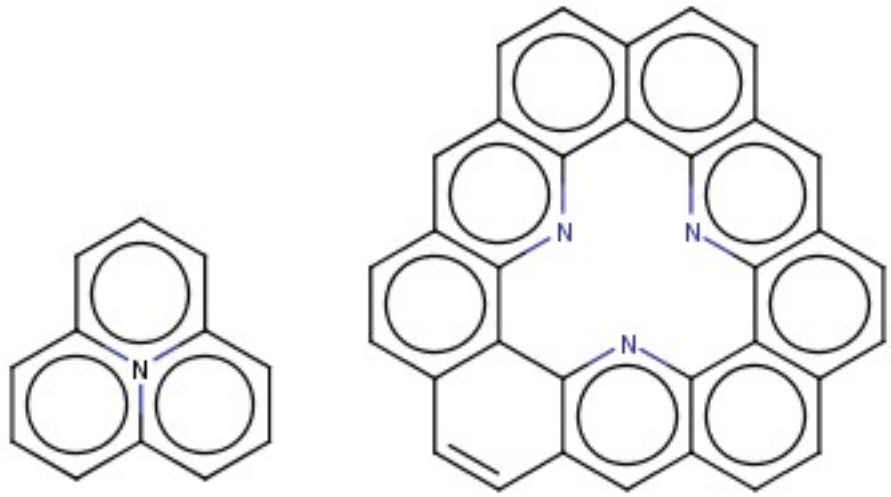

A. B.

Figure 1.1. Representative Nitrogen bonding in CNT lattice (A) substitutional Graphitic-N, and (B) Pyridinic-N with vacancies.

Carbon to carbon bonds comprise σ bonds and π bonds as seen in Figure 1.2. There are six carbon atoms in each aromatic ring, and every carbon atom bonds with three other carbon atoms creating three planar σ bonds via sp^2 orbitals and one delocalized π bond, with the remaining p orbital.

Compared to carbon, nitrogen has one extra electron, and the direct substitution of a nitrogen atom for a carbon atom creates a donor state[7]. Since the CNT lattice carbon provides three sigma bonds and one pi bond, the direct substitution of a nitrogen atom still has one pi and three coplanar sigma bonds, but now there is a free electron that can enhance the electrical conductivity of the NCNT. However, just because nitrogen has an extra electron does not mean that every instance of an atom of nitrogen included in the carbon nanotube lattice is a donor. Pyridinic nitrogen in CNTs represents a second type of nitrogen doping and involves vacancies created in the lattice or an edge bond, as seen in Figure 1.1B.

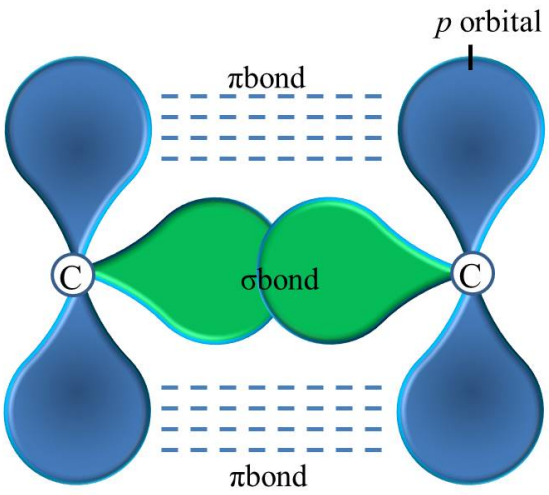

Figure 1.2 Carbon-Carbon bonding

In this case 1, 2, 3, or even 4 nitrogen atoms can replace several carbons in the lattice, but with greater distortion and often with 1 or more vacancies. With a vacancy next to one of the pyridinic nitrogen atoms, as seen in Figure 1.1B, there is an empty p_z electron orbital that creates an acceptor state.[8] If all vacancies are filled or the pyridinic

nitrogen is edge bonded a neutral state created. Pyridinic nitrogen species boost the oxidation reduction reaction (ORR) performance[9] in mesoporous carbon. This is because pyridinic nitrogen provides a 4 electron pathway to reduce oxygen to water as opposed to other nitrogen groups requiring the two step, 2 electron pathway that first reduces to unstable peroxides and in an acidic environment can be further reduced to water. Supercapacitor performance increases with the level of pyridinic nitrogen incorporated in within the nanocarbon matrix.[10] High pyridinic nitrogen content in low dimension carbon nanomaterials also correlates with higher potassium storage levels and electrochemical performance in potassium ion batteries.[11] While NCNT syntheses tend to yield graphitic-N as the dominant form of incorporated nitrogen, this work explores ways to maximize the pyridinic-N content[12, 13].

Czerw et al.[14] used a tight binding model and ab initio calculations to model the properties of this second type of bonding, and confirmed the bonding with X-ray photoelectron spectroscopy (XPS) and Scanning Tunneling Microscopy (STM). The structure was further confirmed by locating the surface distortion and vacancies on the nanotube surface via an STM image. Pyrrolic nitrogen represents a third type of nitrogen functionality in the nanotube lattice, as seen in Figure 1.3 A. This configuration incorporates the nitrogen atom into a five membered ring, increasing the likelihood of Stone-Wales defects[15] as seen in Figure 1.4.

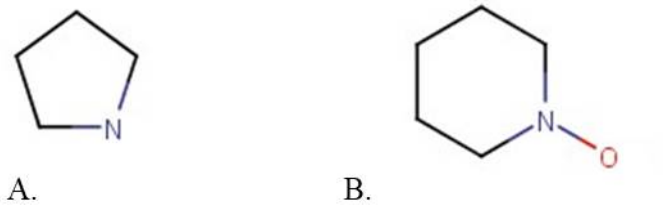

Figure 1.3 A. Pyrrolic and B. Pyridinic Oxide Nitrogen bonds.

This type of doping occurs in lower temperature syntheses, as it is not thermodynamically stable at the higher temperatures we use to synthesize NCNTs. Consequently, we expect to observe relatively small amounts of pyrrolic nitrogen doped CNTs.

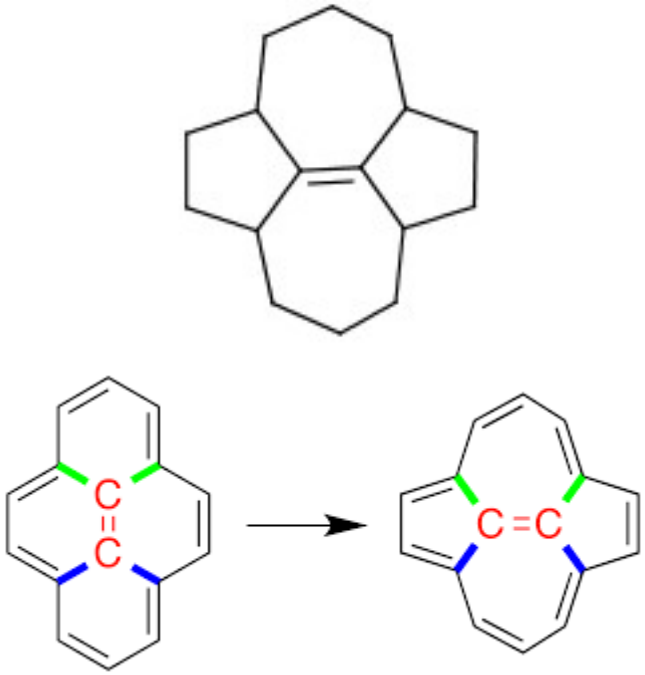

Figure 1.4 Stone-Wales Defect.

Figure 1.5 shows a special configuration with an iron atom bound to nitrogen atoms in the pyridinic structure, and occupying a vacancy in the lattice. In this scenario an individual iron atom will coordinate with unbound orbitals of 1, 2, 3, or 4 nitrogen atoms in the pyridinic formation with vacancies in the form FeN_x, where x=1 - 4. This FeN_x moiety is important for the improvement of oxidation reduction reactions (ORR).[16] Similarly, FeN_x species supported on NCNTs significantly improve the performance of alkaline polymer electrolyte fuel cells (APEFCs).[17] It is believed that Fe atoms, in the form of FeN_x activate and further improve the function of the nitrogen on carbon support,[18] especially in ORR and at trace concentrations of the transition metal.[19] The addition of the Fe to the N/C system allows for the reduction of O_2 directly to OH^- via the 4 electron process.[20] These properties are of particular interest and are one of the main reasons to study this system to determine if the nitrogen content can be maximized and tuned for specific species.

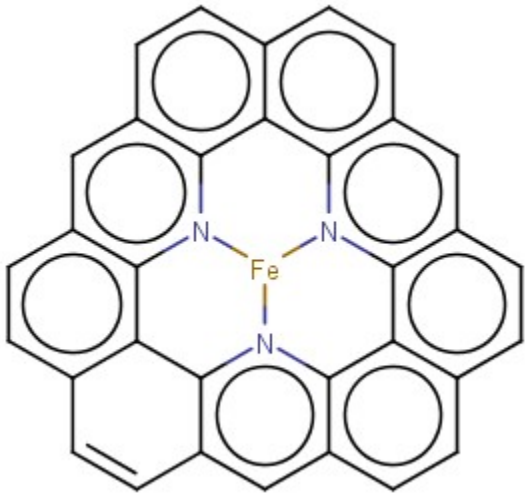

Figure 1.5 Fe-N_3 bond structure.

The remaining nitrogen bonding types include adsorbed oxygen from exposure to air. One is a pyridinic oxide structure, as seen in Figure 1.3B, the other is a higher order NO_x that is bonded to lattice edge nitrogen. Kaukonen et al. did a computational study on the formation energies of all these nitrogen species as well as the vacancy generation.[21] In addition they also looked at the origins of the oxygen reduction reaction of these functional groups and point to why this material is so interesting for that application.

Nitrogen doping in CNTs is of interest because the carbon atoms are relatively inert. However, lattice bound nitrogen atoms exhibit greater reactivity and add a large number of functional sites for bonding, catalysis, and many other applications.

NCNTs are used in sensors[22,23], field emission devices[24], nanocomposite materials[25], fuel cells[26], hydrogen storage[27], lithium ion batteries[28], supercapacitors[29], and as scaffolds for attachment of metal particles[30] and higher order polymeric reactions. One particular area of interest for these materials is in polymer electrolyte membrane fuel cells (PEMFCs). Platinum particles on a carbon support represent the state of the art material used in PEMFCs[31]. The cost of platinum is a major drawback for this technology and has fueled a considerable research on non-noble catalysts for the cathode material. PEMFCs operate in acidic conditions, at a pH of 1, rendering most non-noble metals a poor catalyst choice, since they would corrode under such conditions.[32] $Fe\text{-}N_4$ complexes on carbon supports are acid stable[33]. This complex is interesting because ferrocene can serve as the iron source in our synthesis and the corresponding free iron particles raises the possibility of $Fe\text{-}N_x$ complexes on NCNT supports grown in situ. Lefevre et al.[34] looked at multiple $Fe\text{-}N_x$ active sites on carbon supports for PEMFCs.

They showed FeN, FeN_2, FeN_3, and FeN_4, complexes on carbon supports are stable in acidic media. There are several synthesis methods for nitrogen doped carbon nanomaterials, such as arc discharge,[35] where the nitrogen source is incorporated into the anode and cathode. When the arc is struck between cathode and anode, the nitrogen doped CNTs form in the super-heated plasma around the arc. Another method to incorporate nitrogen in nanomaterials is to post dope by exposing a carbon support to high temperature and NH_3 gas.[36,37] A pristine nanomaterial gets annealed with a nitrogen source such as polyaniline[38], polypyrrole[39], or tripyrrolyl(1,3,5)triazine[40], in a nitrogen atmosphere offering yet another route. Nitrogen sources used in NCNT chemical vapor deposition (CVD) synthesis include pyridine[41], melamine[42], acetonitrile[43], dimethylformamide[44], zinc cyanamide[45], iron (II) phthalocyanine[46], and several aromatic hydrocarbons with NH_3 and H_2, or Ar. Iron, cobalt, and nickel are the most common catalysts used, in the form of a metallocene dissolved in the N-precursor or metal on a support, such as nickel-nitrate hexahydrate on magnesium oxide (MgO)[47]. Of all the methods used to produce nitrogen doping in carbon nanomaterials, CVD synthesis with a metallocene dissolved in a hydrocarbon nitrogen source is the most economical way to synthesize a sizeable amount of material with the highest percentage nitrogen doping.

Lee et al.[48] showed the first temperature evolution study of nitrogen doping in carbon nanotubes using C_2H_2, Ar as a carrier gas, NH_3, and iron pentacarbonyl. They observed an increase in nitrogen concentration from less than 3 atomic percent to almost 7 atomic percent. They produced nanotubes at 950°C, but their run times were only 30 minutes and the large flow of argon as a carrier gas would limit the etch rate of the NH_3.

This is because the NH_3 is less than 10% of the total flow rate and is only acting as a doping source and the etching would be greatly limited by the multitude of argon in the system. Liu et al.[49] synthesized NCNTs with Ferrocene/Pyridine in a hydrogen atmosphere and observed that graphitic-N was the highest N-species as determined by XPS. They found as temperature increased, the graphitic-N/pyridinic-N ratio also increased, to as high as a 10:1, but total atomic percent nitrogen was between one and two percent. In a similar study[50], NCNTs were synthesized with pyridine/ferrocene but, in this case they used pure NH_3 gas. In this report, the graphitic-N/pyridinic-N ratio increased with increasing temperature, but at lower temperatures the ratio of graphitic-N/pyridinic-N starts at 0.5:1, and rises as temperature increases to 1.5:1, with the atomic percent nitrogen peaking at 8.8 percent. In a study by Liu et al., using melamine/ferrocene and ethane with argon as the carrier gas[51], the total atomic percent nitrogen increased as high as 8 atomic percent but again the graphitic-N/pyridinic-N ratio was ~2:1.

NCNTs synthesized via CVD and using iron as the catalyst always have a bamboo structure, but the outer walls typically appear straight as seen in Figure 1.6. These NCNTs usually have 1-2 atomic percent nitrogen in the lattice and use Argon or Hydrogen as the gas source, as shown in previous work from Liu et al.[52]

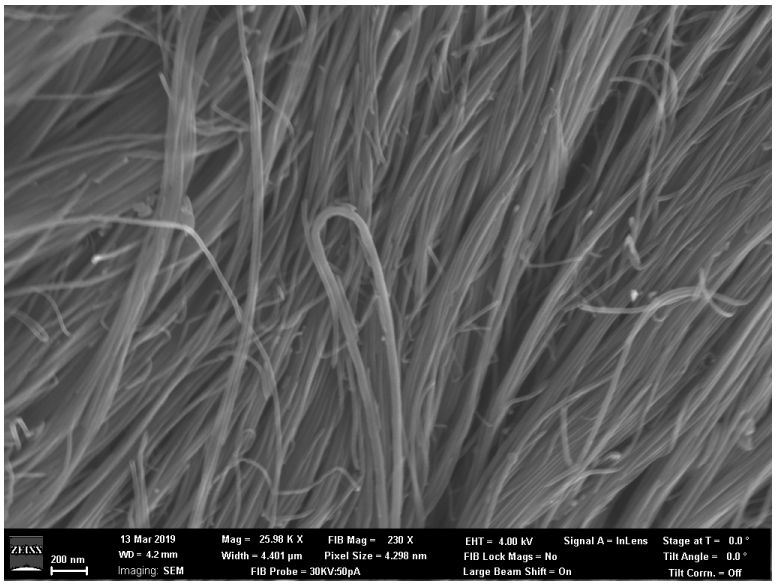

Figure 1.6 SEM of typical NCNT exhibiting straight walls (M. Craps)

These NCNTs were synthesized with hydrogen as the carrier gas in previous work. The walls can have a slightly roughened appearance; you must use a Transmission Electron Microscope (TEM) to view the inner wall bamboo structure seen in Figure 1.7.

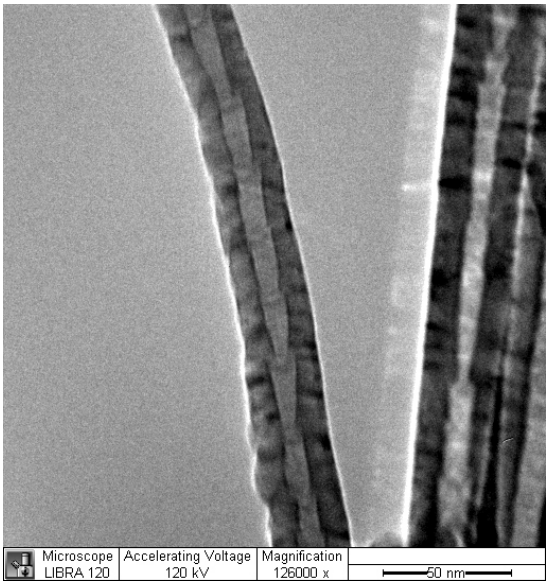

Figure 1.7 TEM of typical NCNT exhibiting straight outer walls but showing internal bamboo structure (M. Craps)

Renu Sharma's groundbreaking environmental TEM studies showed the initial cap formation during early stages of carbon nanotube growth.[53] When NCNTs get synthesized in a pure NH_3 atmosphere as is the case in this work, the structure of the tubes becomes more bulbous, as seen via TEM in Figure 1.8. These extreme lattice distortions can be imaged in SEM as well.

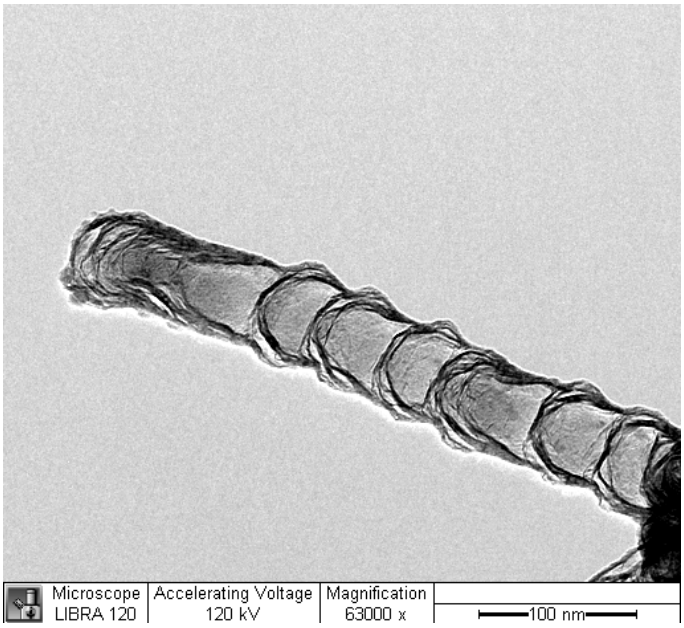

Figure 1.8 TEM of NCNT synthesized in pure NH_3 atmosphere (M. Craps)

NCNTs, when synthesized in a pure NH_3 atmosphere, the extreme curvature of the NCNT tube walls are seen in SEM in Figure 1.9. The extra curvature comes from the added reactivity of the NH_3 and increased nitrogen incorporation into the catalyst particle, which adds more nitrogen defect structure in the NCNT lattice.

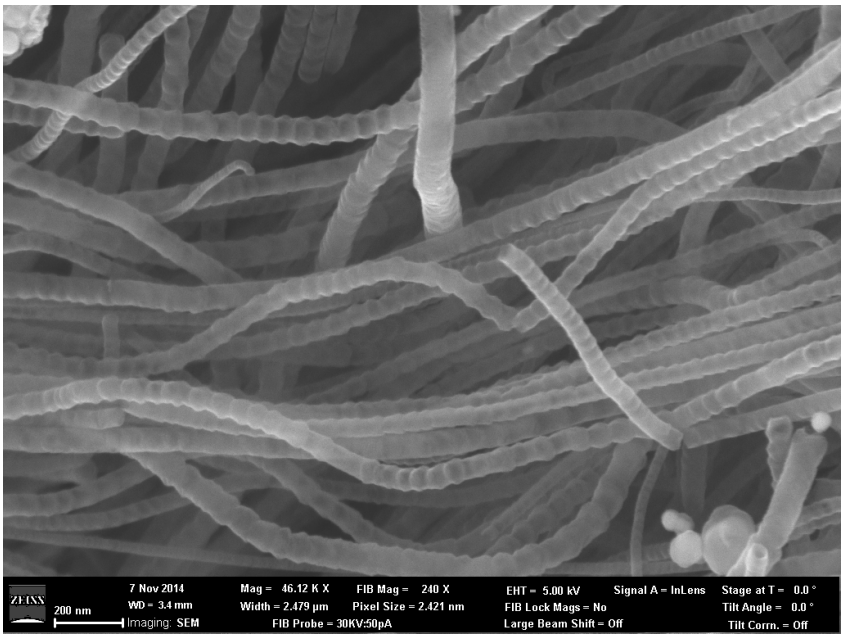

Figure 1.9 SEM of NCNTs synthesized in pure NH_3 atmosphere (M. Craps)

There is still debate on the kinetics of CNT growth. In its simplest form, a hydrocarbon undergoes pyrolysis and further decomposes in the gas phase, on the catalyst particle or dissolves into the particle. Once the catalyst particle is supersaturated CNT growth starts, and continues until the catalyst become poisoned or encapsulated. In the case of the nitrogen doped CNT, the addition of nitrogen to the catalyst particle actually increases the depth, rate, and concentration of carbon[54]. Sharma et al.[55] did a kinetic study on carbon nanotube synthesis in a fixed bed system. Initially, they estimated the rate of NCNT formation by calculating the moles of NCNT formed over the grams of catalyst and support times the reaction time in seconds. They did this because they used a fixed bed reactor with ferrocene on MgO. They don't see a reduction in NCNT formation until 950°C. This is interesting but explained by the usage of acetylene as an added carbon source and argon as the carrier gas. They compared the nitrogen

concentrations of the synthesized material, and the highest nitrogen concentration happened at 600°C at 13.8% then decreased at each temperature through 950°C. These experiments were only carried out for 25 minutes so they don't capture all of the extra data collected in this experimental series with both temperature and time evolution.

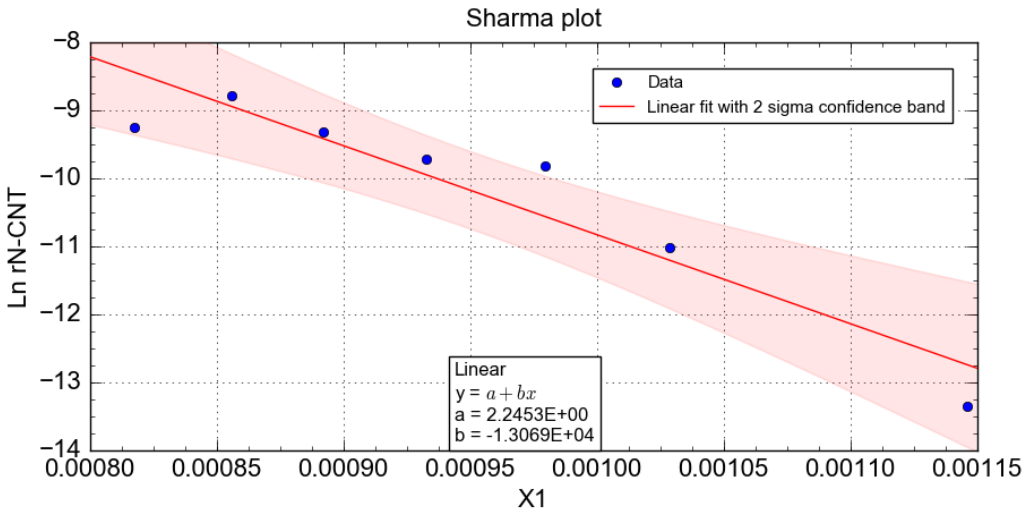

Figure 1.10 Arrhenius plot of NCNT rate from Sharma (band shows 95% confidence interval)

There is a problem with the data in Figure 1.10. First, there is only one data point per temperature. Without a statistically relevant data set, it is not advisable to make an assertion that there is a down turn or deviation from the linear fit when you cannot say one way or the other. Then, there is a data point right in the middle of the data that doesn't fit in the 95%, 2 standard deviation confidence band. They looked at a saturated versus a super saturated model and provide one of the few reasonable analogs to build off. Attention was given to mass of product, partial pressures, and flow rates. No one to my knowledge has attempted to determine the kinetics of NCNT synthesis in a purely

NH_3 environment. And this is interesting because our drive is not to maximize NCNT production but to maximize the percent nitrogen and to tune certain catalytic sites.

In this work, I investigated the CVD synthesis of NCNTs using ferrocene and pyridine precursors in a pure NH_3 environment. To understand the kinetics of nitrogen incorporation in carbon nanotubes, I performed a time and temperature evolution study. We logged the mass of NCNT product collected from each run. We know from literature that post doping carbon nanomaterials with NH_3 increases the total atomic percent nitrogen[56,57]. We also know that synthesis in an NH_3 atmosphere is an effective method to maximize nitrogen percentage. I implemented SEM and TEM to monitor structural changes to the NCNTs, and record lengths and diameters. We used XPS to monitor the percent nitrogen changes in the nanotubes.

Hypothesis 1: At a set temperature, and constant feed rates, atomic percent nitrogen incorporated in the NCNT lattice should remain constant with time.

Prediction 1.1: For set constant feed and gas rates, and a specific reaction temperature, the atomic percent nitrogen observed, via XPS, should remain the same at each reaction time, unless the catalyst becomes poisoned.

Hypothesis 2: The atomic percent nitrogen incorporated in the NCNT lattice should increase with increasing reaction temperature.

Prediction 2.1: Because nitrogen becomes more soluble in iron as the reaction temperature increases, we expect higher percentage nitrogen incorporated in the NCNT lattice with increasing reaction temperature.

Prediction 2.2: Further, increasing reaction tube temperatures drives greater NH_3 decomposition, which yields more nitrogen free radicals and increased nitrogen content in the nanotubes.

CHAPTER II

SYNTHESIS OF HIGHLY DOPED NITROGEN CARBON NANOTUBES

II.1 Introduction

Highly doped NCNTs, synthesized using a pure NH_3 atmosphere, maximize the nitrogen incorporation into the CNT lattice. After a thorough review of the literature, many questions remain around the synthesis of NCNTs in a pure NH_3 atmosphere. We selected NH_3 plus pyridine because when H_2 or Ar is the carrier gas, the concentration of nitrogen doping rarely exceeded 4 atomic percent. By utilizing pure NH_3 as the carrier gas, the nitrogen concentration increases dramatically from 7-13 atomic percent. I conducted a temperature evolution study from 700°C to 850°C, for two hours and only observed a silver flaky product at 850°C and above, along with NCNTs. We also obtained no NCNTs at temperatures above 850°C at the two hour synthesis time, only the shiny, flaky product. To further understand NCNT synthesis kinetics, I conducted a time evolution study from 15 to 120 minutes at several temperatures to resolve any rate changes. All NCNT products were collected, weighed, and recorded for each time and temperature.

II.2 Materials and Equipment

I synthesized NCNTs via chemical vapor deposition (CVD) in a two-furnace system comprised of a Thermcraft preheater in which it vaporizes the precursor solution,

and a higher temperature Thermcraft furnace, seen in Figure 2.1, which facilitates the NCNT synthesis and deposition.

Figure 2.1 Chemical Vapor Deposition system with preheater (left) and furnace (right).

99.995% Ultra high purity nitrogen or helium gas from Airgas was flown through Aalborg mass flow controllers to purge the air from the system for 15 minutes. Then, the helium flow was stopped and 99.99% Anhydrous Ammonia from Airgas (NH_3) gas was flown through an Alicat NH_3 mass flow controller at 200 standard cubic centimeters (sccm) and purged the inert gas from the system for 15 minutes. Then, a 2.7 wt % ferrocene (99.0% Alfa Aesar) in pyridine solution, (99.0% Alfa Aesar kept under argon) weighed on a Mettler Toledo PL602E Precision balance with 0.01 gram resolution, was injected into the preheater, as seen in Figure 2.2. The solution was injected via a syringe and syringe pump with plastic tubing connected to 1/8" stainless tubing connected with Swagelok fittings through custom end caps on a 2" x 80" Quartz tube from National

Quartz. The solution was injected at 5.5 mL/hr. The solution vaporized in the preheater and the vapor carried into the reactor furnace via the flow of 200 sccm of NH_3. The NH_3 flow passed over a bed of CaO to remove any residual moisture from the ammonia gas. Note: Even though I used very pure ammonia gas, before employing the use of CaO to scavenge the residual moisture, some samples exhibited with very high oxygen contents as measured via XPS. Great care was exercised to ensure that oxygen and moisture concentration was minimized. In addition to passing the gas through molecular sieves, Drierite (calcium sulfate), and a CaO trap, H_2O and O_2 sensors monitored and confirmed that moisture and oxygen levels were below 10 parts per million. Preheater temperature is an important factor, as it must be maintained above the boiling point of the pyridine and above the sublimation temperature of ferrocene. We selected a preheater temperature of 210°C for these studies, as we previously determined that the preheater could operate between 170-250°C. The unreacted gas can exhaust by a number of methods, and we chose to use a glycerin filled bubbler flask over a water filled flask to ensure that there was no water vapor backstreamed into the furnace. The nitrogen doped CNT product deposited on the walls of the 2-inch diameter quartz tube. A schematic of the CVD setup used for these experiments is pictured in Figure 2.2.

Experiments ranged in temperature from 700°C - 850°C in a pure NH_3 atmosphere. Above 850°C, I observed no nanotube product. I also conducted a time evolution study to determine the rate of nitrogen inclusion into the CNT lattice. Experiments lasted from 5 minutes to 180 minutes. All NCNT products were collected, weighed, and recorded for each time and temperature for further characterization and

analysis. Samples were collected with a razor blade attached to wooden dowel. Typically, for production purposes, a bottle brush on a long handle would be used for sample collection but the powdered product would generate a lot of static charge and sample would be lost. The razor blade attachment allowed for virtually all the NCNT product to be collected.

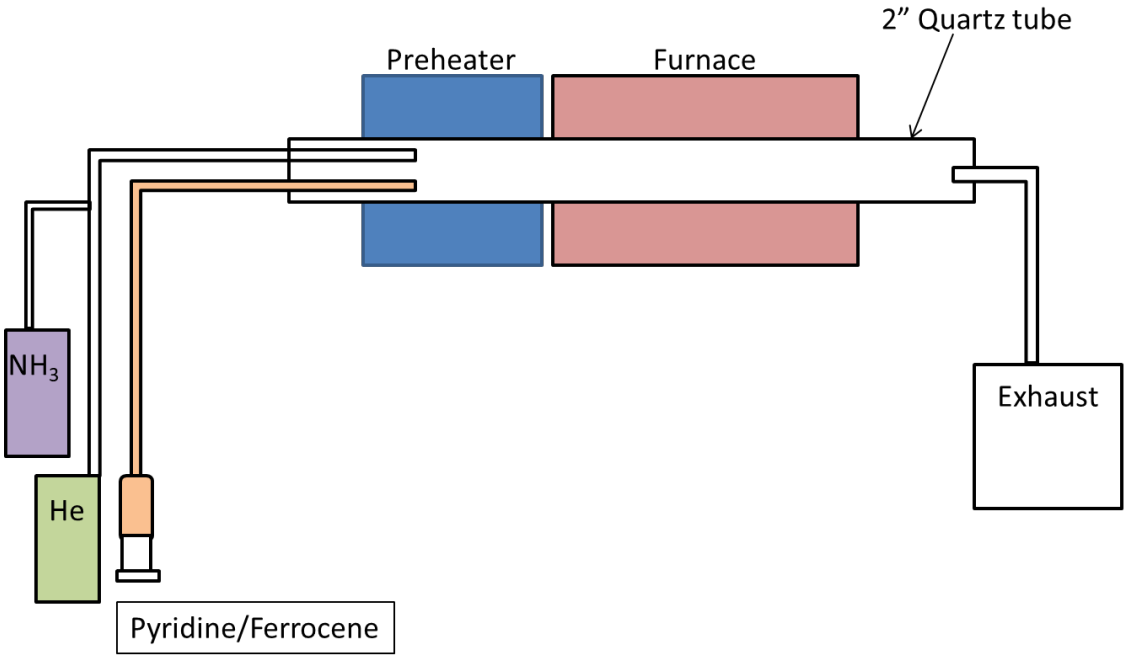

Figure 2.2 Chemical Vapor Deposition set up used for these experiments

II.3 Data and Observations

Table 2.1 Atomic percent nitrogen detected via XPS from time trials. Note: Bolded numbers indicate the median values, with 2 sigma uncertainties

Time (min)	725C (±2σ)	750C (±2σ)	775C (±2σ)	800C (±2σ)	825C (±2σ)	850C (±2σ)
5		6.68, 8.66, 7.55, 8.08, **7.62** (±1.46)	7.78, 8.55, **7.80**, 7.52, 7.83 (±0.77)	7.23, **8.18**, 7.05, 8.83, 8.33 (±1.52)		6.66, **7.35**, 6.10, 7.68, 7.92 (±1.50)
15	**7.40**, 8.13, 7.22 (±0.96)	7.73, 8.81, **8.40**, 7.79, 9.66 (±1.60)	9.62, 8.41, **8.88**, 8.85, 9.53 (±1.02)	8.26, 8.30, 9.26, 8.82, **8.51** (±0.83)	8.14, **8.38**, 9.07 (±0.97)	8.96, 9.61, **8.58**, 8.12, 7.70 (±1.48)
30	**8.62**, 8.89, 8.52 (±0.38)	**8.77**, 8.85, 8.65, 8.3, 9.5 (±0.87)	9.65, 8.90, 10.17, 8.89, **9.16** (±1.10)	9.34, 7.91, **9.52**, 9.36, 9.53, 10.04 (±1.44)	**9.69**, 9.53, 10.75 (±1.33)	**8.69**, 8.70, 8.22, 8.39, 9.32 (±0.84)
60	8.96, 9.44, **9.05** (±0.51)	8.59, 10.02, 10.23, 9.44, **9.59** (±1.27)	**10.22**, 10.76, 10.15, 10.14, 10.58 (±0.57)	9.93, 8.51, 8.39, 10.31, **10.02**, 10.49, 10.73 (±1.88)	**10.82**, 11.18, 10.00 (±1.21)	10.05, 8.61, 8.50, **8.73**, 10.39 (±1.78)
90		10.29, 9.51, 9.55, **10.15**, 11.17 (±1.35)	10.98, 11.52, 11.19, 11.79, **11.48** (±0.63)	10.80, **10.71**, 10.64, 10.52, 10.52, 10.91 (±0.31)		8.66, 7.47, 9.04, **8.79**, 8.79 (±1.24)
120	10.1, 10.53, 9.37, **9.5,** 8.88, 10.47 (±1.32)	11.14, 10.80, 10.03, 10.15, **10.60** (±0.92)	**11.31**, 12.55, 10.87, 11.45, 10.91 (±1.36)	10.60, 11.62, 11.58, 11.30, **11.36** (±0.82)	9.32, 9.17, 9.90, 9.50, **9.36** (±0.56)	**8.53**, 8.31, 8.60, 8.23, 8.71 (±0.40)

Table 2.2 Median mass yields of NCNT's from time evolution studies

Temperature (°C)	15 minutes	30 minutes	60 minutes	120 minutes
725	25 mg	50 mg	110 mg	245 mg
750	20 mg	70 mg	120 mg	260 mg
775	30 mg	70 mg	130 mg	280 mg
800	30 mg	70 mg	140 mg	220 mg
825	30 mg	50 mg	110 mg	200 mg
850	20 mg	40 mg	80 mg	130 mg

II.4 Results

II.4.1 Temperature evolution study

Initially, I conducted a temperature evolution study from 700°C to 850°C in 25 degree intervals for 120 minutes with at least 5 syntheses for each temperature. Given the relatively small sample sizes, I plotted the median data points with ±2σ uncertainties at each temperature. As seen in Figure 2.3, at 700°C the atomic % nitrogen incorporated in the NCNT has a median value of 9.25% with a 95% confidence interval of ± 1.07. At 725°C, the atomic % nitrogen detected in the NCNT rises to 9.80% with a 95% confidence interval of ± 1.32. At 750°C, the atomic % nitrogen incorporated in the

NCNT further rises to 10.60% with a 95% confidence interval of ± 0.92. The atomic % nitrogen rises further still at 775°C, to 11.31% detected in the lattice of the NCNT with a 95% confidence interval of ± 1.36. At 800°C, the atomic % nitrogen levels off to 11.36% with a 95% confidence interval of ± 0.82. This last result is interesting because until this temperature, the rate of increase of nitrogen bonded in the NCNT lattice had been relatively constant and now it has leveled off. At 825°C, the atomic % nitrogen detected in the NCNT dropped to 9.36% with a 95% confidence interval of ± 0.56. Based on the background and hypothesis, the expectation is that the atomic % nitrogen should increase with increasing temperature. However, as seen in the experimental data, something different occurs above 775°C, when the percent nitrogen slows and then decreases with increasing temperature. At 850°C, the atomic % nitrogen included in the NCNT lattice further declines to 8.53% with a 95% confidence interval of ± 0.40. With further increases in temperature, the resulting nitrogen concentration drops to the lowest value in the dataset. This result suggests a competing reaction that dominates at the higher temperatures. At 900°C, I observe no NCNTs at 120 minutes, only a silver flaky product indicating iron carbide formation as measured in XPS.

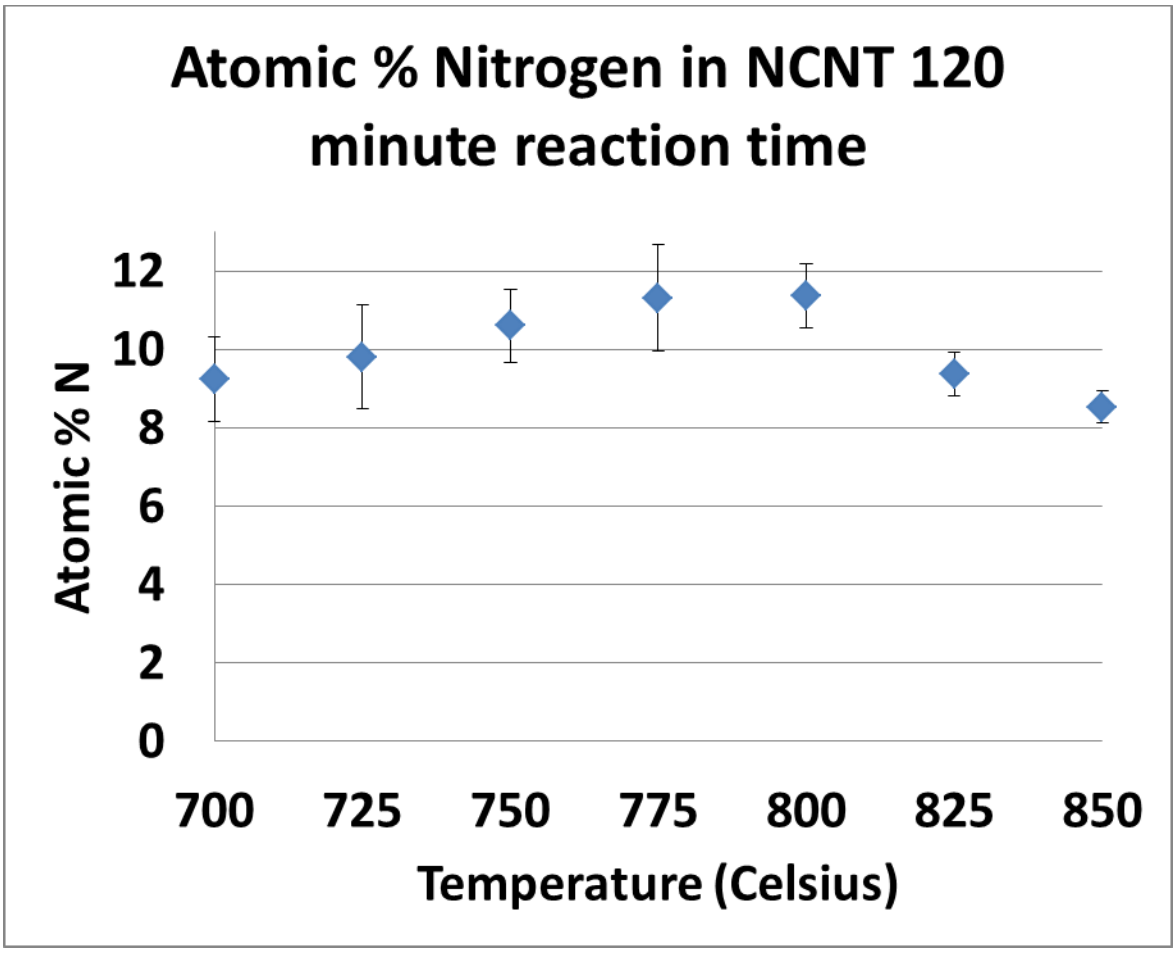

Figure 2.3 Temperature evolution study showing median atomic percent nitrogen with 95% confidence levels after 120 minutes synthesis time in a pure NH_3 environment

II.4.2 Time evolution studies

After observing an interesting change in percent nitrogen incorporated at changing temperatures at 120 minutes, it became clear, to better understand the growth kinetics, I needed to conduct a time evolution study. It is hypothesized that the atomic % nitrogen incorporated in the lattice should increase with time. I carried out a time evolution study from 725°C to 850°C in 25 degree increments. For each unique trial, I

completed at least 3 replicate synthesis runs. Synthesis times were 15, 30, 60, and 120 minutes.

The observed percent nitrogen data was collected via XPS and we report the median data points. In general, the atomic percent nitrogen detected by XPS tends to increase with time and temperature. These results support the hypothesis. However, for 120 minute syntheses at 825°C and 850°C, the percent nitrogen observed actually decreases. If the zero order plots, shown in Figures 2.3a-f, were to support a zero order reaction for nitrogen percentage, the data would need to be linear. While this data suggests zero order behavior at the lower temperatures, at 825°C and 850°C, there is a different reaction order that has yet to be determined.

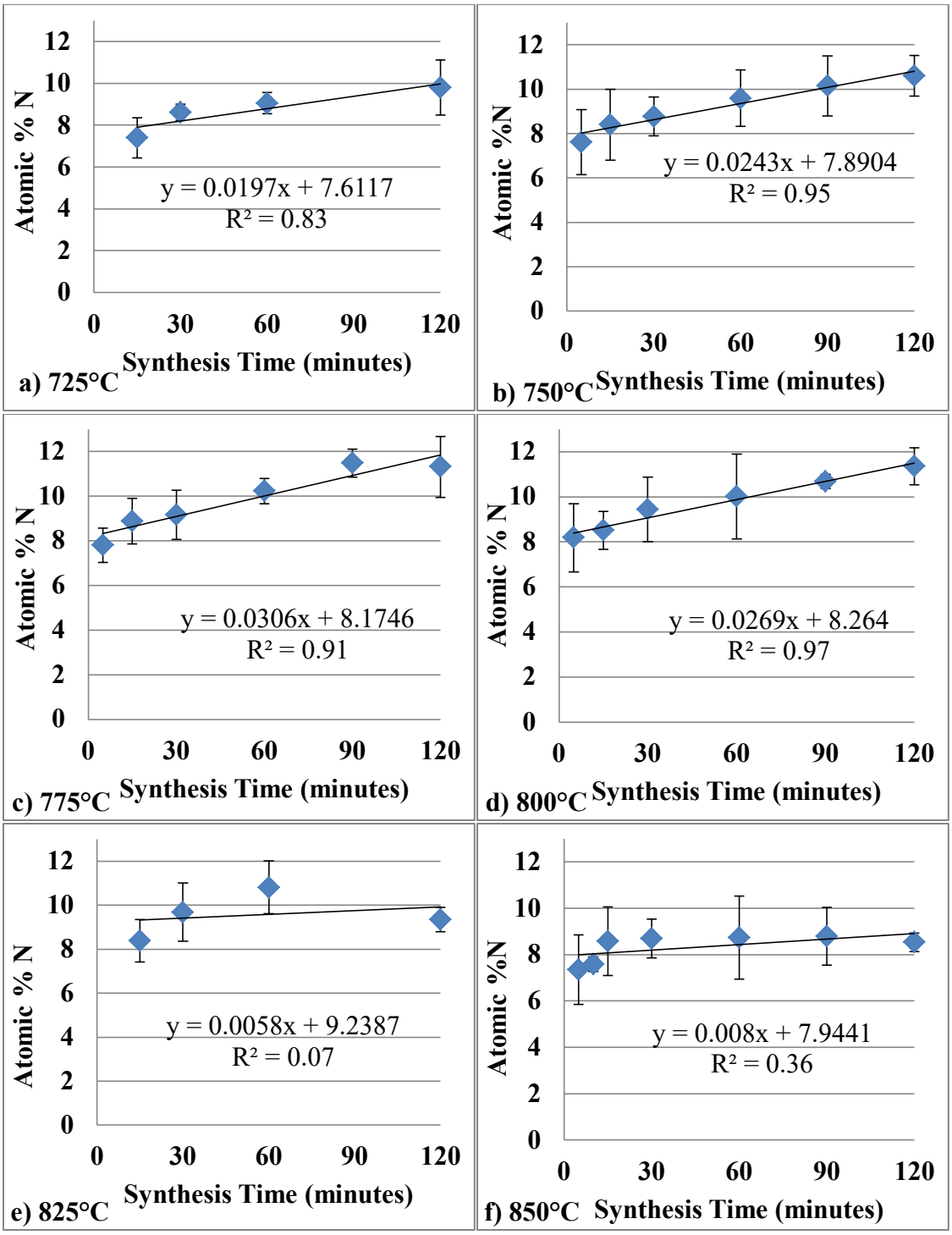

Figure 2.4 Zero order time evolution data showing atomic percent nitrogen in NCNTs synthesized in a pure NH_3 environment from 725°C to 850°C

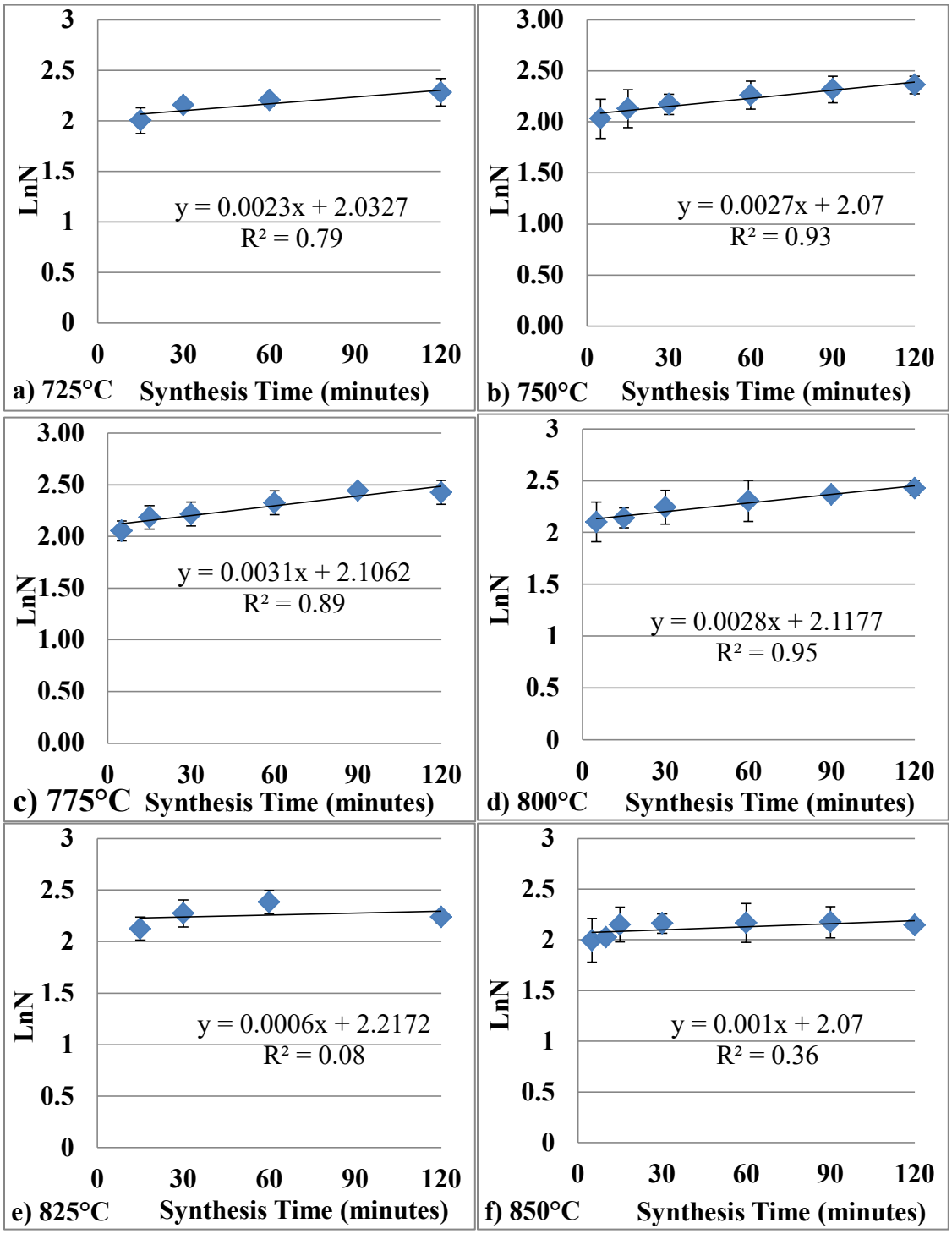

Figure 2.5 1st order Natural Log plots of N concentration versus time

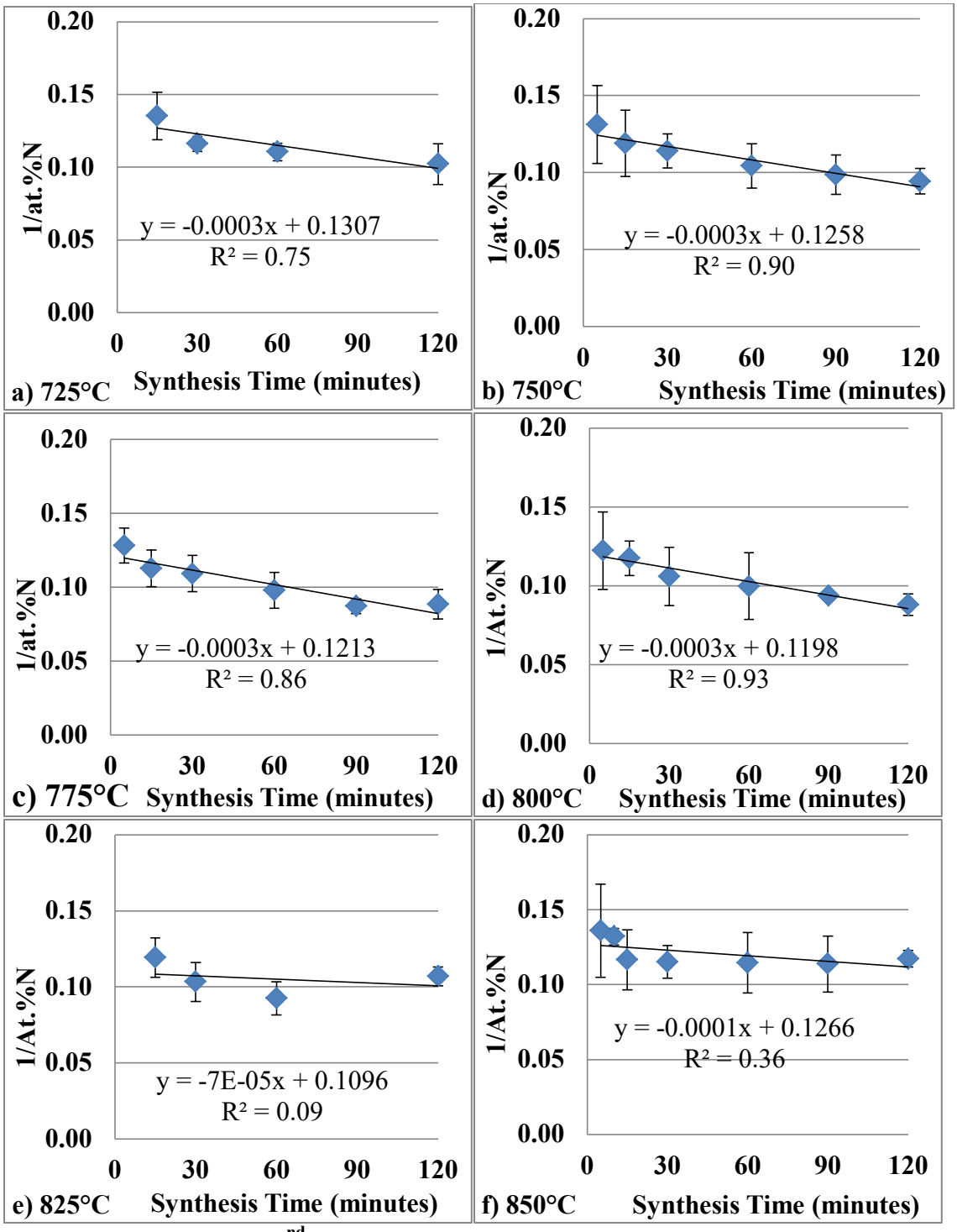

Figure 2.6 2nd order Inverse of N concentration versus time

Table 2.3 Slopes and R^2 goodness of fit values for nitrogen concentration in NCNT

Temperature (°C)	Atomic %N	Ln %N	1/%N
725	y = 0.0197x + 7.6117 R^2 = 0.83	y = 0.0023x + 2.0327 R^2 = 0.79	y = -0.0003x + 0.1307 R^2 = 0.75
750	y = 0.0243x + 7.8904 R^2 = 0.95	y = 0.0027x + 2.07 R^2 = 0.93	y = -0.0003x + 0.1258 R^2 = 0.90
775	y = 0.0306x + 8.1746 R^2 = 0.91	y = 0.0031x + 2.1062 R^2 = 0.89	y = -0.0003x + 0.1213 R^2 = 0.86
800	y = 0.0269x + 8.264 R^2 = 0.97	y = 0.0028x + 2.1177 R^2 = 0.95	y = -0.0003x + 0.1198 R^2 = 0.93
825	y = 0.0058x + 9.2387 R^2 = 0.07	y = 0.0006x + 2.2172 R^2 = 0.08	y = -7E-05x + 0.1096 R^2 = 0.09
850	y = 0.008x + 7.9441 R^2 = 0.36	y = 0.001x + 2.0696 R^2 = 0.36	y = -0.0001x + 0.1266 R^2 = 0.36

After plotting all the slopes and goodness of fit values in Table 2.3, it is unclear whether the reaction rate is zero, first, or second order. From the raw data, the atomic percent nitrogen increases as temperature and time increase until the maximum atomic percent nitrogen incorporated at 775°C and after that point, increasing temperature causes the atomic percent nitrogen to drop. Further, the lack of fit at 825°C and 850°C suggests

something significantly different is happening with respect to time and temperature changes.

As seen in Table 2.2, there is a general trend that the median mass increases up to 775°C, then starts declining but only slightly initially at 800°C, then more dramatically at 825°C and 850°C. After 15 minutes, the results are pretty close to each other but the suggestion to take away from the data is that at 725°C and 750°C the initial rate of growth is slow. However, at 825°C and 800°C each are on par with the yield at 775°C suggesting that the rate of growth increases as temperature increases, to a point. The data suggests that the initial rate of growth may be highest at 800°C. At 30 minutes a similar trend is developed with masses increasing from 50 mg at 725°C, to 70 mg at 750°C, 775°C, and 800°C. At 825°C, there is a reduction in mass, showing a value of 50 mg. At 850°C, the mass at 40 mg, is less than the lowest reported value at 725°C. This suggests that catalyst deactivation and poisoning is quicker at 850°C and that some other factor may be coming into play. At 60 minutes, the trend still holds with increases from 110 mg, 120 mg, to 130 mg, at 725°C, 750°C, and 775°C respectively. At 800°C, the peak is observed at 140mg with reductions in mass to 110 mg and 80 mg at 825°C and 850°C respectively. After 120 minutes, a new trend emerges. Initially the trend holds with mass increases from 245 mg at 725°C, to 260 mg at 750°C, to 280 mg at 775°C. Previously, at 800°C the masses had leveled off being relatively close to 775°C, however, now the mass takes a significant drop to 220 mg. A further drop to 200 mg is reported at 825°C and it falls to a low of 130 mg with all three values falling below the amount at 725°C suggesting a significant change happening at high temperatures. What we see develop

over time is that at low temperature the mass steadily increases but after 60 minutes at 800°C, there is a significant fall off suggesting that there is a competing mechanism or a poisoning of the catalyst particles. Table 2.4 shows the rate of NCNT product formed with the rate equations based off the median mass yields. The rate equations tell an interesting story. The slope of the equations increases from 725°C to 775°C and then decreases from 800°C to 850°C.

Table 2.4 Rate of NCNT product formation from NCNT weight yields

Temperature (°C)	Rate Equation	R^2
725	y = 2.148x - 14.565	0.999
750	y = 2.220x - 7.391	0.994
775	y = 2.359x - 5.217	0.998
800	y = 1.774x + 15.22	0.974
825	y = 1.641x + 5.217	0.996
850	y = 1.038x + 9.130	0.985

The information in Table 2.3 includes the total product produced, not just the nitrogen concentration. The changes in the rate equations further support a more complex change in the mechanism of NCNT growth starting at 800°C. The rate equations in Table 2.4 show an increase in the rate of production with increasing temperature until 775°C and each increase in temperature thereafter results in a decrease in the rate.

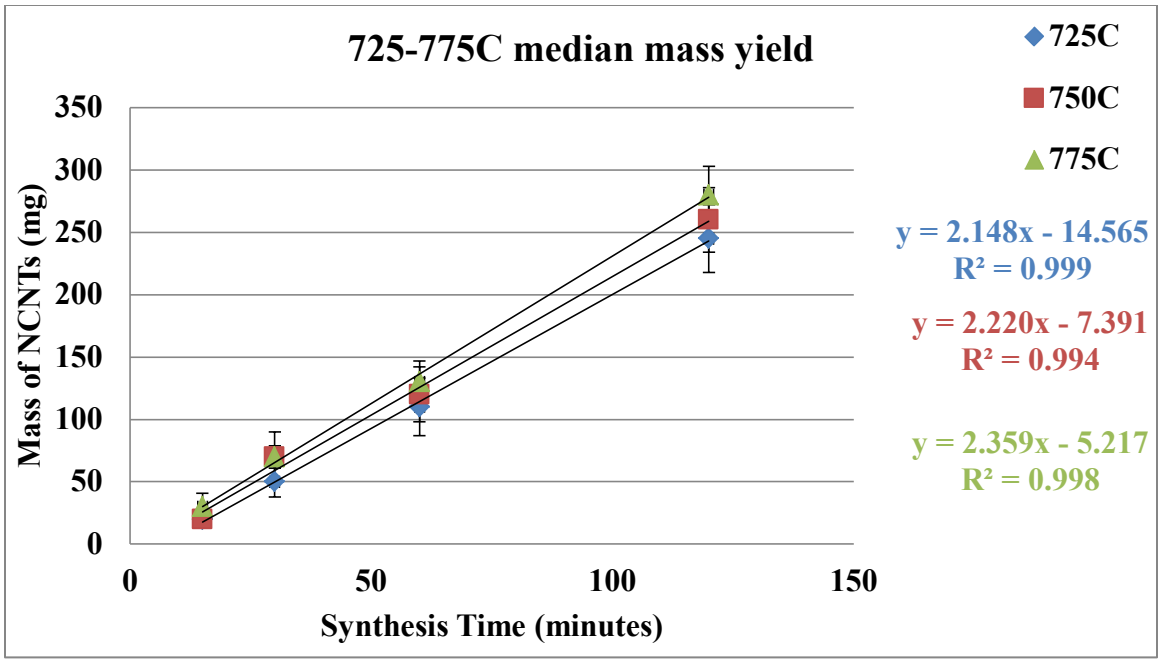

Figure 2.7 Median mass yields from 725-775°C

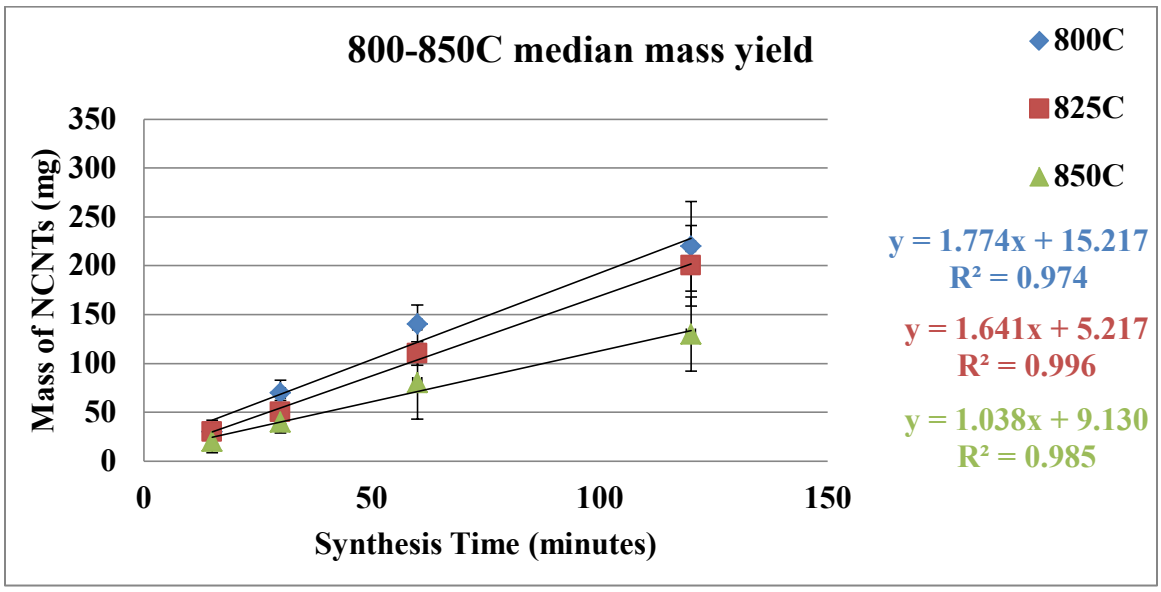

Figure 2.8 Median mass yields from 800-850°C

Figure 2.7 and 2.8 show the mass yields versus time at the two different temperature ranges with their corresponding rates.

II.5 Discussion

NCNTs produced by CVD in a pure NH_3 atmosphere show a nearly linear increase in nitrogen concentration with temperature up until 800°C. But, NCNT samples produced at 825°C and 850°C showed a decline in the nitrogen concentration. This is in agreement with Terrones[58] that it is difficult to incorporate nitrogen into nanotubes at high temperatures, due to the liberation of N_2 gas from the lattice. It is worth noting that Lee[59] found an increase in nitrogen concentration with an increase in temperature that held through 950°C. However, C_2H_2, Ar, and NH_3 were used in that study, so there are different potential mechanisms and rate limiting steps. A closer analog to this study by Liu[60] shows the peak nitrogen concentration at 700°C and decreases steadily as temperature rises to 1000°C. Pure NH_3 and pyridine are used in that study, so it is interesting to note that the results presented here are somewhat contrary to his findings. The experiments presented in Liu's work were based on a one hour synthesis, while the experiments presented here cover a range of times and temperatures, from 5 minutes to 120 minutes, and 700°C to 850°C respectively, in order to gain a deeper understanding of the time and temperature resolved growth kinetics. The first study in this research was conducted for 120 minutes from 700°C to 850°C in 25 degree increments. The result starts at 9.25 atomic percent nitrogen, at 700°C, to 11.36 atomic percent nitrogen, at 800°C, in agreement with the initial hypothesis. Then, the concentration fell to 9.36

atomic percent nitrogen at 825°C, and 8.53 atomic percent nitrogen at 850°C. These findings do not support the initial hypothesis. Originally, the thinking was that the atomic percent nitrogen would increase with increasing temperature. No NCNT product was produced at 120 minutes at 900°C, only a silver flaky product. Synthesis times chosen were 15, 30, and 60 minutes to compliment the 120 minute study. At 60 minutes, the trend holds similar to the 120 minute up to 775°C with 10.22 atomic percent nitrogen, up from 9.59 and 9.05 atomic percent nitrogen at 750°C and 725°C respectively. There is a slight drop at 800°C to 10.02 atomic percent nitrogen, but then at 825°C there is a maximum at 60 minutes of 10.82 atomic percent nitrogen. Finally, at 850°C the value falls off to 8.73 atomic percent. The drop in atomic percent at 800°C is possibly attributed to one synthesis run possibly dragging down the median value and it is likely closer to 10.15-10.20 atomic percent. There is some inherent variability due to some heterogeneity in the samples in terms of lengths and diameters. This is due to the constant feed rate of iron particles and that the catalyst particles will poison at different times during the synthesis. At 825°C, this local maximum stands out at 10.82 atomic percent and with the other raw data values being 11.18 and 10.00 atomic percent nitrogen, it is likely that the average value would be between 10.55 and 10.75 atomic percent as the mean is 10.66 atomic percent. At 30 minutes, the lowest value is 8.62 atomic percent nitrogen at 725°C and climbs steadily to 825°C where it peaks at 9.69 atomic percent nitrogen, which then drops at 850°C to 8.69 atomic percent. At 15 minutes, the data trend mirrors more closely the data at 120 minutes. At 725°C the minimum median value reported is 7.40 atomic percent, which climbs to a maximum at

775°C of 8.88 atomic percent nitrogen. At 800°C, 825°C, and 850°C, reported medians of 8.51, 8.38, and 8.58 atomic percent nitrogen, respectively, suggests that at high temperature there is a significant doping effect initially.

The atomic percent nitrogen increased with every time increase at each temperature supporting hypothesis 1, until 825°C and 850°C at 120 minutes, where it refutes hypothesis 1. The observed data supports hypothesis 2 until 825°C and 850°C where it was refuted.

II.6 Conclusions

NCNTs were successfully produced by a CVD method using NH_3 as the only reactive gas along with pyridine and ferrocene. The NCNT growth conditions were studied to produce the maximum nitrogen content. Based on the data presented, one would conclude that the greatest rate of incorporation happens at 800°C. That inference would be drawn from the atomic % nitrogen incorporated into the final product. However, one cannot assign a rate of growth or nitrogen incorporation without taking into account the total mass of the product produced. Only then, rates could potentially be determined. This aspect will be examined in the next section where a set of time resolved Arrhenius studies will provide deeper insight into the rate of nitrogen in NCNT synthesis.

The results from this initial study raised the question, would the same observed trends be observed at different times at these temperatures. To this end, a time evolution study was devised to synthesize NCNTs under the same NH_3 atmosphere and under the same synthesis conditions. It is observed that something out of the norm is happening to

the rate at high temperatures, and after plotting the natural log of the atomic percent nitrogen concentration and the inverse atomic percent nitrogen concentration to determine if the reaction was first or second order the goodness of fit metrics did not yield a simple result based on atomic concentration alone. Therefore, more information is needed and that comes in the form of median mass yield. Knowing the mass will allow for further calculations on the rates of reaction.

Looking at the trends of the median mass yields provides some evidence of the changing rates of formation. As seen in Table 2.2, as time increases, mass increases as expected. Second, as the temperature increases, the median mass yielded increases, to a point around 775°C to 800°C. At 15 minutes, there isn't a significant variation in mass collected as there isn't much time to make much product, but at the lower temperatures 20 mg is produced and increases up to 30 mg at 800°C, declining to 24 mg at 850°C. At 30 minutes things become a bit more pronounced as 50 mg is produced at 725°C and the yield increases to 70 mg for 750°C, 775°C, and 800°C. Then the median mass declines at 825°C and 850°C to 50 mg and 40 mg respectively. Now this trend starts to tell a story, the masses increase through 775-800°C but then drop significantly after. This same trend continues at 60 minutes where 725°C has a lower mass of 110 mg and then increases up until 800°C where it peaks at 140 mg, and then falls away at 825°C and 850°C significantly to 110 and 80 mg respectively. While 30 minutes showed a slightly less yield at 850°C than 725°C, that is now even more evident at 60 minutes and 850°C is less than the yield of 725°C, by a significant margin. At 120 minutes, the mass at 725°C is 245 mg, and increases to 260 mg and 280 mg at 750°C and 775°C, respectively.

However, now every mass for 800-850°C is less than the mass for 725°C, with 800°C and 825°C both at 220 and 200 mg respectively, and 850°C showing a significant mass reduction at 130 mg. This means that at high temperature there is either a mechanism that is halting the process, or there is a competing mechanism that is causing liberation of the atoms from the lattice, which would account for a significant mass loss, or a combination of both. However, by looking at 725°C through 775°C, one can observe what is happening under normal conditions. The masses increase with both time and temperature. The case of 725°C suggests a much slower rate of growth and nitrogen incorporation, but the effects of poisoning NCNT termination do not appear to show a significant effect. This new information will allow for a better determination of the rates and mechanisms in the next section.

Hypothesis 3: Based on the rates of nitrogen inclusion from previous concentration studies, and assuming a quasi-homogeneous environment, a series of time-resolved Arrhenius plots may elucidate the reaction order of the growth process. Alternatively, such studies could clarify when the competing reaction becomes dominant.

Prediction 3.1: Time resolved Arrhenius plots should show a linear relationship regarding the natural log of rate of nitrogen inclusion. However, based on the empirical data, we predict the reaction is not governed by one rate determining mechanism and there will be a point of delineation.

CHAPTER III

AN ARRHENIUS STUDY ON NCNTS

III.1 Introduction

When trying to determine the reaction order from nitrogen concentration alone, the data suggests a more complex process and mechanism than originally predicted. Looking at the atomic percent nitrogen without taking into account the mass of the product formed provides insufficient information to analyze this growth process. However, if the mass of the product is taken into account, the total moles, moles of carbon, nitrogen, and iron, and ultimately the rate in moles per second can estimate an overall growth rate. This information provides us with a more accurate and complete picture of the system's dynamics. By utilizing an Arrhenius plot, it can be determined if a single mechanism drives the rate of nitrogen inclusion into the NCNT lattice or if there are competing rate limiting steps that dominate at different temperatures. The Arrhenius equation is of the form:

Equation 3.1 $$k = Ae^{-\frac{E_a}{RT}}$$

where k is the rate constant, A is the frequency factor, e is the constant Euler's number and is the base of the natural logarithm, with value 2.718, E_a is the activation energy, R is the gas constant 8.314 J/(mol K), and T is the reaction temperature in degrees Kelvin. It must be noted that this equation is independent of reaction order and is a function only of T and E_a. By taking the natural log of equation number 3.1, linearizes to the form

y=mx+b and a linear relationship with a slope can potentially be plotted, and the equation becomes:

Equation 3.2 $$Lnk = LnA - \frac{E_a}{RT}$$

Where LnA is the natural log of the frequency factor, also known as the steric factor, encompasses the frequency of collisions and the atoms orientation.

III.2 Materials and Methods: See Chapter 2

III.3 Data and Observations:

The data in Table 3.1 is calculated from the XPS survey spectrum and the rate equations shown later in the chapter. Table 3.2 shows the calculated 2 standard deviation error values from all the data.

Table 3.1 Median values of the Natural Log of the Rate

Temperature (C)	1000/T (1000/K)	15 minutes	30 minutes	60 minutes	120 minutes
725	1.00	-15.95	-15.61	-15.45	-15.34
750	0.98	-15.83	-15.30	-15.26	-15.23
775	0.95	-15.42	-15.15	-15.15	-15.04
800	0.93	-15.41	-15.17	-15.18	-15.29
825	0.91	-15.46	-15.48	-15.31	-15.59
850	0.89	-15.70	-15.74	-15.67	-16.10

Table 3.2 2σ Error of the values from Table 3.1

Temperature (C)	1000/T (1000/K)	2σ 15’	2σ 30’	2σ 60’	2σ 120’
725	1.00	0.13	0.27	0.18	0.21
750	0.98	0.18	0.36	0.37	0.13

775	0.95	0.431	0.119	0.131	0.125
800	0.93	0.13	0.25	0.19	0.21
825	0.91	0.357	0.335	0.201	0.28
850	0.89	0.427	0.267	0.470	0.32

III.4 Results

In order to perform an accurate Arrhenius study of nitrogen incorporation into NCNT a number of things must be known. Ultimately, the nitrogen inclusion rate in moles per second must be calculated and, the mass of the product quantified. The product mass from each synthesis experiment was recorded and thermogravimetric analysis (TGA) performed to determine the mass of the iron. The mass recorded from the TGA reflects the mass of iron oxide so the mass of the oxide must be subtracted to yield the true mass of the iron in the NCNTs. Iron comprises ~70% of the mass of iron oxide so the calculation is straightforward. The sample was then characterized with XPS, where the atomic percent nitrogen and carbon are detected. Having subtracted the mass of the iron from the total product, the mass of the nitrogen in the total product can be calculated. The following equations start with the chemical equation of the inputs and outputs in our system and are followed by the rate calculation steps.

Equation 3.3 $C_5H_5N+C_{10}H_{10}Fe+NH_3 \rightarrow NCNT$

Equation 3.4 $Mass(total)-Mass(Fe)=Mass(N+C)$

Equation 3.5 $14.0067*at.\%N+12.01*at.\%C=P(total)$

Equation 3.6 $P(C)/P(total)=wt.\%C$

Equation 3.7 P(N)/P(total)=wt.%N

Equation 3.8 Mass(N+C)*wt%N=Mass(N)

Equation 3.9 Mass(N)/14.0067=moles(N)

Equation 3.10 Rate(N)=moles(N)/synthesis time(s)

Equation 3.11 Rate(N+C)= (moles (N)+moles (C))/synthesis time (s)

Taking the natural log of this trend in rate versus 1/T yields an Arrhenius plot. An Arrhenius plot yields a straight line for reactions with a single dominant rate limiting reaction pathway. The slope of this line corresponds to –Ea/R, from which one can estimate Ea, the reaction's energy of activation. The following Arrhenius plots shown in Figures 3.1 to 3.4, show all the data and straight line plots through the median values. Due to the small sample sizes, the 2σ bands, which reflect at least three replicates for each unique trial, encompass 95% of the possible synthesis outcomes. For ease of viewing the x-axis is labeled as 1000/T instead of 1/T in Kelvin. Please note that 725°C converts to 1.00 on the x-axis and is on the right side of the axis. The values in blue represent the temperatures 725-775°C and climb from right to left. Then, the red values represent the synthesis runs from 800-850°C and descend from right to left from the middle of the Figures. Figure 3.1 depicts the Arrhenius plot after 15 minutes of synthesis time for the rate constant of the nitrogen incorporation in the NCNT lattice. Note the two relatively small error bars at 800°C and 850°C, which suggest a strong possibility that the true variability at 825°C is probably not as large as its error bars indicate. This plot shows two distinct slopes, which indicates that there are two rate limiting processes that

dominate at different temperature ranges. Specifically, a low temperature process from 725°C to 775°C with a slope of -8.78 and a process that dominates at higher temperatures, from 800°C to 850°C, with a slope of 6.20.

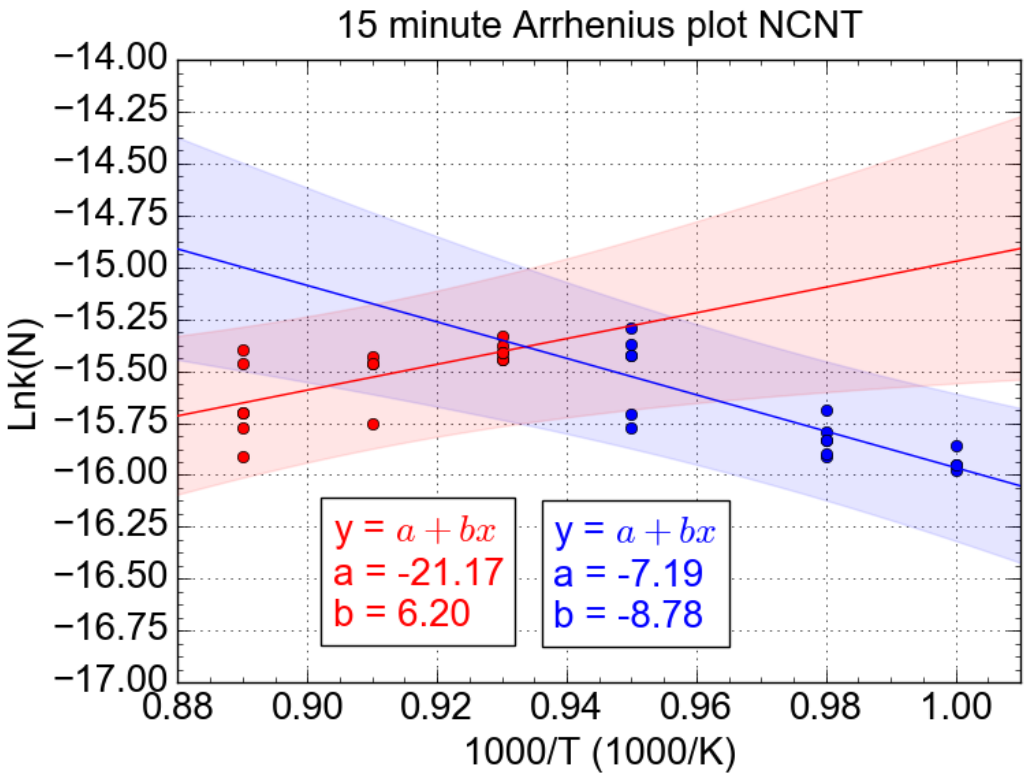

Figure 3.1 Arrhenius plot of the natural log of nitrogen rate of formation in NCNT at 15 minutes from 725°C to 850°C versus the inverse temperature, based on the data shown in the Appendix. The blue data points represent the Ln of the data collected between 725-775°C with an R^2 value of 0.91. The red data points represent the Ln of the data collected between 800-850°C with an R^2 value of 0.86.

As seen in Figure 3.2, the Arrhenius plot for a 30 minutes synthesis time shows a decrease in the magnitude of the slope to -8.80 from 725°C to 775°C. From 800°C to 850°C, the magnitude of the slope more than doubles the amount in Figure 3.1, to 13.25.

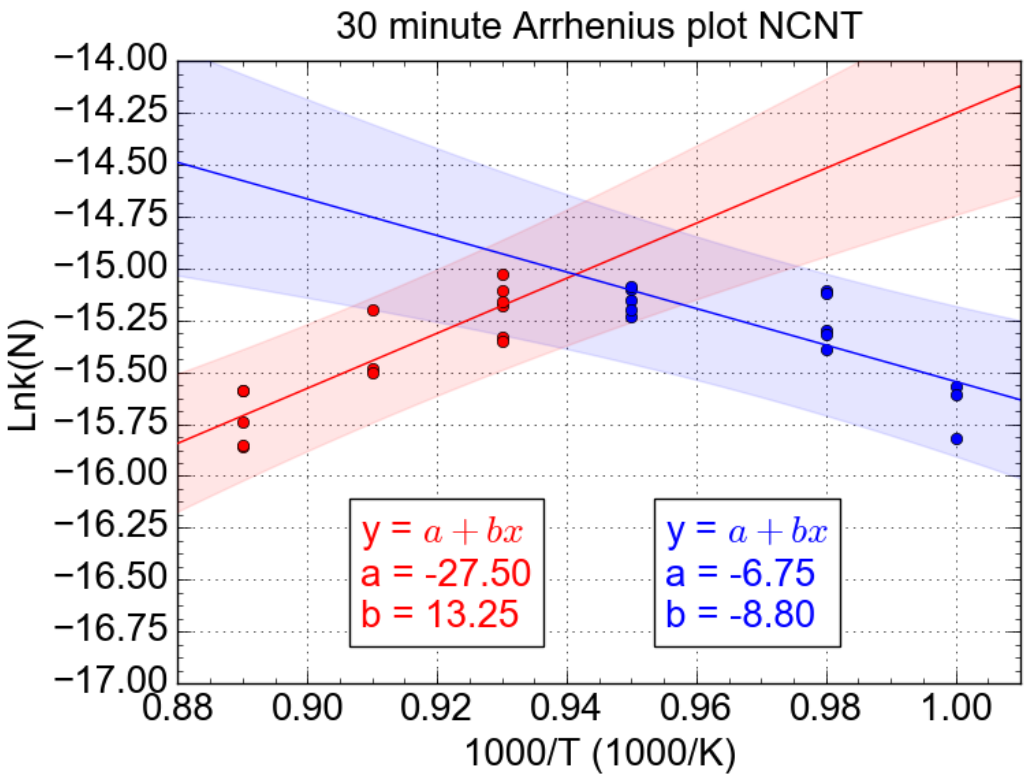

Figure 3.2 Arrhenius plot of the natural log of nitrogen rate of formation in NCNT at 30 minutes from 725°C to 850°C versus the inverse temperature, based on the data shown in the Appendix. The blue data points represent the Ln of the data collected between 725-775°C with an R^2 value of 0.97. The red data points represent the Ln of the data collected between 800-850°C with an R^2 value of 0.99.

Depicted in Figure 3.3 is the Arrhenius plot of the nitrogen incorporation rate after a 60 minute synthesis, shows a decrease in the magnitude of the slope to -4.63 from

725°C to 775°C. From 800°C to 850°C, the slope maintains a similar magnitude at 11.63.

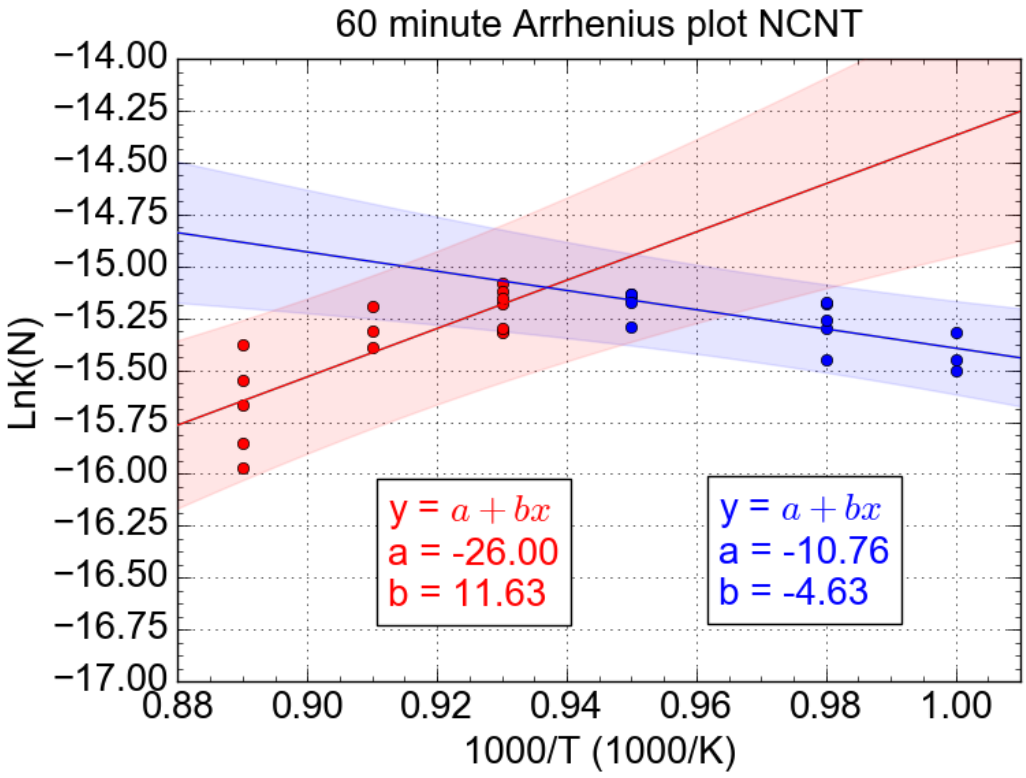

Figure 3.3 Arrhenius plot of the natural log of nitrogen rate of formation in NCNT at 60 minutes from 725°C to 850°C versus the inverse temperature, based on the data shown in the Appendix. The blue data points represent the Ln of the data collected between 725-775°C with an R^2 value of 0.99. The red data points represent the Ln of the data collected between 800-850°C with an R^2 value of 0.93.

The Arrhenius plot for a 120 minute synthesis, shown in Figure 3.4, has a slope of -7.72 from 725°C to 775°C. From 800°C to 850°C, the slope increases by nearly double to 17.25.

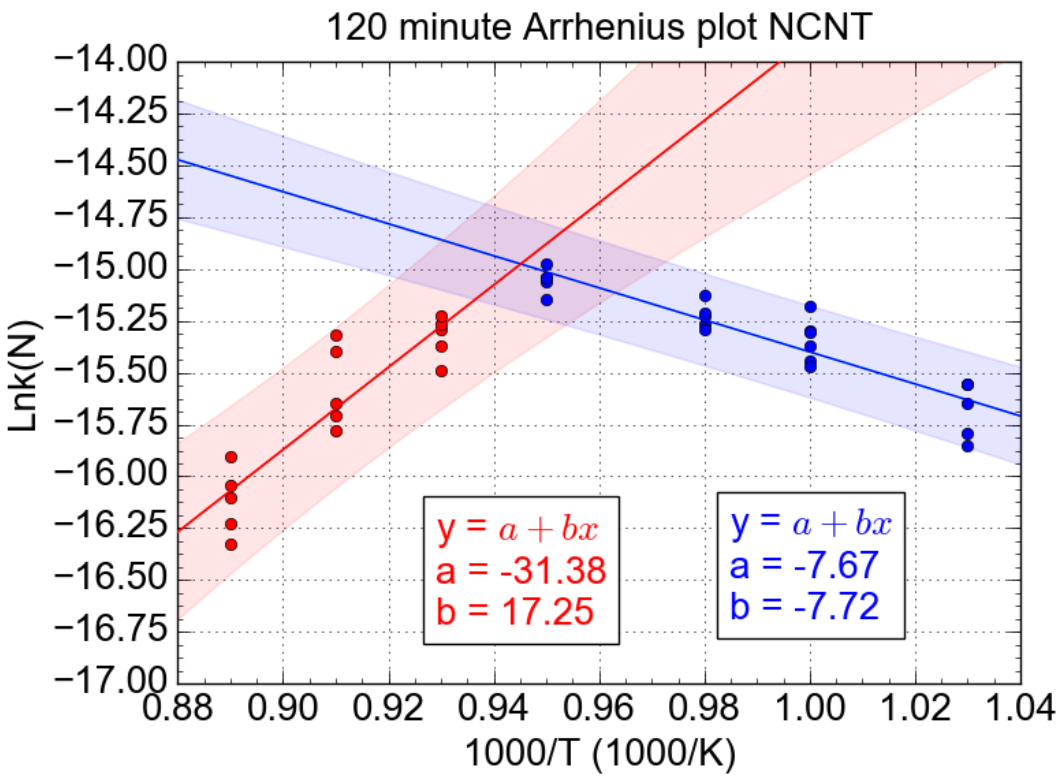

Figure 3.4 Arrhenius plot of the natural log of nitrogen rate of formation in NCNT at 120 minutes from 700°C to 850°C versus the inverse temperature, based on the data shown in the Appendix. The blue data points represent the Ln of the data collected between 700-775°C with an R^2 value of 0.98. The red data points represent 775-850°C with an R^2 value of 0.98.

A linear fit on an Arrhenius plot indicates a single rate limiting step dominates the reaction with the temperature range considered. In these Arrhenius plots, at all synthesis times, there are two different slopes, one positive and one negative. Two slopes of opposite sign suggest a significant dominant change in mechanism at elevated temperature. A negative slope suggests that the reaction is endothermic but after 800°C as the slope shifts to a positive value, the reaction is more complex and takes on a

significant exothermic component. Table 3.3 summarizes the differing slopes and linear correlation coefficients at the two temperature ranges for each time component.

Table 3.3 Arrhenius plot slopes and goodness of fit

Synthesis Time	725°C to 775°C	800°C to 850°C
15 minutes	y = -8.18x – 7.19 R^2 = 0.906	y = 6.20x - 21.17 R^2 = 0.856
30 minutes	y = -8.80x – 6.75 R^2 = 0.966	y = 13.25x – 27.50 R^2 = 0.999
60 minutes	y = -4.63x – 10.76 R^2 = 0.986	y = 11.63x - 26.00 R^2 = 0.928
120 minutes	y = -7.72x – 7.67 R^2 = 0.976	y = 17.25x – 31.38 R^2 = 0.976

The most important point to note from the rates calculated in the Arrhenius plots is that there are two, very clear, distinct regions in which the slopes are opposite and clearly point to the fact that a single mechanism cannot explain the full temperature synthesis range. At the lower temperatures from 725°C to 775°C, the rate does appear to have one mechanism of growth. However, at the upper temperatures from 800°C to 850°C, while the data suggest linear behavior, the positive slope means that a single rate

limiting process cannot explain the rate. The rate of nitrogen incorporation in NCNTs at the higher temperature regime is more complex.

III.5 Discussion

When plotting the Arrhenius equation, it takes the form of y=mx+b, where y is equivalent to the natural log (Ln) of the rate constant k, m is the slope of the line and is equivalent to $-E_a/R$.

The activation energies calculated from the slope are shown in Table 3.4

Table 3.4 Activation energies at different temperature ranges

		15 minutes	30 minutes	60 minutes	120 minutes
E_a725-775°C	eV	0.95	0.84	0.54	0.53
E_a800-850°C	eV	-0.59	-1.19	-1.02	-1.68

The activation energy E_a for the incorporation of nitrogen in to the NCNT lattice from 725-775°C after 15 minutes requires 0.95 eV of energy in the presence of the iron catalyst. After 30 minutes, the E_a drops to 0.84 eV and levels off after 60 minutes to 0.54, and 0.53 eV after 120 minutes. This suggested trend towards lower activation energy suggests that initially there is a larger barrier to nitrogen incorporation and over time that barrier drops making it easier to insert more nitrogen atoms in the lattice. This drop in barrier is likely from the interaction of NH_3 with the side walls of the NCNTs and doping occurring at defect sites. In the temperature range of 800-850°C, the observed activation energies are negative. This information suggests that a second, competing

mechanism is hampering the rate of nitrogen inclusion into the CNT lattice. This is possible if the rate is in the form of $k_{total}=k_1/k_{2,}$ where k1 and k2 are rates at different temperatures, normally low to high temperature, and both rate constants fit an Arrhenius form yielding a result that is proportional to $e^{-(E1-E2)/RT}$. For all practical purposes the apparent activation energies in the higher temperature range are not real but give us important information about the difference in how much nitrogen could have been in the lattice if the trend had continued from the lower temperature regime versus what has really happened to the rate of inclusion. Now, if we assume the rate of nitrogen entering the lattice remains a constant proportional to the original k_1 from 725-775°C, in the higher temperature range, then one could infer that the reason for the negative slope in activation energy is due to nitrogen atoms leaving the NCNT lattice at a significant rate. This would be an exothermic event because the NCNT would actually be losing atoms from gasification while gaining atoms from growth.

When taking into account the full information of mass, atomic concentration of nitrogen, and the growth rates, it is apparent that there are two distinct temperature regions of interest. At low temperatures, i.e., <775°C, the observed growth rate is governed by a single rate limiting step. At the higher temperature regime >800°C, there is another rate limiting process that dominates the observed rate. However, it is a convolution of an endothermic growth process expected from the linear extension of the lower temperature process and an exothermic mass loss component. These results support the original predictions from chapter 2 for the low temperature regime and refute these predictions for syntheses at and above 800°C.

III.6 Conclusions

Why does the rate turn to a loss mechanism in the Arrhenius plot? The previous results in the high temperature regime do not support the predictions proposed at the end of chapter 2. Something dramatically different is happening to the growth rate at higher temperatures. Based on these results we now hypothesize the following new understanding for this growth process at high temperatures.

Hypothesis 4: De-doping of nitrogen occurs at high temperature and is the competing mechanism that causes the decreasing rate change.

Prediction 4.1: If nitrogen dedoping is occurring at the higher reaction temperatures, then XPS analysis will show a loss of nitrogen with time at the highest synthesis temperatures.

Prediction 4.2: Additionally, the loss of nitrogen should be observed by a post synthesis heat treatment of reaction products from a lower temperature synthesis.

CHAPTER IV

KINETICS AND DEDOPING OF NCNTS

IV.1 Introduction

Little is known about the rate of nitrogen doping in a pure NH_3 atmosphere into the carbon lattice of the NCNT. In this work, we report a significant drop in NCNT-bound nitrogen for NCNT syntheses temperatures above 800°C. This observation, agrees with Koos et al.[61] who suggests the liberation of nitrogen from the lattice at high temperature. The paper reports using benzylamine to synthesize NCNTs, but under an argon atmosphere. Koos et al. observe significantly lower %N incorporation than we find for syntheses under an NH_3 atmosphere. Also, that work provides little insight into the dedoping mechanism or kinetics. Fujimoto and Saito report a density functional theory calculation on a 10,0 CNT with different nitrogen site bonds and vacancies[62]. They found that when a vacancy was present, pyridinic nitrogen was the preferred bonding configuration. Further, their calculations suggested that the trimer pyridinic-N plus di-vacancy was the most stable form of the pyridinic-N species in the case of the 10,0 CNT. Their simulations estimated the $C_{76}N_3$ trimerized pyridinic energy of formation to be 2.16 eV, while the $C_{79}N$ graphitic nitrogen configuration was found to have a significantly higher energy of formation of 7.02 eV. Ultimately, it was found that as vacancies formed, there was a much greater probability for the N-dopant to bond

preferentially at a vacancy in the immediate vicinity of the pyridinic site. Based on our previously reported Arrhenius studies, we propose that above 800°C there is a second mechanism that becomes dominant that will be referred to as de-doping. At 825°C and 850°C, this loss in atomic percent nitrogen is dramatic. At 800°C, while the effects of de-doping are seen, it is nearly in balance with the rate of inclusion as is evidenced by the product retaining a high atomic percent nitrogen concentration but showing a reduction in mass as compared to 775°C. This point of turnover is denoted on the Arrhenius plots of nitrogen inclusion as the point where the two opposing slopes intersect.

IV.2 Materials

Materials used in addition to the set of materials listed in Chapter 2 are as follows:

NCNTs synthesized at 775°C with a high nitrogen content

TGA pan

99.999% Ultra high purity argon

IV.3 Equipment

Equipment used in addition to the set of items listed in Chapter 2 are as follows:

TA Thermogravimetric Analyzer

Thermo Scientific Escalab XPS

IV.4 Methods

I developed a method to estimate the rate of atomic nitrogen lost at high temperature to gain insight into why the nitrogen concentration rate declines at high temperature. A sample that was previously synthesized, with 10-11 at.% nitrogen doping, was weighed in TGA under ultra-high purity argon gas at 140°C after a 10 minute gas purge from the sample cell. Then, the sample was loaded in a 2" quartz tube on a quartz slide in the TGA pan. End caps were put on both ends and ultra-high purity helium gas was allowed to flow for 15 minutes to purge all oxygen from the tube. During this time period, the furnace was brought up to the selected reaction temperature. The following temperatures were used in this study to determine the rate of de-doping; 700°C, 750°C, 775°C, 800°C, and 850°C. The tube was then loaded in the furnace. Typically, it takes about one minute for the temperature in the tube to stabilize. At this point the timer was started. I examined de-doping times of 15, 30, 60, 120, and 180 minutes in triplicate at each temperature. At the conclusion of each de-doping time period, the tube was removed from the furnace and placed in a tube holder to quickly cool in air so as to quench the de-doping. After 10 minutes, the tube was sufficiently cooled to remove the end caps and harvest the material from the furnace. Once the sample was retrieved, it was again loaded in the TGA and weighed again at 140°C after a gas purge, which ensured that the material was free from adsorbed oxygen or moisture. Upon completion of the de-doping, XPS analysis was performed on all samples.

IV.5 Data and Observations

From the original synthesis runs, a drop in yield and concentration of nitrogen above 800°C suggested that a second rate limiting step dominated the reaction rate at high temperature. This theory was further confirmed after performing a temperature evolution study at 725°C, 750°C, 775°C, 800°C, 825°C, and 850°C. As seen in Figure 4.1, for a run at 850°C, suggests that there is a fast drop in atomic % nitrogen in the first 15 minutes. After this point, the nitrogen de-doping rate slows significantly.

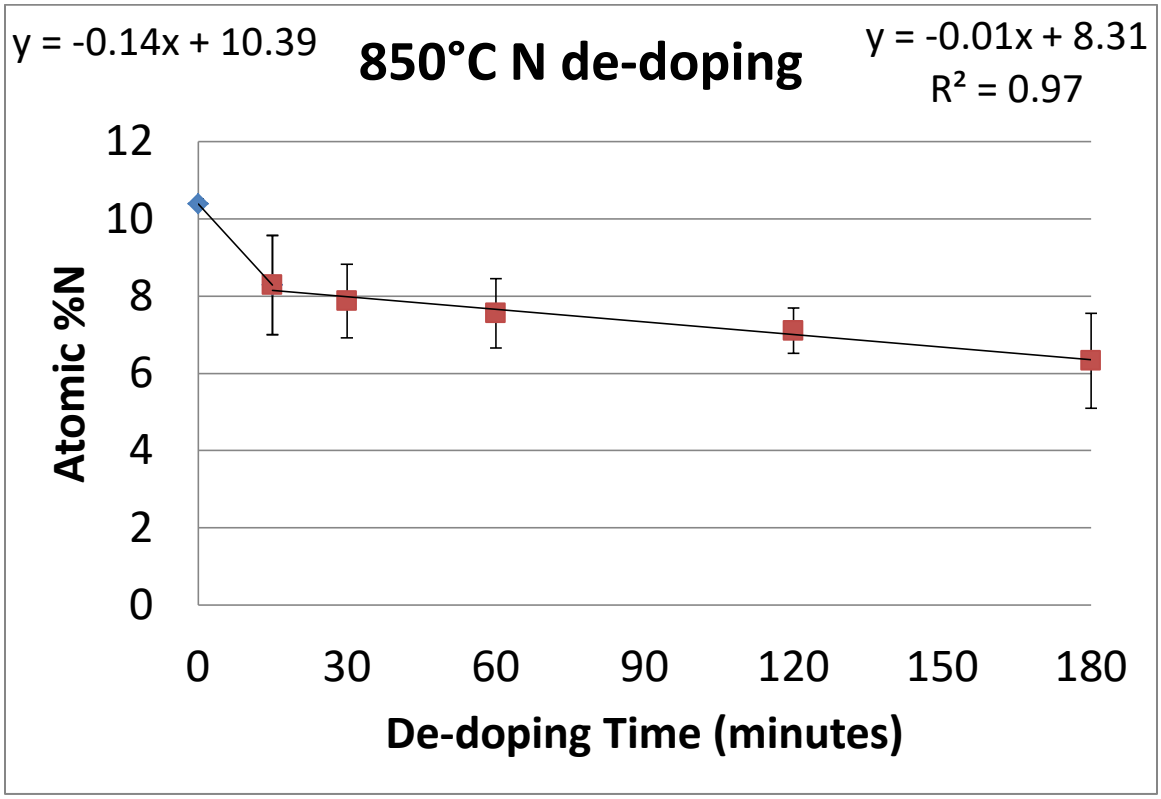

Figure 4.1 Nitrogen de-doping of NCNTs at 850°C as a function of time at temperature, which shows the median values with 2σ error and, an initial high rate of loss and then a steady much slower de-doping rate after 15 minutes.

At 850°C, 2.1 atomic percent nitrogen (±2σ=1.28) is lost in the first 15 minutes, and a little over 4 atomic percent nitrogen (±2σ=1.23) is lost after 180 minutes. The 2

standard deviations in all this data are due to very small sample sizes. For each experiment, 10 mg of sample was all that would fit into the TGA pan. This constraint led to higher statistical uncertainty. However, the reproducibility of these observations suggest that the qualitative trends are significant. In contrast to this high temperature de-doping process, at 700°C a significantly slower rate of de-doping is observed. In the first 15 minutes, only 0.18 atomic percent nitrogen ($\pm 2\sigma = 0.57$) is lost. In total, after 180 minutes only 1.37 atomic percent nitrogen ($\pm 2\sigma = 1.39$) is liberated from the NCNT lattice as seen in Figure 4.2. This result is interesting in that there is significant de-doping at high temperature and that rate appears to be higher in the first few minutes of the trial. It appears there are two different rates in the lower temperature regime as well, just much slower.

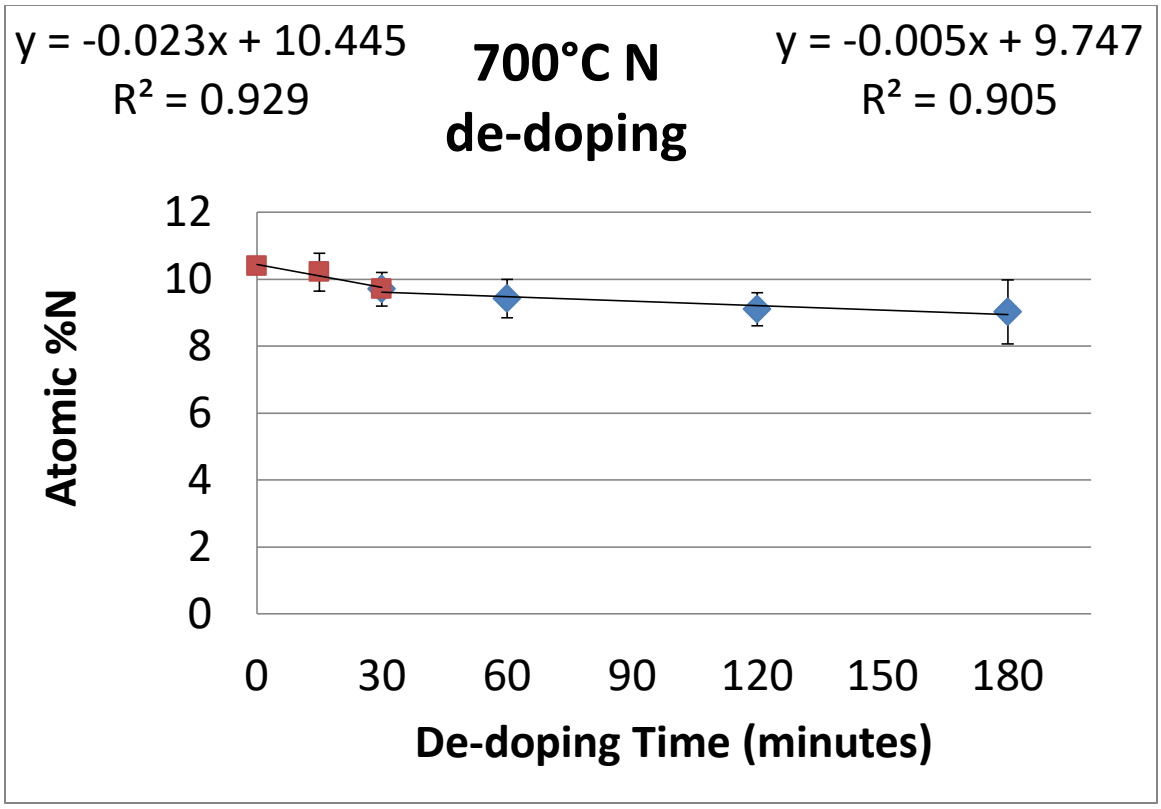

Figure 4.2 De-doping study over time at 700°C showing a slow rate of nitrogen loss from the CNT lattice. Data shown are median values with 2σ error bars.

This finding confirms that there is a competing de-doping reaction at high reaction temperature that becomes the dominant rate limiting step at some time in the NCNT synthesis. This de-doping mechanism dominates when the observed growth rate slows and eventually stops.

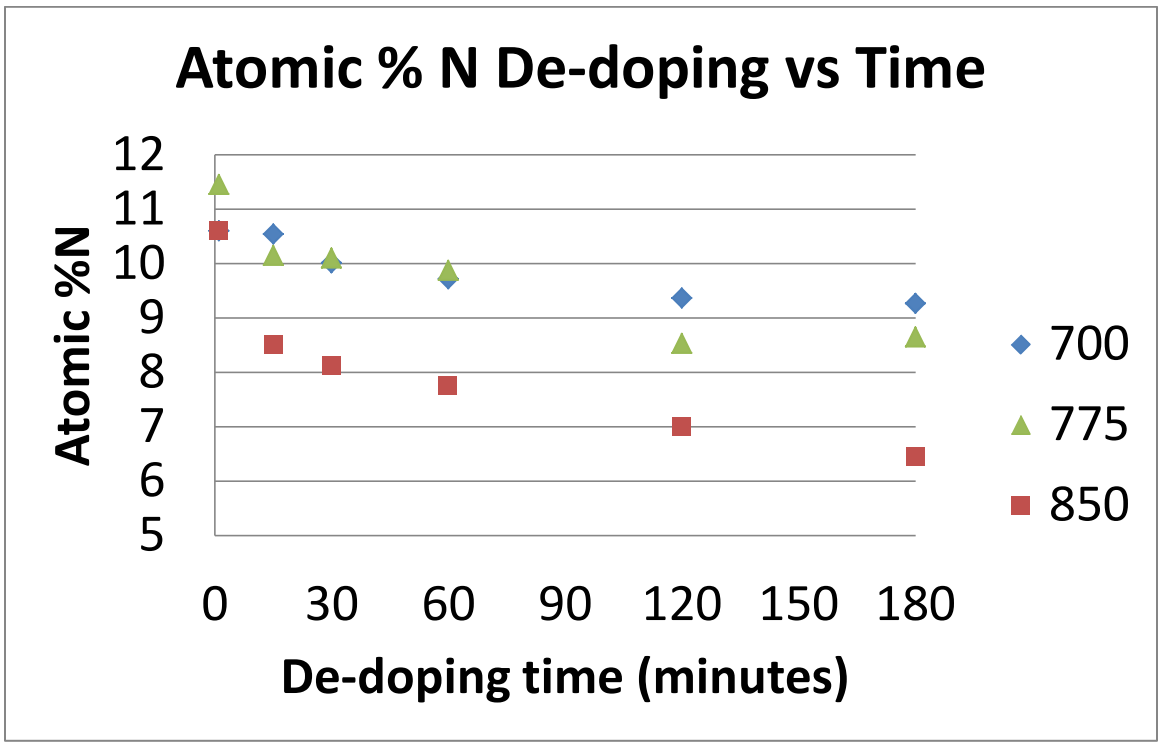

Figure 4.3 De-doping study with three temperatures showing the median values.

The data shown in Figure 4.3 demonstrate that the rate of de-doping is temperature dependent and that at 775°C there is not as significant a rate of loss as at 850°C. The only disadvantage of viewing the data in this way is that the starting concentration for the 775°C sample was 11.45% nitrogen, while the other two samples had a starting concentration of 10.6%. Perhaps, a better way to compare the rates of loss would be to compare the normalized loss of nitrogen, or the ratio of N/N_0, where N_0 is the starting concentration as seen in Figure 4.4.

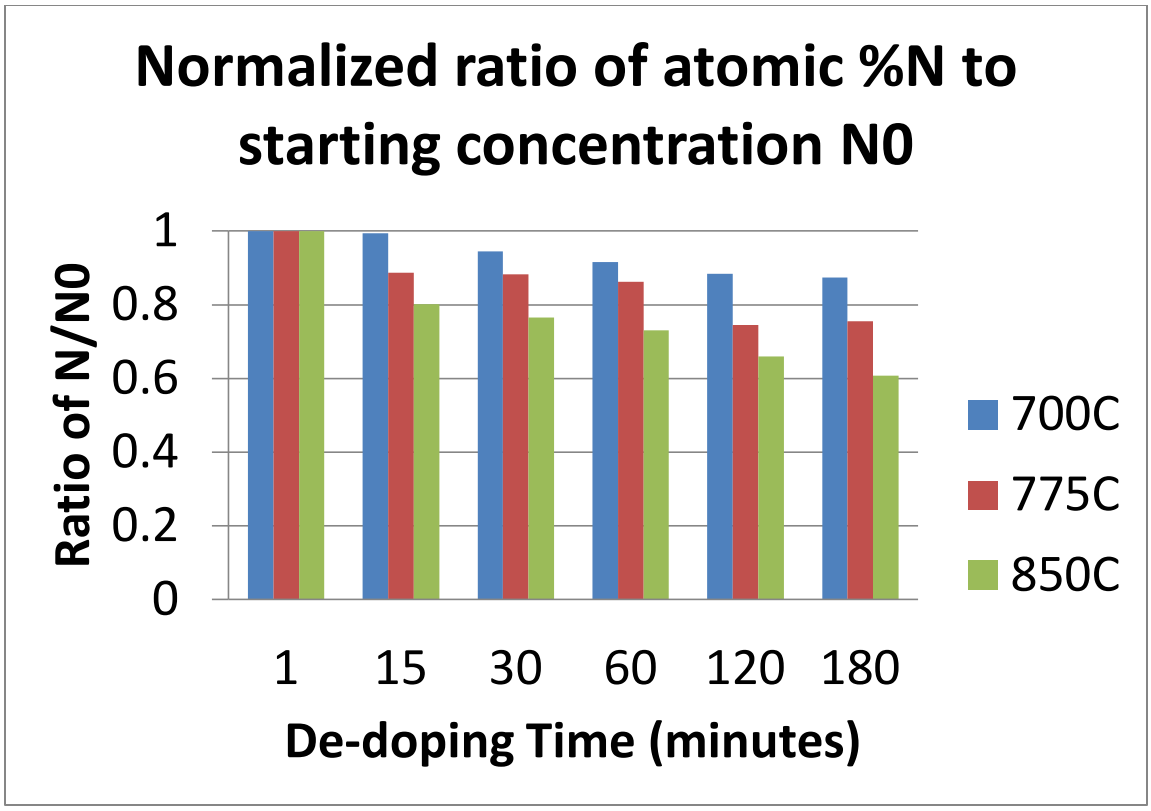

Figure 4.4 De-doping study showing the ratio of nitrogen to the initial concentration based off median values

At 700°C, the rate of nitrogen lost from the lattice of the NCNT is very slow and after 15 minutes the sample has only lost roughly 1%. After 30', 60', 120', and 180', the relative loss of nitrogen climbs to 5%, 8%, 12%, and 13%, respectively. At 775°C, the sample loses ~11% in the first 15 minutes but that rate slows significantly thereafter. After 30', 60', 180', the sample loses 12%, 14%, and 26%, of its nitrogen respectively, which is twice that observed at 700°C. At 850°C, the initial rate of nitrogen lost is significant, at 20% after just 15 minutes. After 30', 60', 120', and 180', the nitrogen loss climbs to 23%, 26%, 34%, and 39%, respectively.

Hypothesis 5: Since we observe a loss of nitrogen at high reaction temperature, we should be able to identify with XPS, which specific type of nitrogen is lost from the NCNT matrix. The nitrogen species lost from gasification should primarily be pyridinic because of its lower binding energy, relative to the other types of nitrogen in the NCNTs. Local vacancies associated with the bond are shown in Chapter 1, Figure 1.1 B.

Prediction 5.1: At the higher reaction temperatures, we expect that XPS measurements will show a greater stability for graphitic nitrogen by revealing less graphitic nitrogen mass loss as compared to pyridinic species. We think this that graphitic nitrogen's direct substitution into the lattice makes it inherently more stable, than pyridinic nitrogen, which is associated with vacancies.

While performing de-doping studies and observing increasing rates of loss of nitrogen from the NCNT lattice with increasing temperature and time, I considered the possibility of detecting a specific nitrogen loss mechanism, i.e., pyridinic, pyrrolic, graphitic, etc. While conceptually clear, these studies would be difficult to perform, as the measured weight changes would be based on the differences of small masses with significant uncertainties. When viewing the reported data, one must understand that when calculating the percentages of the different species, all amounts will have to add up to 100%. So then, the reported amounts are relative and there could be an observed increase over time. This actually means that there are other species that were lost at a higher rate making the relative percent of a given species increase as can be seen in Figure 4.5, with the graphitic-N species.

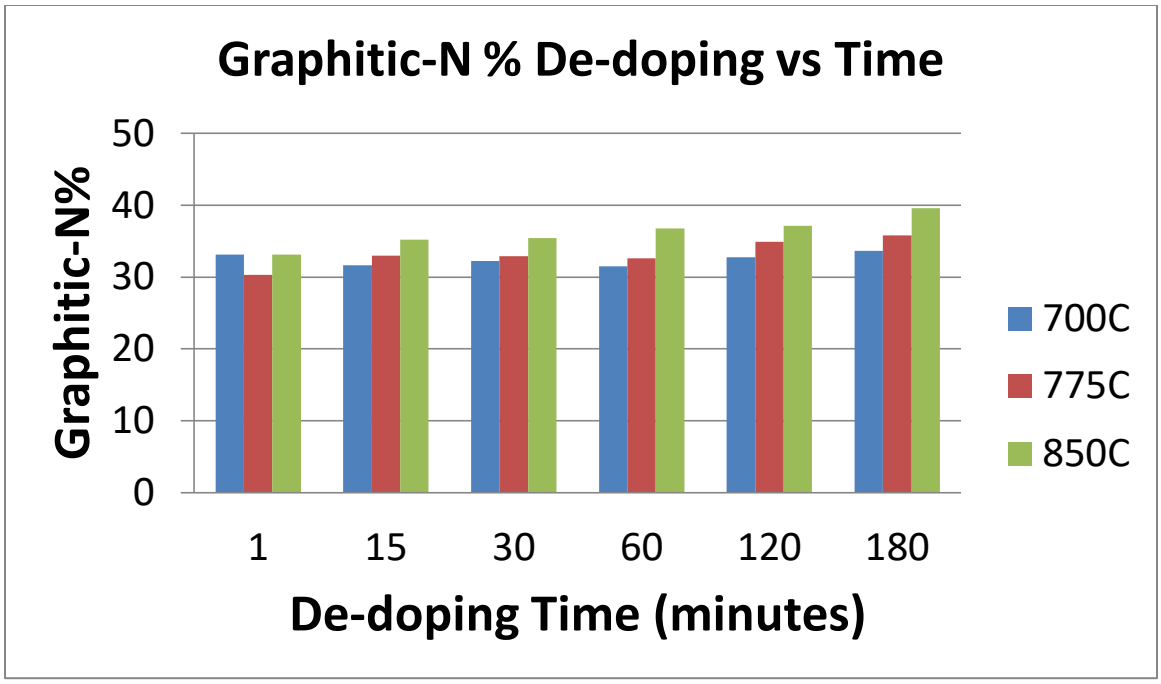

Figure 4.5 XPS of the Graphitic-N relative % over time based off median values.

At 700°C, 775°C, & 850°C, after 180', there is 1.5%, ~5%, and ~ 6.5%, deviation from the relative starting percentage of Graphitic-N, respectively. By looking at each species more knowledge can be garnered about the relative selectivity in the sequence of nitrogen de-doped and, which species may selectively de-dope first. After XPS N1s spectra were acquired, we observe a relative drop in Pyridinic-N from 46% to 41% while the relative Graphitic-N increases from 30% to 39% as seen in Figure 4.6. This data suggests that the pyridinic species is less stable and the first to gasify in the de-doping step.

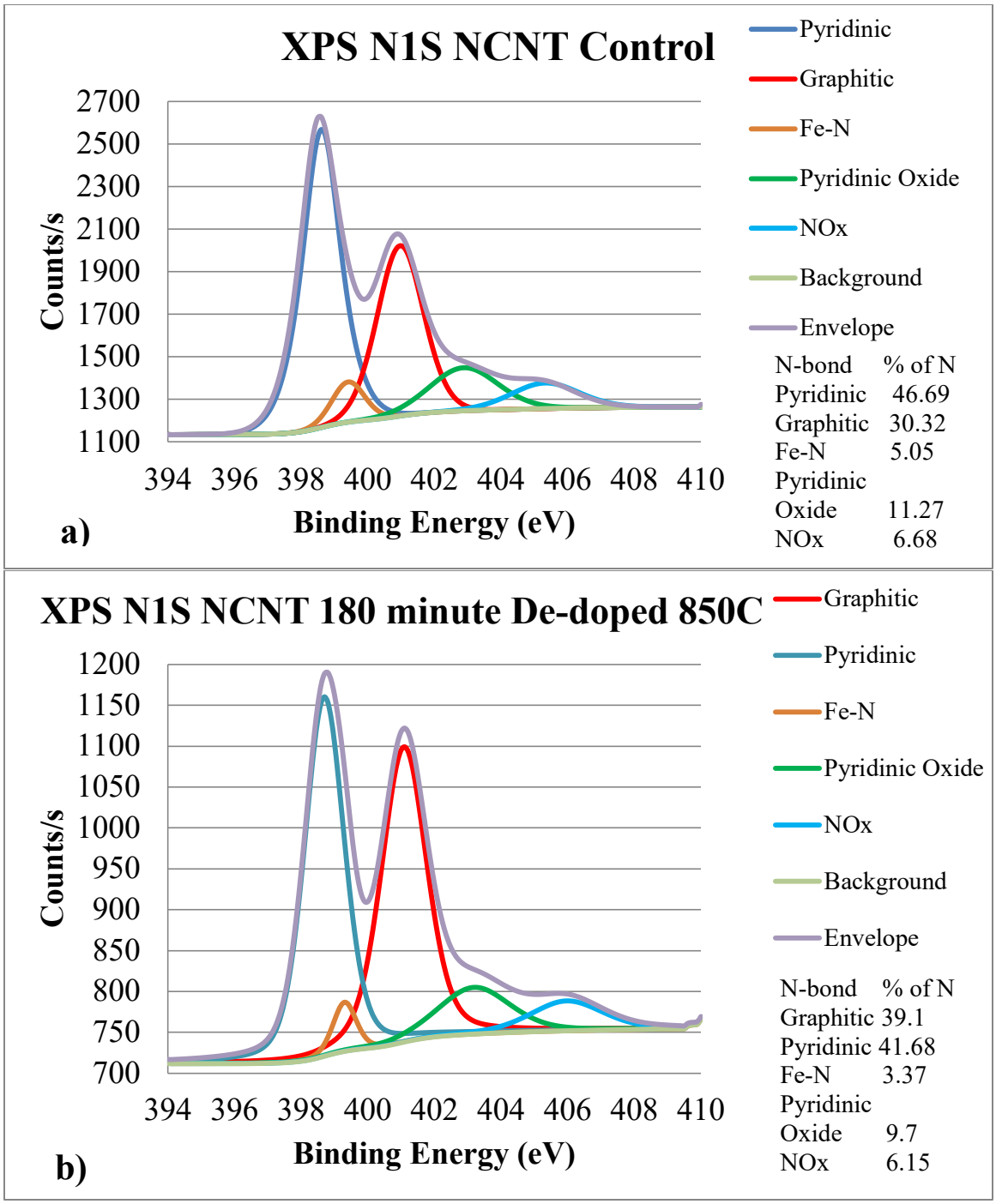

Figure 4.6 XPS of the N1s of the NCNT a) before (top) and b) after (bottom) de-doping

The most dominant species in all of our syntheses in a pure NH_3 environment is Pyridinic-N and its rate of change can be seen in Figure 4.7.

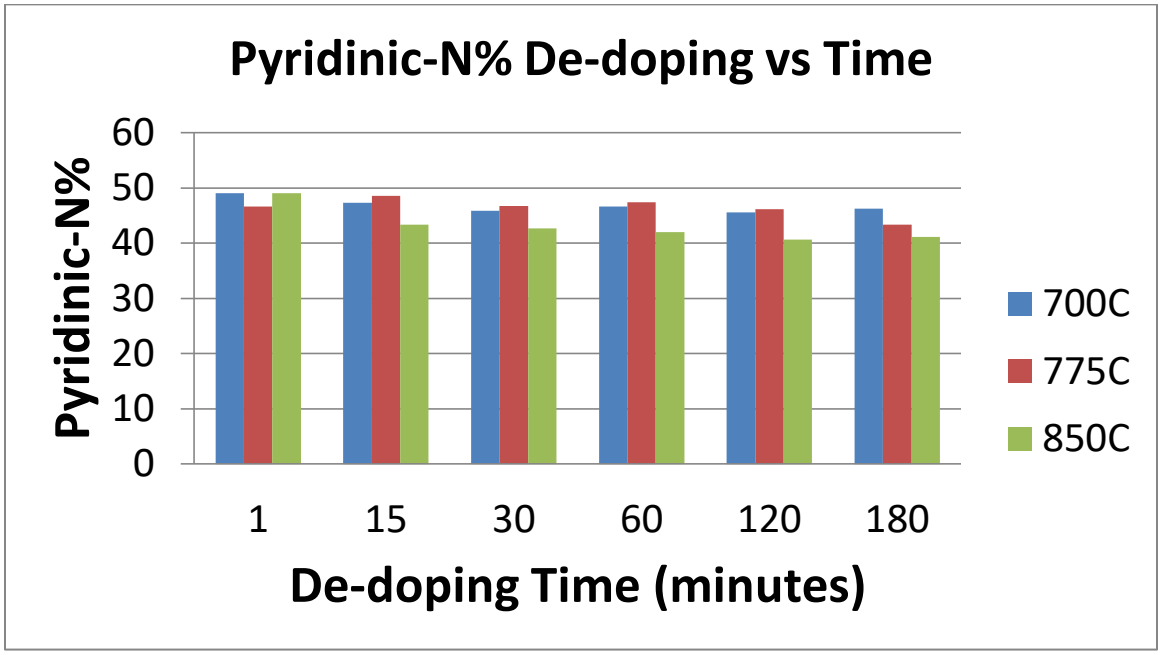

Figure 4.7 XPS of the Pyridinic-N relative % over time based of median values.

At 700°C, the relative % Pyridinic-N lost is ~2.7% after 180 minutes, at 775°C, ~3.3%, at 850°C, ~8%. For the Fe-N species, the Pyridinic-N plus vacancies allow for a Fe-N_x bonding, as seen in Figure 1.5, where x can equal 1, 2, 3, or 4. The changes in the Fe-N species over time can be seen in Figure 4.8.

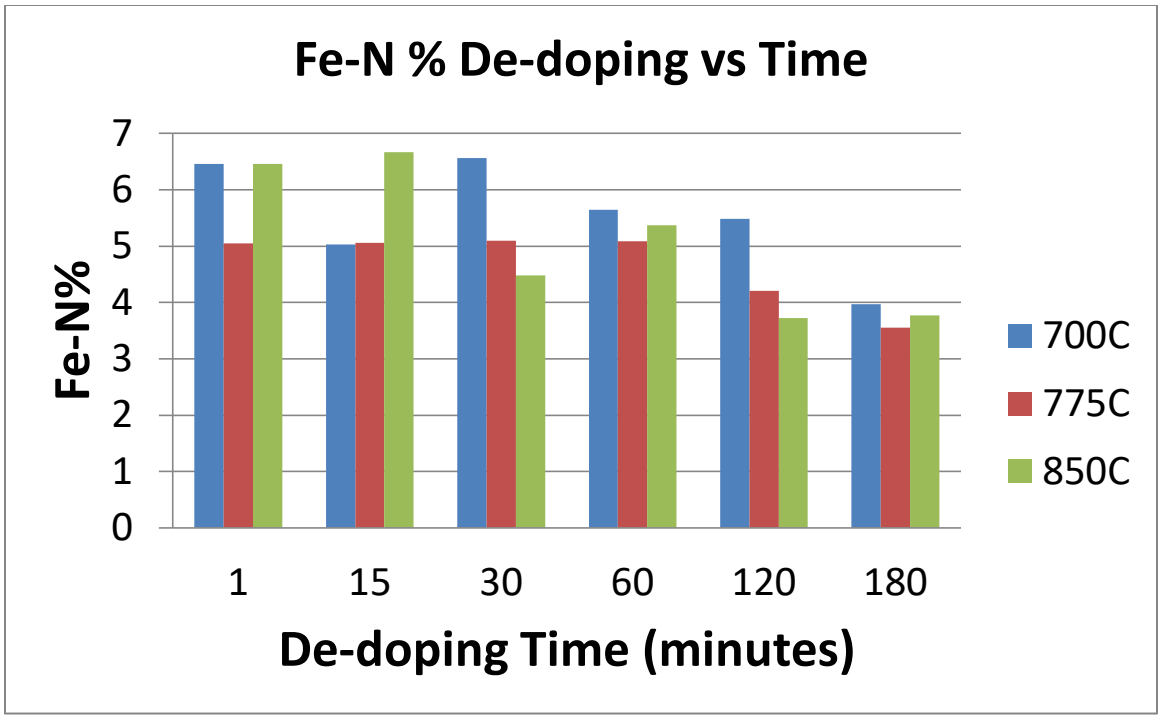

Figure 4.8 XPS of the Fe-N species relative % change over time based off medians.

At 700°C, a relative loss of ~2.5% of the Fe-N species occurs after 180 minutes. It is worth noting that after 15 minutes the relative percent drop is nearly 1.5% then after 30 minutes the relative percent returns to the starting level, and declines at a steady rate thereafter. This finding is not surprising as the relative percentages could fluctuate with respect to each other, as all are dependent. At 775°C, the relative % of Fe-N does not significantly change for the first 60 minutes. Then after 120 and 180 minutes, the relative % drop is ~1% and ~1.5% respectively. At 850°C, the relative % of Fe-N goes unchanged after 15 minutes, and a relative 2% drop after 30 minutes, with a total loss of ~3% of the Fe-N species after 180 minutes. It is worth noting that at all temperatures, the relative loss of the Fe-N species comprises 30-40% of the total starting Fe-N concentration.

There are three species that comprise the Pyridinic structure, the Fe-N species, the Pyridinic-N, and the Pyridinic Oxide, which is a Pyridinic-N with a vacancy that picks up an oxygen bond from the air after the material is harvested and exposed to oxygen in the air. It may be of value to look at the changes of these three species as a whole since the observation shows a loss of pyridinic species in previous Figures. All three species of pyridinic nitrogen can be seen in Figure 4.9.

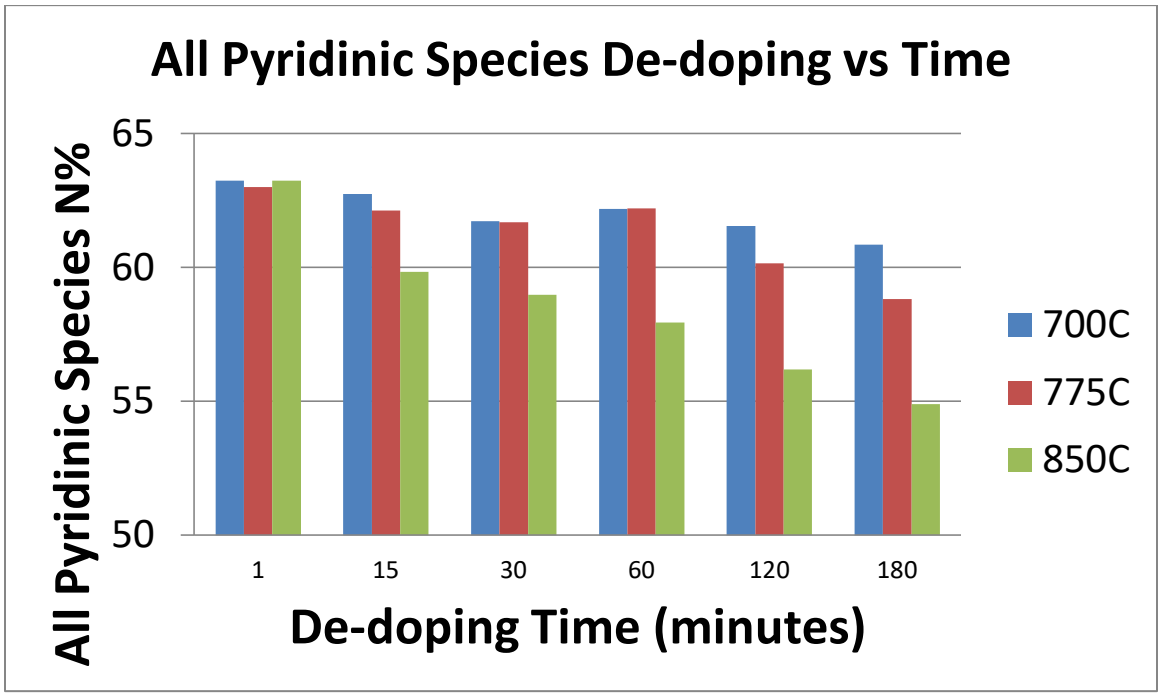

Figure 4.9 XPS of all three Pyridinic species (Pyr-N,Fe-N,Pyr-Ox) relative % change over time based of median values.

At 700°C, the relative % lost for all pyridinic species was ~2.5% after 180 minutes, at775°C, ~4.2%, at 850°C, ~8.5%. But more importantly after just 15 minutes, the lower temperatures lost less than 1% while at the highest temperature the % lost in those first 15 minutes is 3.5% which is significant. For completeness, as seen in Figure

4.10, please note that the Fe-N and Pyridinic-N species without the Pyridinic Oxide, as the binding energy for the Pyridinic Oxide is 4-6eV higher.

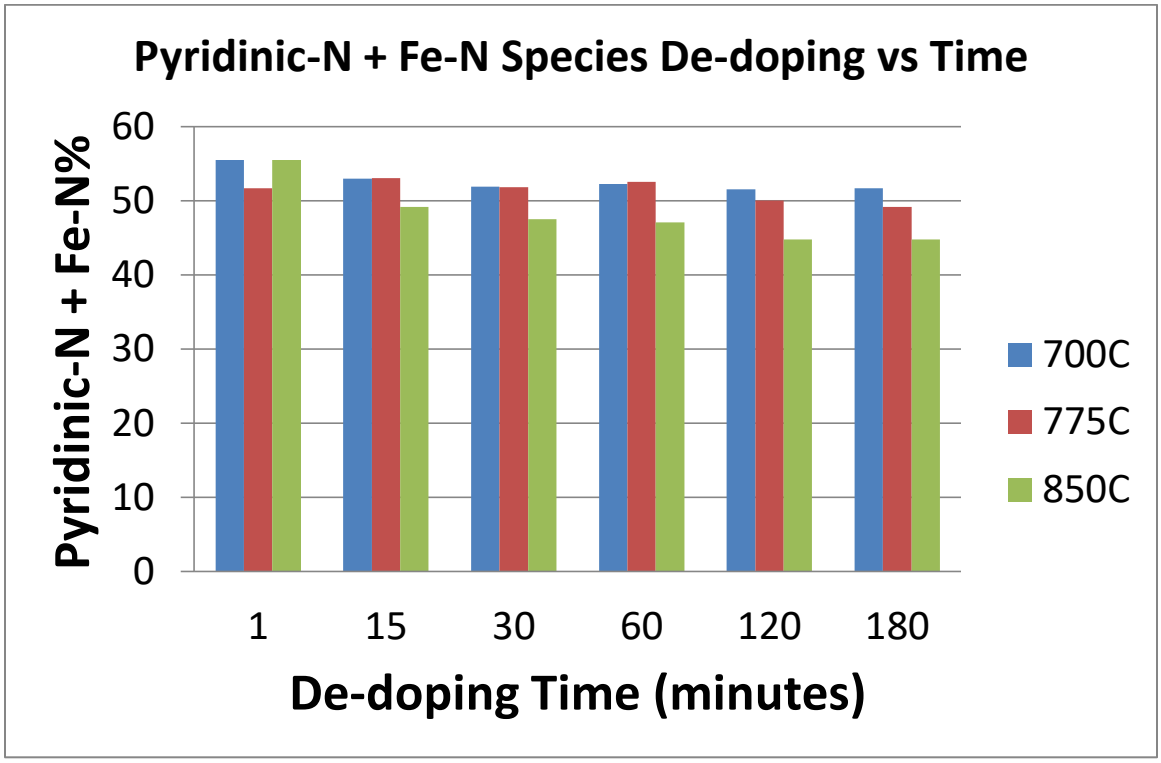

Figure 4.10 XPS of the relative % change over time of the Pyridinic-N + Fe-N species.

At 700°C, the total relative % lost is ~3.7% after 180 minutes, at 775°C, ~2.5%, and at 850°C, ~10.7%. It is noteworthy that at this high temperature ~6.3% is lost in the first 15 minutes. This information tells us that the Pyridinic-N and Fe-N species appear to lose a significant fraction of nitrogen in the first 15 minutes and over the total 180 minutes. This means that after 15 minutes, there is a relative increase of the Pyridinic Oxide. This observation suggests that while the Fe-N and Pyridinic-N drop, it is entirely

possible that some of them converted to pyridinic oxide upon exposure to oxygen in the air after the de-doping was complete.

IV.6 Discussion

The data and observations presented in the previous section support the hypothesis that de-doping happens at high temperature, i.e., above 800°C. Hypothesis 5 stated that we could confirm with XPS which nitrogen bond is more stable and which de-dopes first. The data provides support for this hypothesis. The initial apparent fast rate of de-doping at 850°C is consistent with nitrogen atoms from the surface being liberated in the gas stream. After 15 minutes the rate slows down quite a bit and this is likely due to the remaining surface nitrogen atoms being more stable and the nitrogen atoms lost now are coming from inner walls and have to diffuse out of the tube wall, thereby slowing the rate of de-doping.

Initially, this experiment was attempted in the TGA. Gas impurities and air backstreaming from the exhaust or other valves contributed to significant noise and signal variability in the curves. A series of bubblers and positive pressure systems were also tried to reduce variability with no success. Ideally these studies would be performed in a vacuum TGA system, but we did not have access to this equipment, which would provide valuable information in a future experiment. From 700° C to 775° C the dominant mechanism is nitrogen doping as there is an increased percentage of nitrogen incorporation into the CNT lattice. The results at 800°C indicate similar atomic concentrations of nitrogen to 775°C, but the mass yields are less and suggest that the second mechanism is starting to have a competing effect. However at 825° C and at 850°

C a second mechanism dominates. At high temperature it becomes clear that there are two causes for competing reactions, doping and de-doping mechanisms. While the de-doping study was carried out to 180 minutes, for the purpose of this work, no NCNT synthesis lasted longer than 120 minutes. The de-doping study was performed under a helium atmosphere. When the study was attempted under an ammonia atmosphere, the reactivity of ammonia at elevated temperatures completely consumed the starting NCNT material. When considering the rate of nitrogen loss, since the current study is not feeding a source of nitrogen or carbon, the rate of loss is likely higher than in the normal synthesis conditions. However, the finding that a pure ammonia environment in de-doping completely consumes the NCNTs over time suggests that there is a highly reactive nature to the ammonia atmosphere and an optimal reaction condition for nitrogen incorporation. In practice, it is most likely that in the synthesis experiment, as time is progresses, and with an excess supply of iron, nitrogen, and carbon, that there is a give and take of doping and de-doping that is always in competition with each other. Doping likely proceeds through two routes, the first directly through the catalytic reaction over and through the catalyst particle as the carbonaceous and nitrogenous species, including the breakdown of ammonia to its different radical states, and polymerizes to form the NCNTs. The second route likely proceeds via the free nitrogen radicals and the reactivity of ammonia gas with the sidewalls of the NCNT. The sidewalls provide a scaffold where more defects can either be created or the current defects can be vapor doped from the free nitrogen radicals. The initial rate of loss is important as well, as it gives a clue as to the instantaneous and initial de-doping state.

The XPS data of the N1s peaks for the nitrogen loss in the de-doping study show that at low temperatures very little nitrogen is lost, and only 1% lost in the first 15 minutes. At the highest temperature 850°C, there is significant atomic % nitrogen lost from the lattice on the order of 40%, losing 20% in the first 15 minutes. The data suggest that at high temperatures, there is a clear initial rate of loss, followed by a second and slower rate of loss. This observation of a two rate loss mechanism suggests that initially there is a quick loss of nitrogen atoms from the outer surface of the NCNT. The second slower rate may be a diffusion limited loss mechanism from the inner walls of the NCNT. These initial rates of loss are most important because they are an indication of the initial rate loss mechanism, when the NCNT is in its fully doped state and most vulnerable for nitrogen exchange in the NCNT lattice. Further, the data shows that the primary nitrogen bond lost in the de-doping step is of one of the pyridinic species as seen in the N1s spectra from XPS. The data also suggest that graphitic nitrogen is likely more stable as we saw their relative percentages rise. These results support our previous hypotheses.

We believe the nitrogen is lost through gasification of the nitrogen atoms leaving the NCNT lattice. We wondered whether nitrogen vaporizes with amorphous carbon. The observed 40% nitrogen loss confirms that while some small percent could be lost with amorphous carbon and likely is, there is far too much nitrogen lost at the highest temperatures to suggest this could be the only way it is lost. Alternatively, interstitial nitrogen gas trapped in between the walls of the NCNT might diffuse out of the system. If this were the case, the NCNTs would surely de-dope over time just by diffusion, which has yet to be observed. Further, the initial 15 minute de-doping study at 700°C showed

no nitrogen loss, which suggests there is no interstitial nitrogen. One must also consider that the de-doping study was performed under a He atmosphere instead of the NH_3 atmosphere of synthesis. The de-doping study does not work in a pure NH_3 atmosphere of the synthesis. The de-doping study was not conducted in a pure NH_3 atmosphere because the NH_3 is very reactive and it would consume the NCNTs in a short period of time. During synthesis, there is a constant feed rate of the nitrocarbon precursor so there is always fresh carbon to react and keep the NCNTs growing. This means that the actual mechanism of nitrogen lost could be slightly different than what we observe from the He atmosphere de-doping study, which warrants consideration in a future study.

IV.7 Conclusions

The results presented here demonstrate that at temperatures above 800°C, a significant atomic percent of nitrogen is lost via gasification in the first few minutes. This process is then followed by a second slower diffusion limited loss mechanism. Further, the species of nitrogen lost in this initial step at high temperature is pyridinic. At lower temperatures no significant rate of loss is observed in the initial 15 minutes. The second diffusion limited rate is much slower than the initial rate and this is understandable if the easy nitrogen loss from the surface happens first and then the next nitrogen atoms to gas off would come from the inner layer of the NCNT. Another consequence of the first rate being fast and the data pointing to a relative increase in the graphitic nitrogen and a decrease in the pyridinic nitrogen, is that it is highly likely that more pyridinic species reside on the outer layers of the NCNT and/or are less stable and

the graphitic species are more stable. After performing this experiment we can confirm that nitrogen is being liberated. There is a possibility that there is also carbon being liberated from the product. It is also possible that some of the nitrogen and carbon that come off could be in the form of an amorphous coating, although the significant losses at higher temperature along with the mass reductions during synthesis suggest this is not a significant source of de-doping and mass loss. In future experiments, this study could be performed again in vacuum TGA to yield a better understanding of the volatile components and their temperature dependence. Based on the information gathered to this point, a few inferences can be made about what we expect to see in the next chapter's SEM characterization studies.

Hypothesis 6: We expect that NCNT length will increase with reaction time until the second de-doping mechanism dominates the growth process. We also expect that NCNT diameters will increase with increasing temperature.

Prediction 6.1: Based on continuing polymerization of the NCNT and Ostwald ripening of the catalyst particle from the constant feed source of catalyst. We expect NCNT length and diameter, much like for CNT growth, will increase with increasing temperature.

Hypothesis 7: Utilizing a pure NH_3 atmosphere will alter the nature of the nitrogen species incorporated into the NCNT lattice due to increased nitrogen solubility and defect creation.

Prediction 7.1: NH_3 has greater reactivity than hydrogen, and thus will impart more nitrogen into the lattice. We expect the added solubility of nitrogen in the iron

catalyst particles will create more defects and vacancies, allowing for more non-graphitic nitrogen substitutions. We also expect a larger percentage of pyridinic species created due to the added reactivity of the NH_3 and added defect creation in the sidewalls of the NCNT.

CHAPTER V

CHARACTERIZATION OF NCNTS

V.1 Introduction

NCNTs were characterized by SEM, TEM, and X-ray Photoelectron Spectroscopy (XPS). The SEM study provides an excellent opportunity to give a broad overview of a material and characterize various aspects of NCNT morphology as well as measure diameter and lengths. We examine representative samples from each time and temperature evolution point in the study. XPS provides elemental and chemical information of a material's top several atomic layers of a material. When a sample is exposed to X-rays, photoelectrons are released from the material into ultra-high vacuum and are detected by the electrostatic spherical sector analyzer as a function of energy in electron volts (eV). The corresponding spectrum plots electron counts on the y-axis versus the binding energy on the x-axis.

V.2 Materials

Materials used were previously listed in Chapter 2.

V.3 Equipment

Equipment used in addition to the previous listed in Chapter 2 are as follows:

Thermo Scientific ESCALAB 250 Xi

Zeiss Auriga Scanning Electron Microscope

Zeiss Libra Transmission Electron Microscope

V.4 Methods

For this work the ESCALAB 250 Xi by Thermo Scientific with a monochromatic (1486.6 eV) Al Kα-ray source with a 400 micron spot size. A pass energy of 200 eV was utilized for the survey experiments. The adventitious C1s peak was set at 284.5 eV to calibrate binding energies. Survey spectra were collected for each sample to evaluate the surface elemental composition. The pass energy of 20 eV was selected and signals were averaged over 60 scans for the N1s and other element scans to produce high quality curves to assess and deconvolute the different nitrogen peaks. Avantage processing software was used to analyze all samples. XPS is a powerful surface and depth analysis tool for the characterization of NCNTs. It is important to assign the best accepted peaks in the N1s spectrum for deconvolution so that proper peak assignments can be made. Pyridinic nitrogen has an XPS peak at 398.5 eV with a full width at half maximum (FWHM) of 1.4 eV. Graphitic nitrogen has an XPS peak at 401.0 eV with a FWHM of 1.7 eV. An important assignment is the location of the Fe-N_x deconvolution. It can be seen from Jiang et al.[63] that the Fe-N_x peak, where x=1-4, shows XPS peaks between 399.3-399.7 eV depending on the N coordination number. The accepted full width at half maximum value for this peak is 1.2 eV. Pyridinic oxide has an XPS peak generally centered near 402.5 eV with a FWHM of 2.5 eV. Any other higher order NOx compounds have an XPS peak around 405 eV with a FWHM of 2.5 eV. .

V.5 Data and Observations

The following series of SEM images shows a representative sample from each relevant synthesis time and temperature used in this study. Those will be followed by a few representative TEM images generally showing the NCNT bamboo structures. First, the median length and diameters can be seen in Table 5.1 and 5.2, respectively.

Table 5.1 Median Lengths of NCNTs in microns

	725°C	750°C	775°C	800°C	825°C	850°C
15 min	2.4±3.3	4.0±5.0	8.8±3.9	7.0±4.6	9.7±5.0	26.0±11.9
30 min	3.6±1.1	8.3±0.9	15.0±9.7	33.0±14.1	12.0±6.5	26.0±8.1
60 min	5.8±2.9	12.2±12.1	33.0±13.6	48.5±7.1	48.0±24.7	28.5±12.8
120 min	8.0±12.9	31.9±16.1	50.0±13.9	63.0±79.6	91.0±21.2	33.0±29.5

Table 5.2 Median Diameters of NCNTs

	725°C	750°C	775°C	800°C	825°C	850°C
15 min	56.0±34.5	77.0±40.5	74.0±39.2	22.0±14.5	28.0±22.6	65.0±75.5
30 min	62.0±11.0	24.0±9.7	69.0±34.6	59.0±35.9	38.0±20.4	50.0±37.8
60 min	60.0±26.9	38.5±26.4	60.0±35.0	82.0±18.4	72.0±35.7	73.0±66.5
120 min	87.0±39.6	85.0±40.6	62.0±16.8	88.5±59.1	92.0±27.3	60.0±43.7

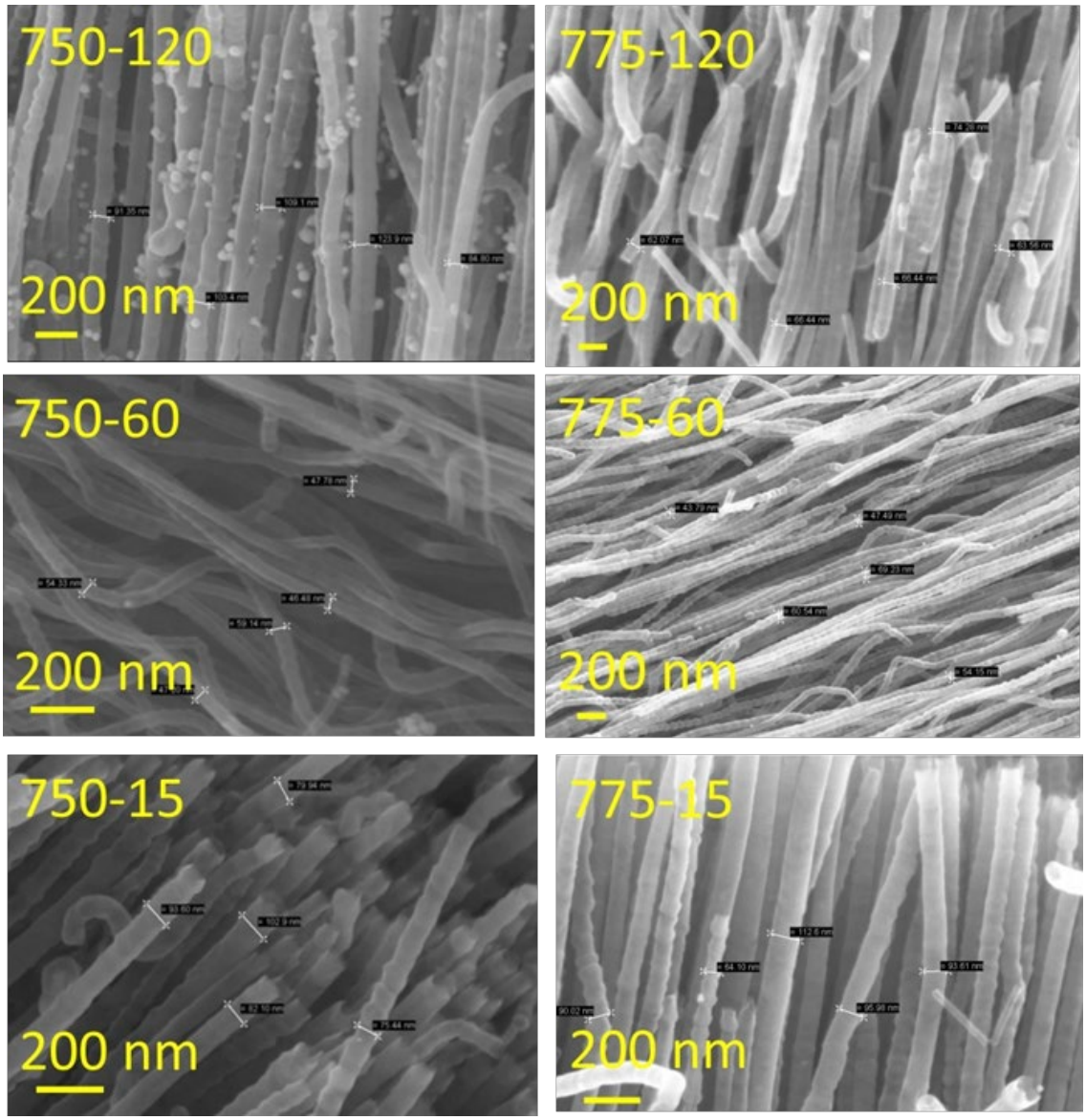

Figure 5.1 SEM showing NCNTs produced at different times at 750°C and 775°C.

As seen in Figure 5.1 the NCNTs have a bulbous shape in the wall structure. The median lengths increase at 750°C from 4, to 12.2, to 31.2 microns at 15', 60', and 120', respectively. At 775°C, the most efficient synthesis happens and we observed median lengths of 8.8, 33.0, and 50.0 microns at 15', 60' and 120' respectively. Median

diameters at 750°C were 77.0, 38.0 and 85.0 nanometers at 15', 60' and 120' respectively. Median diameters at 775°C were 74.0, 60.0, and 62.0 nanometers at 15', 60' and 120' respectively.

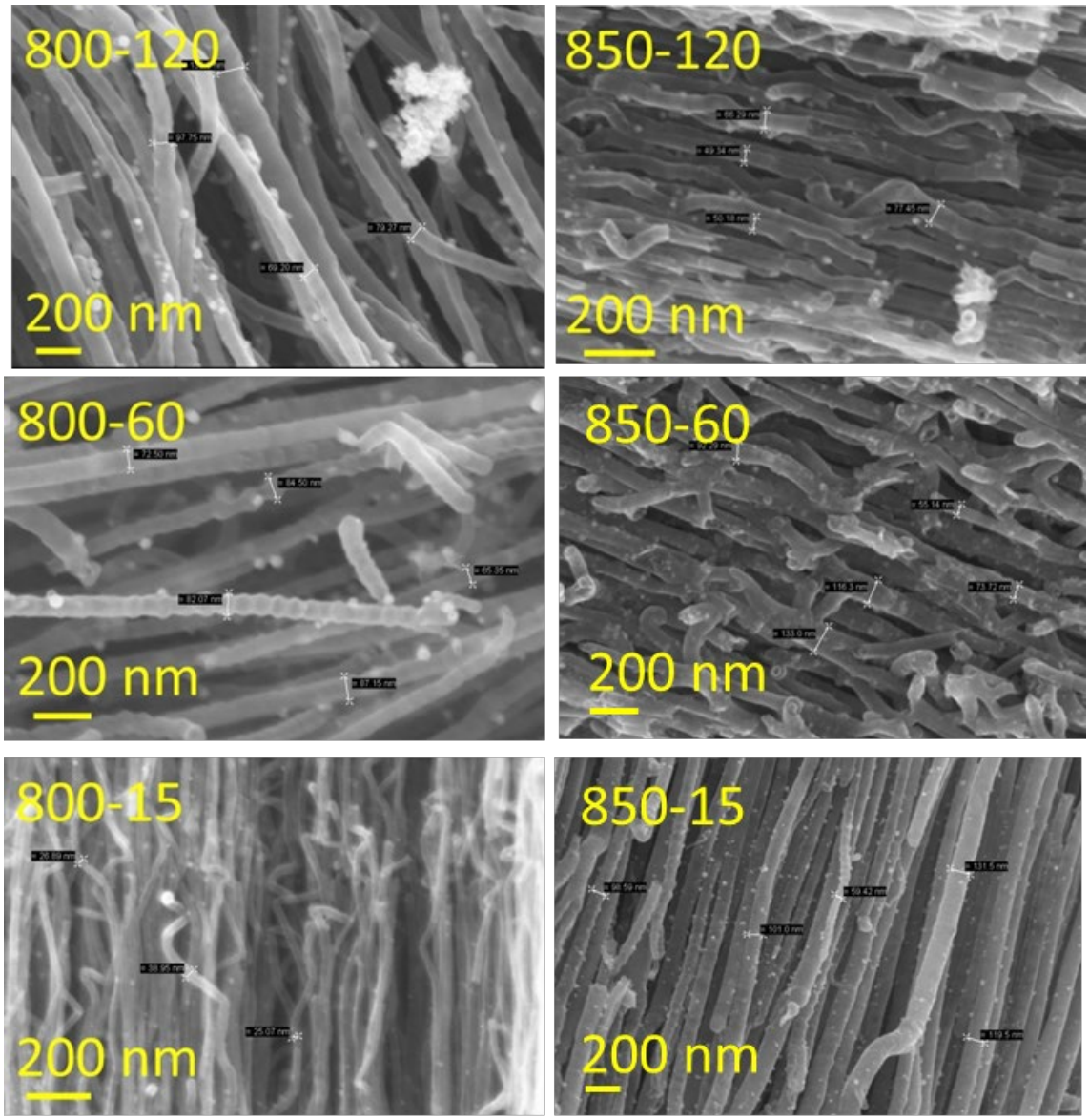

Figure 5.2 SEM showing NCNTs produced at different times at 800°C and 850°C.

As seen in Figure 5.2 the NCNTs still have a bulbous shape, but at 850°C there is significant sidewall damage, branching, and iron decoration on the surface of the NCNTs. The median lengths at 800°C were 7.0, 48.5, 63.0 microns at 15', 60', and 120', respectively. The median diameters were 22.0, 82.0, and 88.5 nanometers 15', 60', and 120', respectively. At 850°C the median lengths were 26.0, 28.5, and 33.0 microns at 15', 60', and 120', respectively. The median diameters were 65.0, 73.0, and 60.0 nanometers at 15', 60', and 120', respectively.

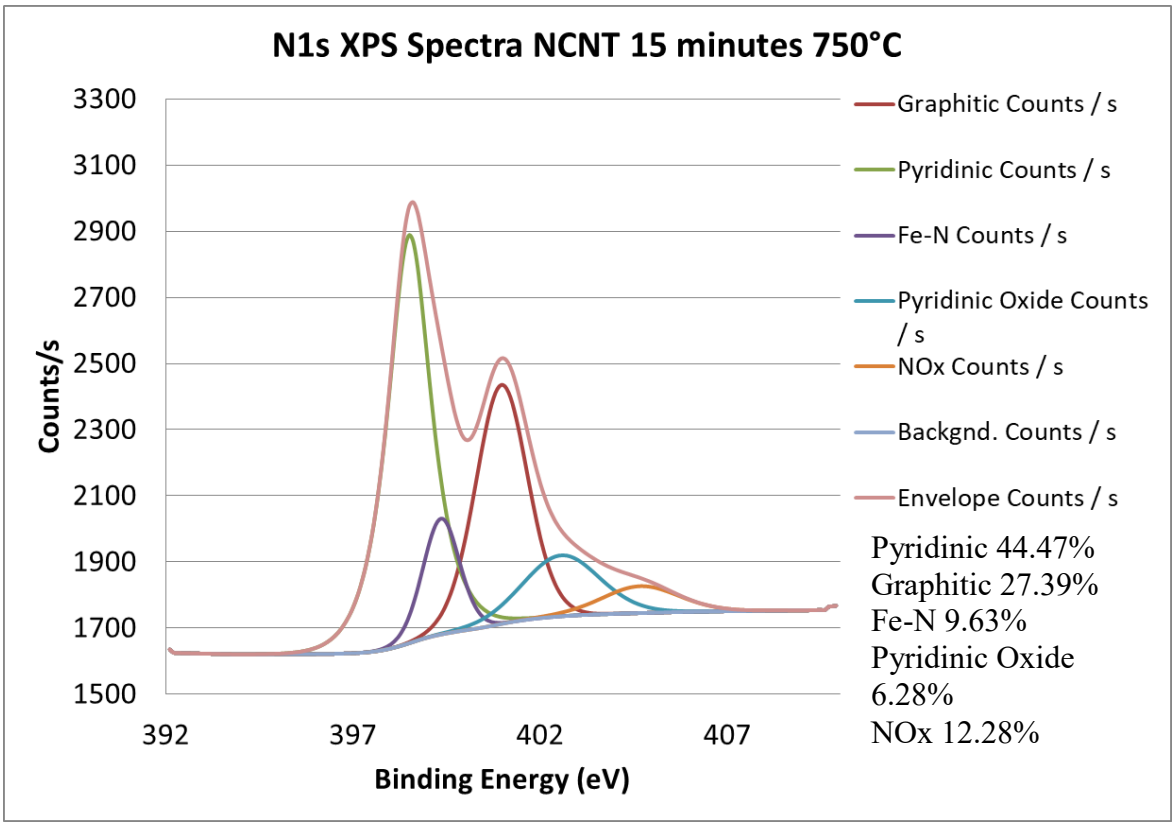

Figure 5.3 XPS N1s scan after 15 minutes at 750°C.

The N1s spectrum shown in Figure 5.3, after a 15 minute synthesis shows a preference toward pyridinic nitrogen. The N1s spectrum yields a 44.47% pyridinic nitrogen content, 27.39% graphitic, 9.63% Fe-N, 12.23 % pyridinic oxide, and 6.28% NOx content. This spectrum exemplifies a typical N1s spectrum. In every instance, the most prevalent nitrogen species in the spectrum is pyridinic.

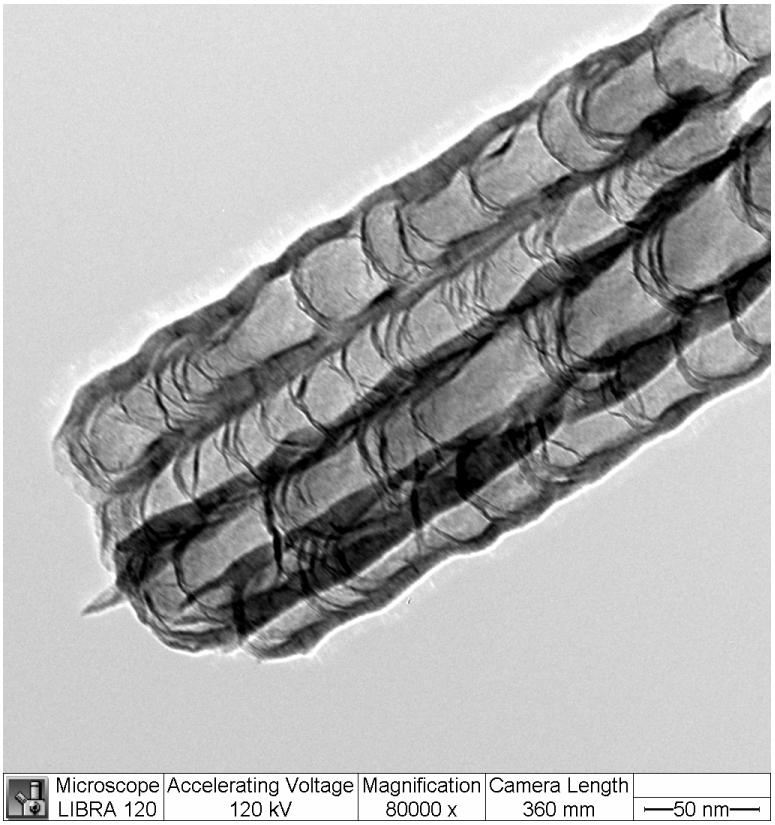

Figure 5.4 TEM of the NCNTs showing the bamboo structure

Transmission electron microscopy reveals the internal structure of the NCNTs. Figure 5.4 is a representative image showing the bulbous walls.

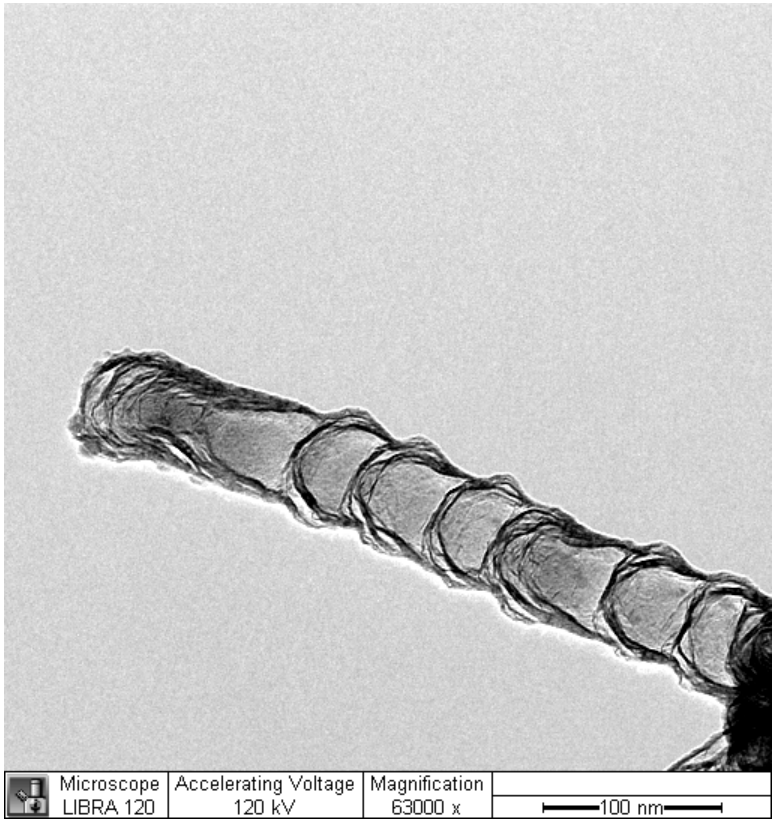

Figure 5.5 TEM of NCNT.

Shown in Figure 5.5 is another representative TEM showing a typical NCNT produced in a pure NH_3 atmosphere. The bulbous compartments appear to have a fairly regular periodicity.

V.6 Results

At 725°C, the rate of growth is very slow only growing 2 microns in 15', and only 8 microns in 120'. At 750°C, the maximum length increases to 32 microns, and 50 microns at 775°C. At 800°C the maximum length increases to 63 microns, and 91 microns at 825°C. There is a marked difference at 850°C, where the length starts at 26 microns in 15 minutes suggesting a fast starting growth rate, but at 30 minutes it is still

26 microns, and only increases to 29 and 33 microns at 60 and 120 minutes respectively. This result suggests that at 850°C, while the initial growth rate is very high, the catalyst particle is poisoned very quickly, most likely in the first 15-20 minutes. Iron is constantly fed into the system from ferrocene dissolved in the pyridine precursor. The NCNTs likely grow for less than 15 minutes and there are just multiple cycles of sub-15 minute growths that add to the yield. But, the degenerative effects from the NH_3 and the lesser components and free radicals at this elevated temperature have a significant effect on the sidewalls of the NCNT. It is known now that there is a competing rate of de-doping that dominates the growth kinetics at 850°C and there is rapid gasification of the nitrogen from the lattice at this temperature as we showed in chapter 4. It is possible that carbon could gas off with the nitrogen making HCN. This assertion is consistent with the drastic drop in mass yields observed at 850°C as discussed in chapter 2.

V.7 Discussion

The hypothesis put forward at the beginning of this section stated that with increasing temperature, NCNT diameter will increase. In reality, based on the empirical evidence, the diameters appear to be only weakly dependent on temperature. However, diameters tend to increase with reaction time. The other hypothesis put forward was that lengths also would increase with reaction time. The results generally support this hypothesis but, the NCNT lengths also exhibit temperature dependence. The last hypothesis stated that NH_3 had greater reactivity than hydrogen and thus, synthesis in a pure NH_3 environment imparts more nitrogen into the NCNT lattice. XPS data confirms

that while typical syntheses of NCNTs in argon or hydrogen environments often yields less than 5 atomic % nitrogen, this work demonstrates that syntheses in a pure NH_3 environment yield 8-13% nitrogen. Further, pyridinic nitrogen was predicted to become the preferential bond over graphitic nitrogen which is the normal dominant species. The XPS N1s data also confirms this prediction that pyridinic nitrogen does become the dominant species and the sidewall structural bending as observed by SEM and TEM points to greater defect generation.

V.8 Conclusions

Highly doped NCNTs were successfully synthesized and characterized via XPS to yield 8-13 atomic % nitrogen. SEM analysis elucidates trends in the NCNT lengths and diameters. The SEM study appears to make some diameters look to be increasing but with larger counts from more images shows that trend was even except at the lowest synthesis temperatures where diameters stayed small. Lengths generally show a dependence with temperature and time. Utilization of XPS allows for the resolution of atomic percent nitrogen incorporation as well as deconvolution of the N1s spectra to determine the relative concentration of the different nitrogen species. The complete set of XPS surveys and N1s data, summarized in the Appendix, also support the findings from chapters 2 through 5.

CHAPTER VI

OVERALL CONCLUSIONS

The following table summarizes the predictions and whether the results support or refute the hypotheses.

Table 6.1 Predictions

Prediction #	Prediction	Result	Prediction confirmed or refuted
1.1	%N stays constant with increased reaction time	%N increases with increasing time except at highest reaction temperatures	Supports through 775 Refutes 800-850
2.1	%N increases with increased reaction temperature	%N increases with temperature except at highest reaction temperatures	Supports through 775 Refutes above 775
2.2	%N increases as a byproduct of NH_3 decomposition	Holds for low temperature, 825°C and 850°C show some %N drop with time evolution	Supports through 775 Refutes at 825, 850
3.1	Reaction not governed by one rate determining mechanism	Arrhenius plots show a clean break in the Ln of the rate between 775 & 800°C	Supports
4.1	XPS will show a %N loss at high temperatures in a post	XPS confirms considerable %N loss at 850°C	Supports

	processing heat treatment		
5.1	XPS will show greater stability for graphitic N when N is lost by dedoping	XPS confirms graphitic-N is more stable to dedoping than pyridinic-N	Supports
6.1	NCNT length and diameter will increase with increasing temperature	Diameter not totally dependent on temperature, length generally increases with temperature	Inconclusive on diameter Supports on length
7.1	NH_3 greater reactivity, will impart more N into the lattice, pushing more defects and vacancies pushing more pyridinic-N	XPS confirms more pyridinic-N is incorporated during synthesis	Supports

Summary observation 1.1.1: The empirical observation of the atomic percent nitrogen in the NCNT lattice shows a general trend of increasing nitrogen percent with increasing time from 725°C to 800°C. However, at 825°C and 850°C, the same general trend of increasing nitrogen concentration with time does not hold. At some time point at these two higher temperatures, the atomic percent nitrogen observed in the NCNT lattice actually drops.

Summary observation 2.1.1: As the temperature increases, the solubility of carbon and nitrogen in the iron catalyst particle increases, reaching supersaturation quicker and results in a higher rate of polymerization. At low reaction times the rate increases with increasing temperature. However, at 825°C and 850°C, the higher rate holds at low

reaction times but then a second mechanism causes the atomic percent nitrogen to level off and eventually reduces.

Summary observation 2.2.1: Typically, as observed from hypothesis one, with the longest times, more nitrogen was found in the NCNT product. So by looking at the 120 minute synthesis times, we observe that the percent nitrogen increased from 700°C to 800°C, and then we observed a lower percentage at 825°C and 850°C. It is worth noting that if we only looked at maximum percent nitrogen concentrations, at 825°C after 60 minutes the concentration was 1.5% higher than at 120 minutes. This suggests that something significantly different is happening at the higher temperatures that is competing with the normal formation mechanism.

Summary observation 3.1.1: All the Arrhenius plots show a clear break between 775°C and 800°C. There is a clear Arrhenius plot rate from 725C to 775C with a good fit that shows how things should track at higher temperatures but above the inflection point the competing reaction dominates and completely flips the slope to a loss mechanism.

Summary observation 4.1.1: XPS of de-doping studies does in fact show that at high temperatures a significant percent of nitrogen is lost to gasification. At lower temperatures the rate of loss is significantly lessened and almost nonexistent at the lowest synthesis temperatures.

Summary observation 5.1.1: XPS does show graphitic nitrogen as the more stable species, and pyridinic is lost at a greater percentage.

Summary observation 6.1.1: Based on the empirical evidence, the diameters were not overly dependent on temperature. However, there is a general trend with increasing time,

diameters increase as well. The other part of the hypothesis states NCNT lengths would increase with time. This trend generally holds true but, there is also temperature dependence. Except at 850°C, where the growth rate is initially very fast but also appears to poison the catalyst particle much more quickly.

Summary observation 7.1.1: Nearly every other synthesis route without pure NH_3, shows a preference to forming graphitic nitrogen as the majority species. In these experiments, where NH_3 was the only gas used, pyridinic nitrogen was the more favorable nitrogen group.

We learned from this series of experiments, and this dissertation, that the type of nitrogen in the NCNT lattice can be tuned from graphitic nitrogen dominant to pyridinic nitrogen dominant by switching from an argon or hydrogen atmosphere to a pure NH_3 atmosphere using pyridine and ferrocene as the precursor material. Furthermore, it appears that the reactive nature of the NH_3 imparts more nitrogen into the lattice. While diameter is not overly dependent on temperature, NCNTs trended longer with increasing temperature and time except at the highest synthesis temperatures. Weights of product increased with temperature until 775°C at which point with increasing temperature weights decreased. Following this trend the rate of NCNT formation and the rate of nitrogen inclusion increased with increasing temperature until 775°C and then the trend slowed and even completely flipped to a positive slope. This change in slope on the Arrhenius plots showed us that there was not one single rate limiting mechanism that governs the synthesis temperature range but, that just above 775°C at roughly 790°C a second mechanism dominates the reaction for the rest of the upper synthesis temperature

limit to 850°C and while we produced NCNTs at 900°C after 30 minutes, no NCNTs were produced after120 minutes. We found that this second mechanism was the dedoping of nitrogen. The dedoping study showed that graphitic nitrogen was more stable in the lattice than the pyridinic species. As temperature increases, NH_3 reactivity increases as well, fueling a second source to put more nitrogen into the NCNT lattice. However, at 825 & 850°C the reactivity of the NH_3 likely becomes so reactive that it does damage to the sidewalls and on top of gasification, at the most extreme temperatures, actually start to consume the NCNTs.

VI.1 Future Perspectives

In the future, it would be very interesting to see the de-doping study performed in a vacuum TGA as it could be performed much more quickly and with greater accuracy, as there may be more than one rate limiting, temperature dependent step that contributes to the de-doping process. I would like to see a GC/Mass spec connected to a furnace to analyze the effluent gas stream in real time. Additionally, time evolution studies at temperatures above 850°C could be conducted to determine when NCNTs are consumed and if growth is even possible at these temperatures as we originally screened at 120 minutes and none of those temperatures produced NCNTs. Also, our results also suggest that ~790°C represents the near optimum temperature for incorporating nitrogen into the NCNT lattice during synthesis. It would be quite interesting to do the time evolution study to confirm whether this synthesis temperature provides the highest percent nitrogen and best yield of NCNTs. Finally, as Fe-Nx structures appear to have very interesting

catalytic properties, I would like to see extremely high resolution TEM like high-angle annular dark-field scanning transmission electron microscopy to see the individual moieties, as this tool can resolve individual atoms. In summary, this work has opened the door to a new domain of research that promises to significantly enhance our understanding of heteroatom nanotube growth processes and provide guiding principles for designing high performance catalysts.

REFERENCES

[1] Iijima, S. (1991). Helical microtubules of graphitic carbon. Nature, 354(6348), 56.
[2] Radushkevich, L. V., & Lukyanovich, V. M. (1952). On the carbon structure formed during thermal decomposition of carbon monoxide in the presence of iron. Zhurnal Fizicheskoi Khimii, 26, 88-95.
[3] Endo, M. (1988). Grow carbon fibers in the vapor phase. Chemtech.
[4] Stephan, O., Ajayan, P. M., Colliex, C., Redlich, P., Lambert, J. M., Bernier, P., & Lefin, P. (1994). Doping graphitic and carbon nanotube structures with boron and nitrogen. Science, 266(5191), 1683-1685.
[5] Czerw, R., Terrones, M., Charlier, J. C., Blase, X., Foley, B., Kamalakaran, R., ... & Blau, W. (2001). Identification of electron donor states in N-doped carbon nanotubes. Nano Letters, 1(9), 457-460.
[6] Yi, J. Y., & Bernholc, J. (1993). Atomic structure and doping of microtubules. Physical Review B, 47(3), 1708.
[7] Stephan, O., Ajayan, P. M., Colliex, C., Redlich, P., Lambert, J. M., Bernier, P., & Lefin, P. (1994). Doping graphitic and carbon nanotube structures with boron and nitrogen. Science, 266(5191), 1683-1685.
[8] Ewels, C., Glerup, M., Krstic, V., Basiu, V., & Basiuk, E. (2007). Nitrogen and boron doping in carbon nanotubes. Doped Nanomaterials and Nanodevices, 3.
[9] Rauf, M., Zhao, Y. D., Wang, Y. C., Zheng, Y. P., Chen, C., Yang, X. D., ... & Sun, S. G. (2016). Insight into the different ORR catalytic activity of Fe/N/C between acidic and alkaline media: protonation of pyridinic nitrogen. Electrochemistry Communications, 73, 71-74.
[10] Faisal, S. N., Haque, E., Noorbehesht, N., Zhang, W., Harris, A. T., Church, T. L., & Minett, A. I. (2017). Pyridinic and graphitic nitrogen-rich graphene for high-performance supercapacitors and metal-free bifunctional electrocatalysts for ORR and OER. RSC advances, 7(29), 17950-17958.
[11] Xie, Y., Chen, Y., Liu, L., Tao, P., Fan, M., Xu, N., ... & Yan, C. (2017). Ultra-high pyridinic N-doped porous carbon monolith enabling high-capacity K-ion battery anodes for both half-cell and full-cell applications. Advanced Materials, 29(35), 1702268.
[12] Chen, Z., Higgins, D., Tao, H., Hsu, R. S., & Chen, Z. (2009). Highly active nitrogen-doped carbon nanotubes for oxygen reduction reaction in fuel cell applications. The Journal of Physical Chemistry C, 113(49), 21008-21013.
[13] Sharifi, T., Hu, G., Jia, X., & Wagberg, T. (2012). Formation of active sites for oxygen reduction reactions by transformation of nitrogen functionalities in nitrogen-doped carbon nanotubes. ACS nano, 6(10), 8904-8912.
[14] Czerw, R., Terrones, M., Charlier, J. C., Blase, X., Foley, B., Kamalakaran, R., ... & Blau, W. (2001). Identification of electron donor states in N-doped carbon nanotubes. Nano Letters, 1(9), 457-460.

[15] Bettinger, H. F. (2005). The reactivity of defects at the sidewalls of single-walled carbon nanotubes: The Stone− Wales defect. The Journal of Physical Chemistry B, 109(15), 6922-6924.
[16] Zhang, H., Hwang, S., Wang, M., Feng, Z., Karakalos, S., Luo, L., ... & Shao, Y. (2017). Single atomic iron catalysts for oxygen reduction in acidic media: particle size control and thermal activation. Journal of the American Chemical Society, 139(40), 14143-14149.
[17] Ren, H., Wang, Y., Yang, Y., Tang, X., Peng, Y., Peng, H., ... & Zhuang, L. (2017). Fe/N/C nanotubes with atomic Fe sites: A highly active cathode catalyst for alkaline polymer electrolyte fuel cells. ACS Catalysis, 7(10), 6485-6492.
[18] Oh, H. S., & Kim, H. (2012). The role of transition metals in non-precious nitrogen-modified carbon-based electrocatalysts for oxygen reduction reaction. Journal of Power Sources, 212, 220-225.
[19] Masa, J., Zhao, A., Xia, W., Sun, Z., Mei, B., Muhler, M., & Schuhmann, W. (2013). Trace metal residues promote the activity of supposedly metal-free nitrogen-modified carbon catalysts for the oxygen reduction reaction. Electrochemistry communications, 34, 113-116.
[20] Masa, J., Zhao, A., Xia, W., Muhler, M., & Schuhmann, W. (2014). Metal-free catalysts for oxygen reduction in alkaline electrolytes: influence of the presence of Co, Fe, Mn and Ni inclusions. Electrochimica Acta, 128, 271-278.
[21] Kaukonen, M., Kujala, R., & Kauppinen, E. (2012). On the origin of oxygen reduction reaction at nitrogen-doped carbon nanotubes: a computational study. The Journal of Physical Chemistry C, 116(1), 632-636.
[22] Adjizian, J. J., Leghrib, R., Koos, A. A., Suarez-Martinez, I., Crossley, A., Wagner, P., ... & Ewels, C. P. (2014). Boron-and nitrogen-doped multi-wall carbon nanotubes for gas detection. Carbon, 66, 662-673.
[23] Koós, A. A., Nicholls, R. J., Dillon, F., Kertész, K., Biró, L. P., Crossley, A., & Grobert, N. (2012). Tailoring gas sensing properties of multi-walled carbon nanotubes by in situ modification with Si, P, and N. Carbon, 50(8), 2816-2823.
[24] Ghosh, K., Kumar, M., Maruyama, T., & Ando, Y. (2010). Tailoring the field emission property of nitrogen-doped carbon nanotubes by controlling the graphitic/pyridinic substitution. Carbon, 48(1), 191-200.
[25] Arjmand, M., Chizari, K., Krause, B., Pötschke, P., & Sundararaj, U. (2016). Effect of synthesis catalyst on structure of nitrogen-doped carbon nanotubes and electrical conductivity and electromagnetic interference shielding of their polymeric nanocomposites. Carbon, 98, 358-372.
[26] Chen, Z., Higgins, D., & Chen, Z. (2010). Nitrogen doped carbon nanotubes and their impact on the oxygen reduction reaction in fuel cells. Carbon, 48(11), 3057-3065.

[27] Chen, L., Xia, K., Huang, L., Li, L., Pei, L., & Fei, S. (2013). Facile synthesis and hydrogen storage application of nitrogen-doped carbon nanotubes with bamboo-like structure. International Journal of Hydrogen Energy, 38(8), 3297-3303.
[28] Guo, B., Wang, X., Fulvio, P. F., Chi, M., Mahurin, S. M., Sun, X. G., & Dai, S. (2011). Soft-templated mesoporous carbon-carbon nanotube composites for high performance lithium-ion batteries. Advanced Materials, 23(40), 4661-4666.
[29] Dubal, D. P., Chodankar, N. R., Caban-Huertas, Z., Wolfart, F., Vidotti, M., Holze, R., ... & Gomez-Romero, P. (2016). Synthetic approach from polypyrrole nanotubes to nitrogen doped pyrolyzed carbon nanotubes for asymmetric supercapacitors. Journal of Power Sources, 308, 158-165.
[30] Jiang, K., Eitan, A., Schadler, L. S., Ajayan, P. M., Siegel, R. W., Grobert, N., ... & Terrones, M. (2003). Selective attachment of gold nanoparticles to nitrogen-doped carbon nanotubes. Nano Letters, 3(3), 275-277.
[31] Wu, G., & Zelenay, P. (2013). Nanostructured nonprecious metal catalysts for oxygen reduction reaction. Accounts of chemical research, 46(8), 1878-1889.
[32] Gottesfeld, S., & Zawodzinski, T. A. (1997). Polymer electrolyte fuel cells. Advances in electrochemical science and engineering, 5, 195-302.
[33] Byon, H. R., Suntivich, J., Crumlin, E. J., & Shao-Horn, Y. (2011). Fe–N-modified multi-walled carbon nanotubes for oxygen reduction reaction in acid. Physical Chemistry Chemical Physics, 13(48), 21437-21445.
[34] Lefèvre, M., Dodelet, J. P., & Bertrand, P. (2002). Molecular oxygen reduction in PEM fuel cells: evidence for the simultaneous presence of two active sites in Fe-based catalysts. The Journal of Physical Chemistry B, 106(34), 8705-8713.
[35] Glerup, M., Steinmetz, J., Samaille, D., Stephan, O., Enouz, S., Loiseau, A., ... & Bernier, P. (2004). Synthesis of N-doped SWNT using the arc-discharge procedure. Chemical Physics Letters, 387(1-3), 193-197.
[36] Jaouen, F., Lefèvre, M., Dodelet, J. P., & Cai, M. (2006). Heat-treated Fe/N/C catalysts for O2 electroreduction: are active sites hosted in micropores?. The Journal of Physical Chemistry B, 110(11), 5553-5558.
[37] Nagaiah, T. C., Kundu, S., Bron, M., Muhler, M., & Schuhmann, W. (2010). Nitrogen-doped carbon nanotubes as a cathode catalyst for the oxygen reduction reaction in alkaline medium. Electrochemistry Communications, 12(3), 338-341.
[38] Jin, C., Nagaiah, T. C., Xia, W., Spliethoff, B., Wang, S., Bron, M., ... & Muhler, M. (2010). Metal-free and electrocatalytically active nitrogen-doped carbon nanotubes synthesized by coating with polyaniline. Nanoscale, 2(6), 981-987.

[39] Zhao, A., Masa, J., Muhler, M., Schuhmann, W., & Xia, W. (2013). N-doped carbon synthesized from N-containing polymers as metal-free catalysts for the oxygen reduction under alkaline conditions. Electrochimica Acta, 98, 139-145.
[40] Yang, M., Yang, D., Chen, H., Gao, Y., & Li, H. (2015). Nitrogen-doped carbon nanotubes as catalysts for the oxygen reduction reaction in alkaline medium. Journal of power sources, 279, 28-35.
[41] Xu, E., Wei, J., Wang, K., Li, Z., Gui, X., Jia, Y., ... & Wu, D. (2010). Doped carbon nanotube array with a gradient of nitrogen concentration. Carbon, 48(11), 3097-3102.
[42] Terrones, M., Ajayan, P. M., Banhart, F., Blase, X., Carroll, D. L., Charlier, J. C., ... & Kohler-Redlich, P. (2002). N-doping and coalescence of carbon nanotubes: synthesis and electronic properties. Applied Physics A, 74(3), 355-361.
[43] Hao, Y., Qingwen, L., Jin, Z., & Zhongfan, L. (2003). The effect of hydrogen on the formation of nitrogen-doped carbon nanotubes via catalytic pyrolysis of acetonitrile. Chemical Physics Letters, 380(3-4), 347-351.
[44] Tang, C., Bando, Y., Golberg, D., & Xu, F. (2004). Structure and nitrogen incorporation of carbon nanotubes synthesized by catalytic pyrolysis of dimethylformamide. Carbon, 42(12-13), 2625-2633.
[45] Becker, M., Bender, H., Jansen, M., Kienle, L., & Assenmacher, W. (2001). Efficient access to bamboo-like carbon micro and nanofibres by pyrolysis of zinc cyanamide. Journal of Physics and Chemistry of Solids, 62(8), 1431-1433.
[46] Wang, X., Hu, W., Liu, Y., Long, C., Xu, Y., Zhou, S., ... & Dai, L. (2001). Bamboo-like carbon nanotubes produced by pyrolysis of iron (II) phthalocyanine. Carbon, 39(10), 1533-1536.
[47] Vanyorek, L., Muránszky, G., Fiser, B., Sikora, E., Hutkai, Z. G., & Viskolcz, B. (2019). Adsorption capacity of oxidized nitrogen-doped bamboo-like carbon nanotubes. Journal of Dispersion Science and Technology, 1-6.
[48] Lee, C. J., Lyu, S. C., Kim, H. W., Lee, J. H., & Cho, K. I. (2002). Synthesis of bamboo-shaped carbon–nitrogen nanotubes using C2H2–NH3–Fe (CO) 5 system. Chemical physics letters, 359(1-2), 115-120.
[49] Liu, J., Czerw, R., & Carroll, D. L. (2005). Large-scale synthesis of highly aligned nitrogen doped carbon nanotubes by injection chemical vapor deposition methods. Journal of Materials Research, 20(2), 538-543.
[50] Liu, J., Webster, S., & Carroll, D. L. (2005). Temperature and flow rate of NH3 effects on nitrogen content and doping environments of carbon nanotubes grown by injection CVD method. The Journal of Physical Chemistry B, 109(33), 15769-15774.
[51] Liu, H., Zhang, Y., Li, R., Sun, X., Désilets, S., Abou-Rachid, H., ... & Lussier, L. S. (2010). Structural and morphological control of aligned nitrogen-doped carbon nanotubes. Carbon, 48(5), 1498-1507.

[52] Liu, J., Czerw, R., & Carroll, D. L. (2005). Large-scale synthesis of highly aligned nitrogen doped carbon nanotubes by injection chemical vapor deposition methods. Journal of Materials Research, 20(2), 538-543.
[53] Feng, X., Chee, S. W., Sharma, R., Liu, K., Xie, X., Li, Q., ... & Jiang, K. (2011). In Situ TEM observation of the gasification and growth of carbon nanotubes using iron catalysts. Nano Research, 4(8), 767.
[54] Jäniche, W., Dahl, W., Klärner, H. F., Pitsch, W., Schauwinhold, D., Schlüter, W., & Schmitz, H. (2013). Werkstoffkunde Stahl: Band 1: Grundlagen. Springer-Verlag.
[55] Sharma, A., Dasgupta, K., Patwardhan, A., & Joshi, J. (2017). Kinetic study of nitrogen doped carbon nanotubes in a fixed bed. Chemical Engineering Science, 170, 756-766.
[56] Guellati, O., Antoni, F., Guerioune, M., & Bégin, D. (2018). New doping process mode to synthesize in situ N-MWNTs in novel coaxial nanostructure. Catalysis Today, 301, 164-171.
[57] Kundu, S., Xia, W., Busser, W., Becker, M., Schmidt, D. A., Havenith, M., & Muhler, M.(2010). The formation of nitrogen-containing functional groups on carbon nanotubesurfaces: a quantitative XPS and TPD study. Physical Chemistry Chemical Physics,12(17), 4351-4359.
[58] Terrones, M., Redlich, P., Grobert, N., Trasobares, S., Hsu, W. K., Terrones, H., &Rühle, M. (1999). Carbon nitride nanocomposites: formation of aligned CxNynanofibers. Advanced materials, 11(8), 655-658.
[59] Lee, C. J., Lyu, S. C., Kim, H. W., Lee, J. H., & Cho, K. I. (2002). Synthesis ofbamboo-shaped carbon–nitrogen nanotubes using C2H2–NH3–Fe (CO) 5 system.Chemical Physics Letters, 359(1-2), 115-120.
[60] Liu, J., Webster, S., & Carroll, D. L. (2005). Temperature and flow rate of NH3 effectson nitrogen content and doping environments of carbon nanotubes grown by injectionCVD method. The Journal of Physical Chemistry B, 109(33), 15769-15774.
[61] Koós, A. A., Dowling, M., Jurkschat, K., Crossley, A., & Grobert, N. (2009). Effect ofthe experimental parameters on the structure of nitrogen-doped carbon nanotubesproduced by aerosol chemical vapour deposition. Carbon, 47(1), 30-37.
[62] Fujimoto, Y., & Saito, S. (2011). Energetics and electronic structures of pyridine-typedefects in nitrogen-doped carbon nanotubes. Physica E: Low-dimensional Systems andNanostructures, 43(3), 677-680.
[63] Jiang, W. J., Gu, L., Li, L., Zhang, Y., Zhang, X., Zhang, L. J., ... & Wan, L. J. (2016).Understanding the high activity of Fe–N–C electrocatalysts in oxygen reduction: Fe/Fe3Cnanoparticles boost the activity of Fe–N x. Journal of the American Chemical Society,138(10), 3570-3578.

APPENDIX

APPENDIX A: SEM OF NCNTS

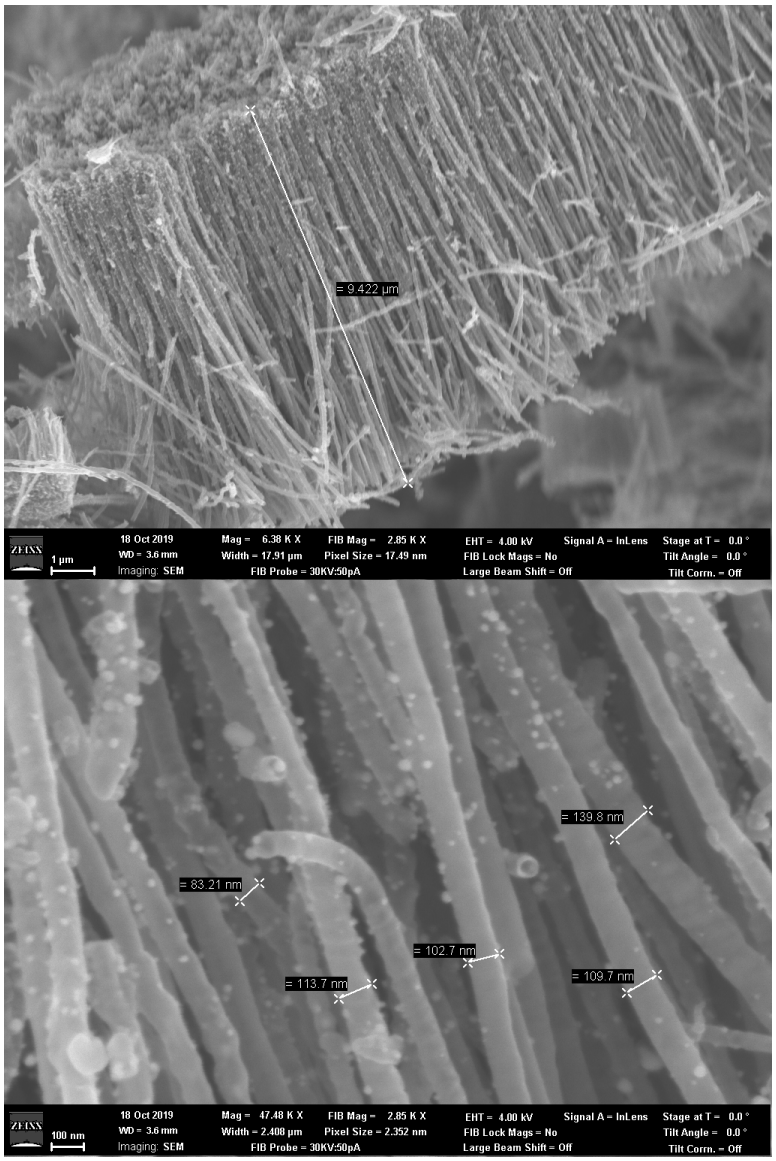

Figure A.1 SEM of lengths and diameters of NCNTs after 120 minutes at 700°C

After 120 minutes at 700°C, the median length of the NCNT is 10 microns and the median diameter is 105 nm and as seen in Figure A.1, there is iron decoration of the sidewalls, and while the tubes still appear to be bamboo in nature, the amount of sidewall curvature is less than those observed at other temperatures.

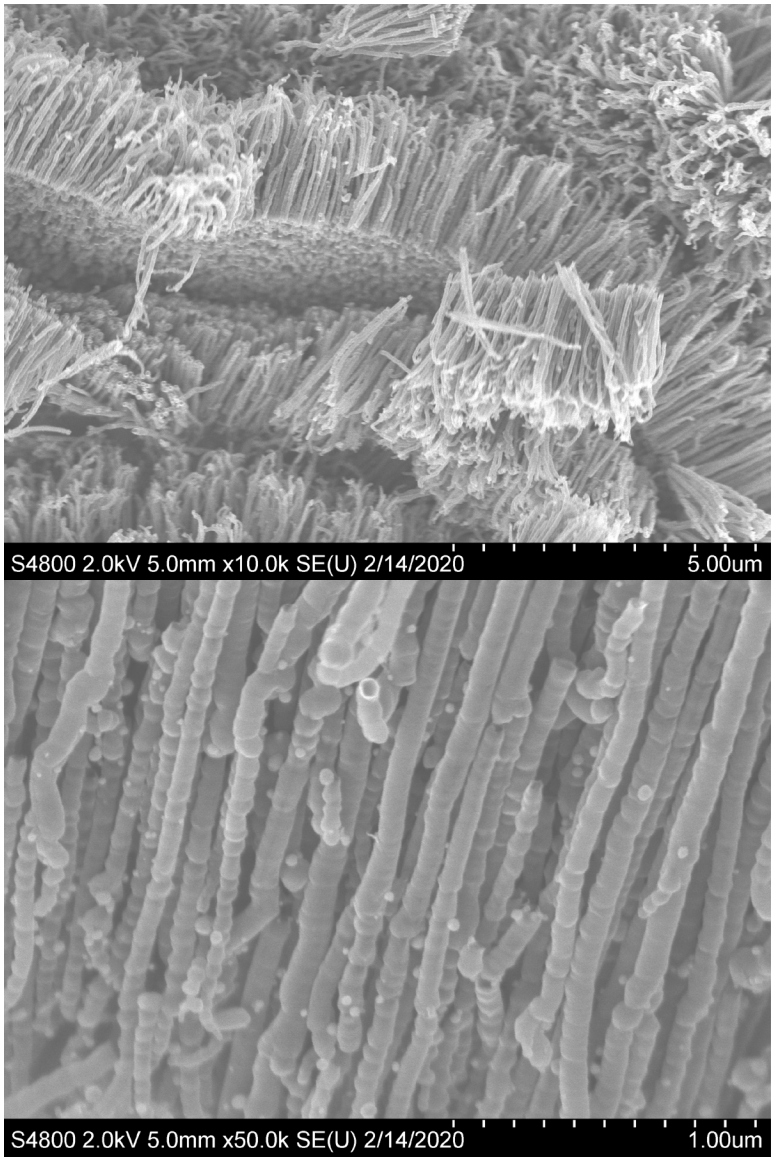

Figure A.2 SEM of lengths and diameters of NCNTs after 15 minutes synthesis at 725°C

At 15 minutes synthesis time at 725°C, the median length is 2 microns with a median diameter of 56 nanometers. As seen in Figure A.2, the NCNTs are relatively clean and have a bulbous bamboo shape.

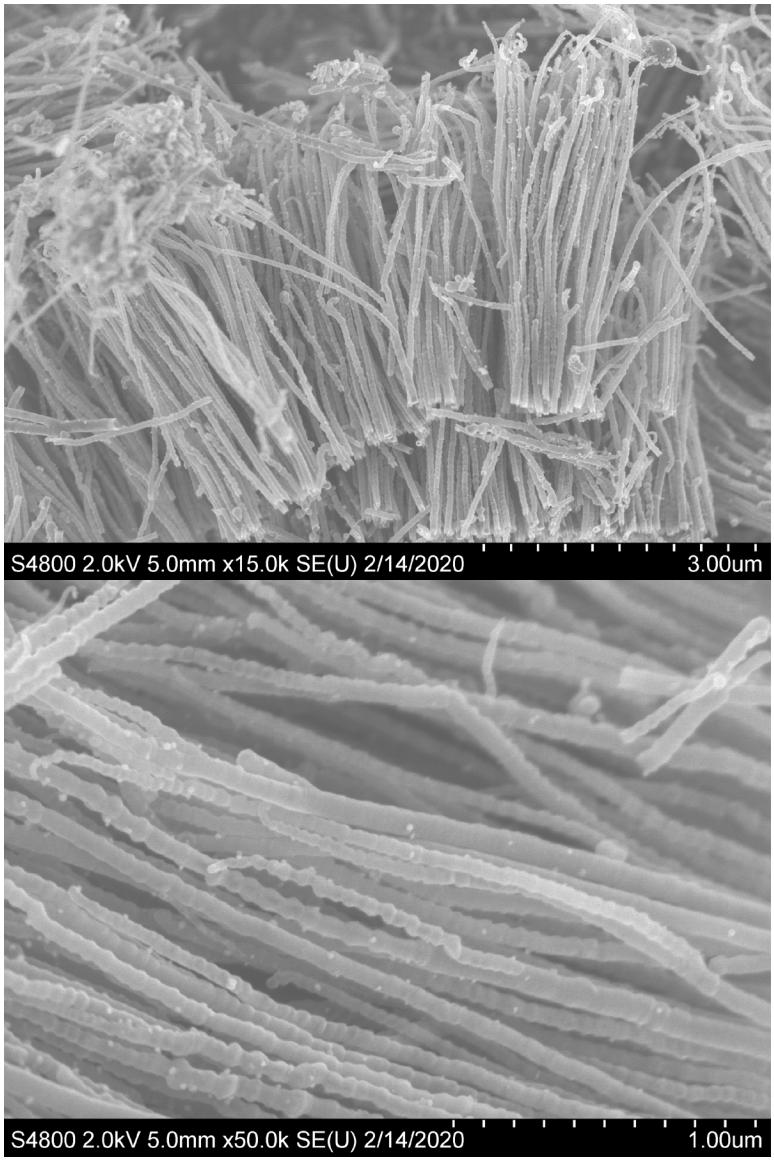

Figure A.3 SEM of NCNTs lengths and diameters of NCNTs after 30 minutes synthesis at 725°C

At 30 minutes synthesis time at 725°C, the SEM in Figure A.3 shows a NCNT median length of 4 microns and a median diameter of 62 nanometers. The NCNTs are relatively clean and have bulbous bamboo shape.

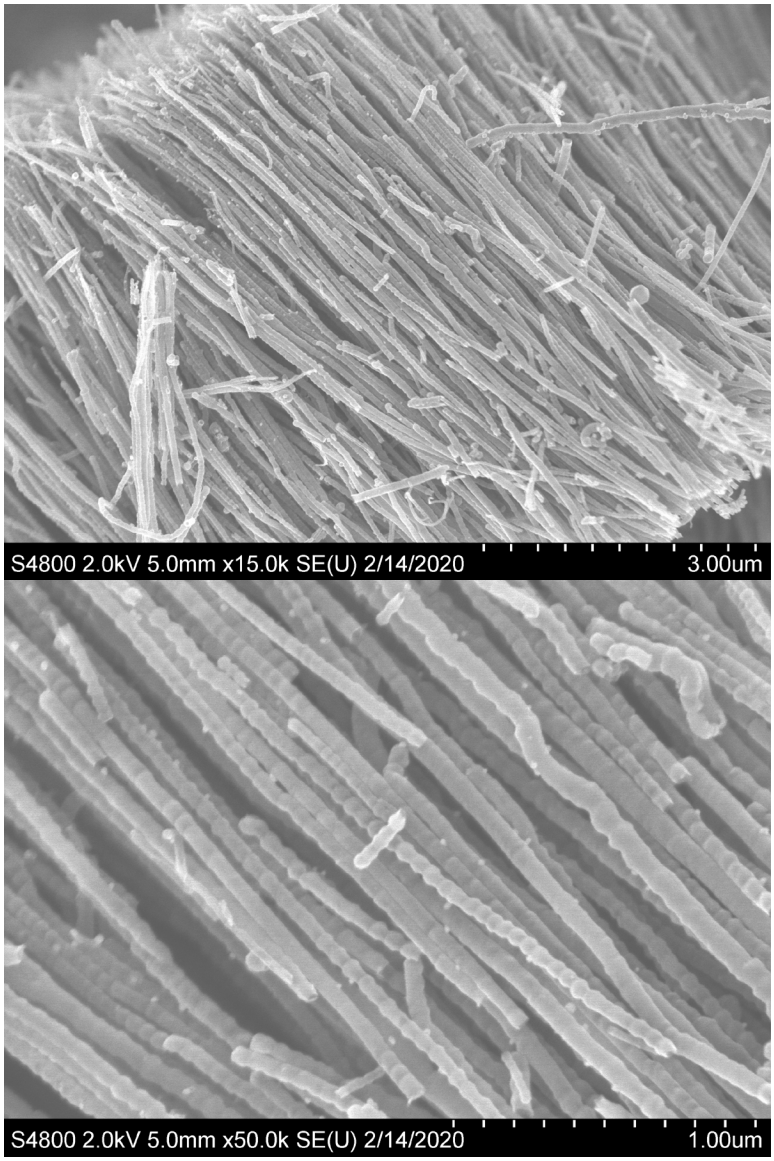

Figure A.4 SEM of lengths and diameters of NCNTs of NCNTs after 60 minutes synthesis at 725°C

After 60 minutes of NCNT synthesis at 725°C, the median length is 6 microns and the median diameter is 60 nanometers. The nanotubes are relatively clean and have a bulbous shape.

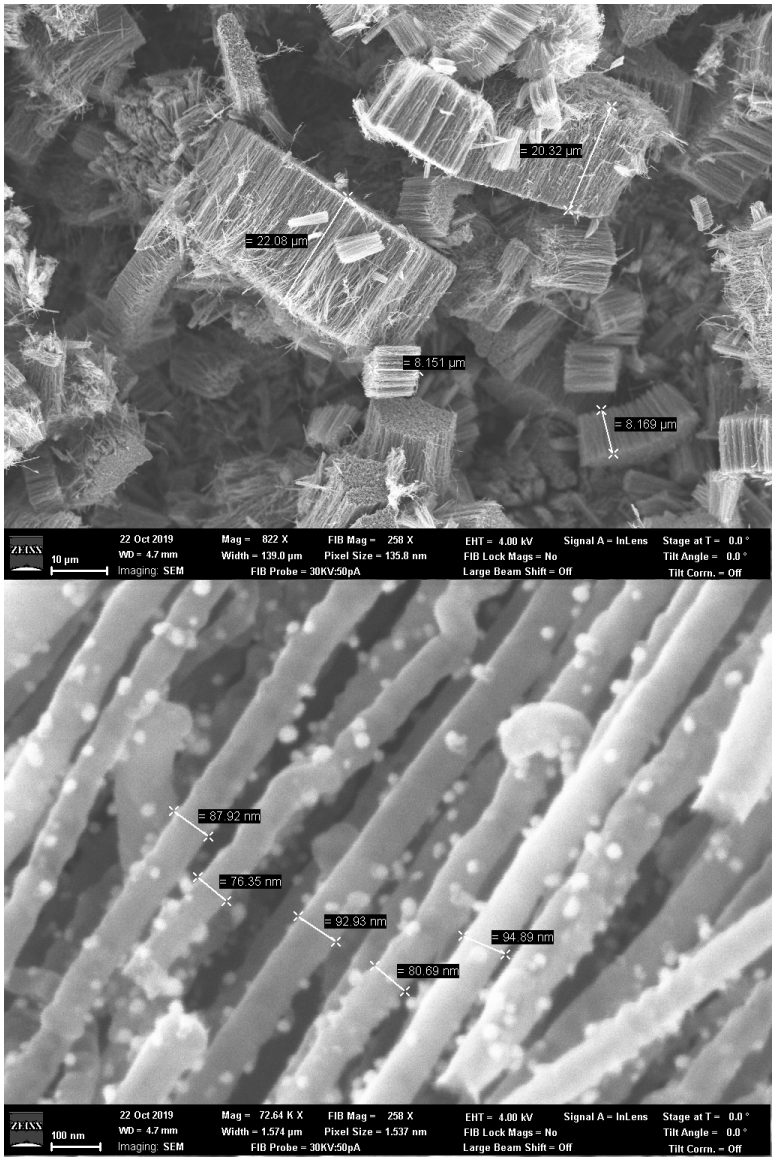

Figure A.5 SEM of lengths and diameters of NCNTs after 120 minutes at 725°C

At 120 minutes of synthesis time at 725°C, the median length is 8 microns and the median diameter is 87 nanometers. The nanotubes have considerable iron nanoparticle decoration and bulbous sidewall structure.

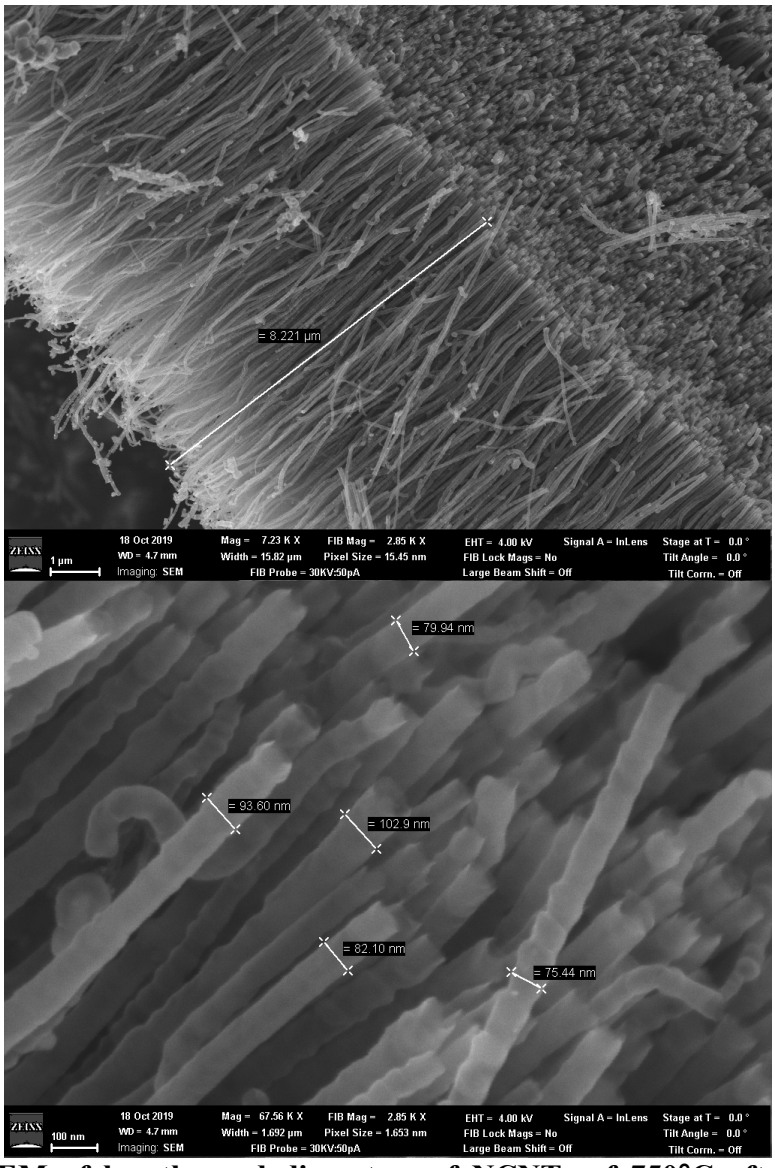

Figure A.6 SEM of lengths and diameters of NCNTs of 750°C after 15 minutes synthesis time

After 15 minutes synthesis time at 750°C, the NCNTs have clean walls with a bamboo structure. They have a median length of 4 microns, and a median diameter of 77 nm.

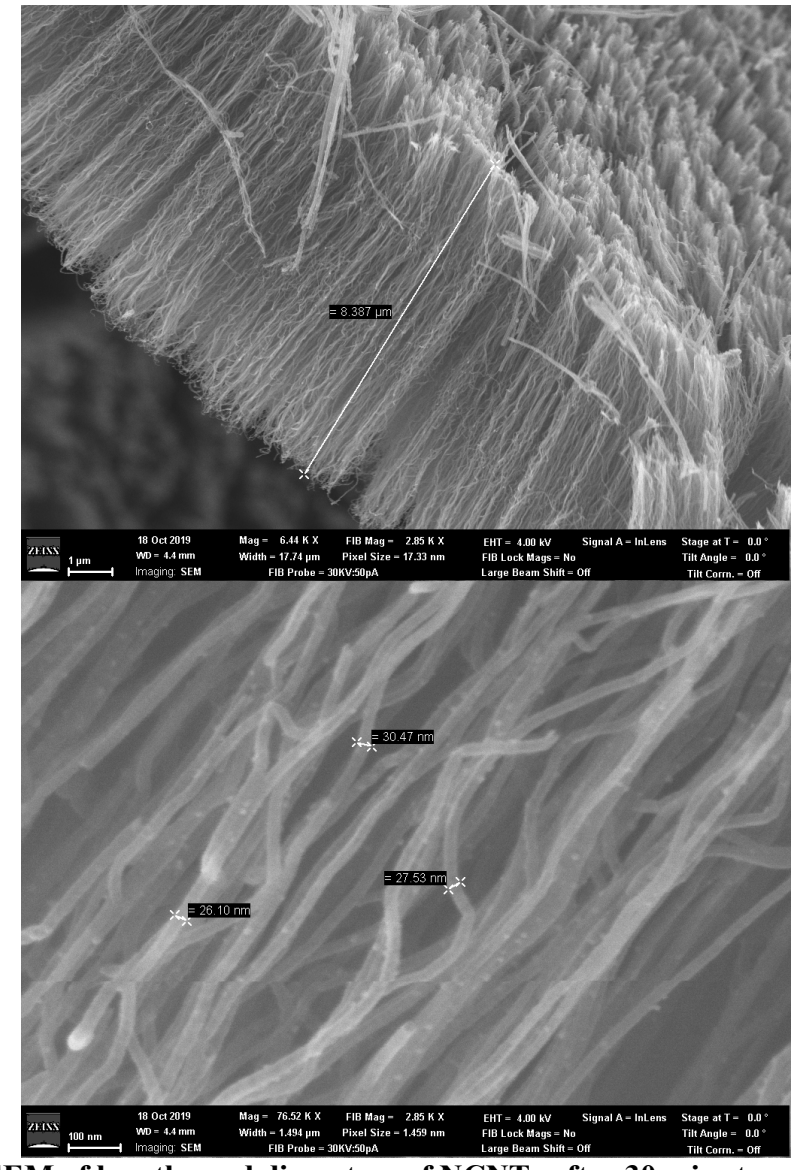

Figure A.7 SEM of lengths and diameters of NCNTs after 30 minutes at 750°C

After 30 minutes synthesis time at 750°C, the NCNTs show some iron decoration, and have a median length of 8 microns with a median diameter 24 nm.

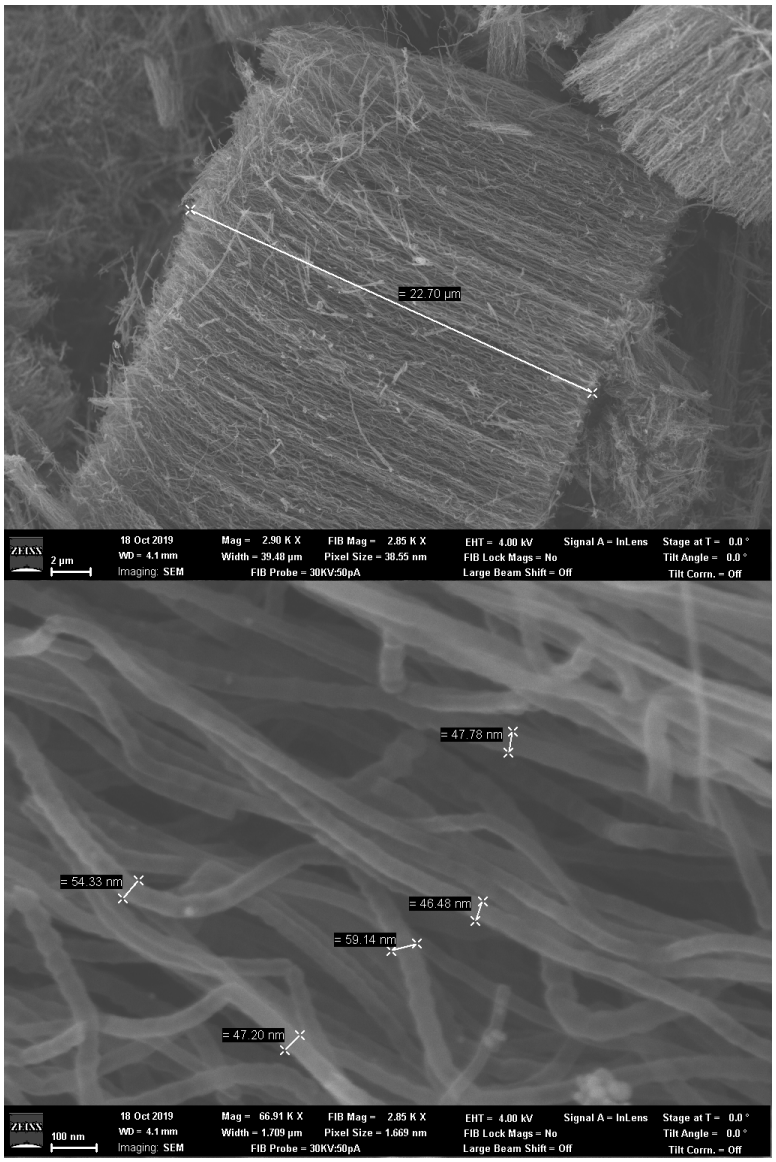

Figure A.8 SEM of lengths and diameters of NCNTs after 60 minutes at 750°C

The NCNTs synthesized after 60 minutes at 750°C, have a bulbous bamboo structure with very little iron decoration. The median length is 12 microns and the median diameter is 39 nm.

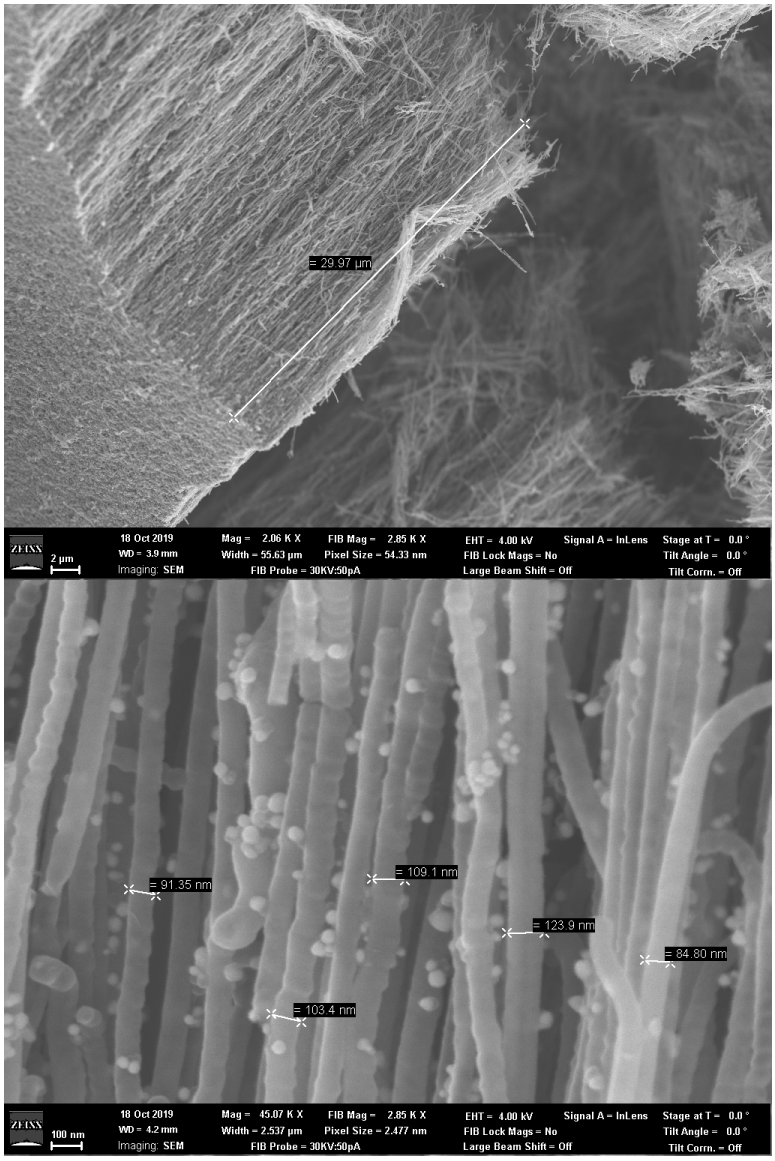

Figure A.9 SEM of lengths and diameters of NCNTs after 120 minutes at 750°C

After 120 minutes synthesis of the NCNTs at 750°C, there is iron decoration, and a bulbous structure. The NCNTs have a median length of 32 microns with a median diameter of 85 nm.

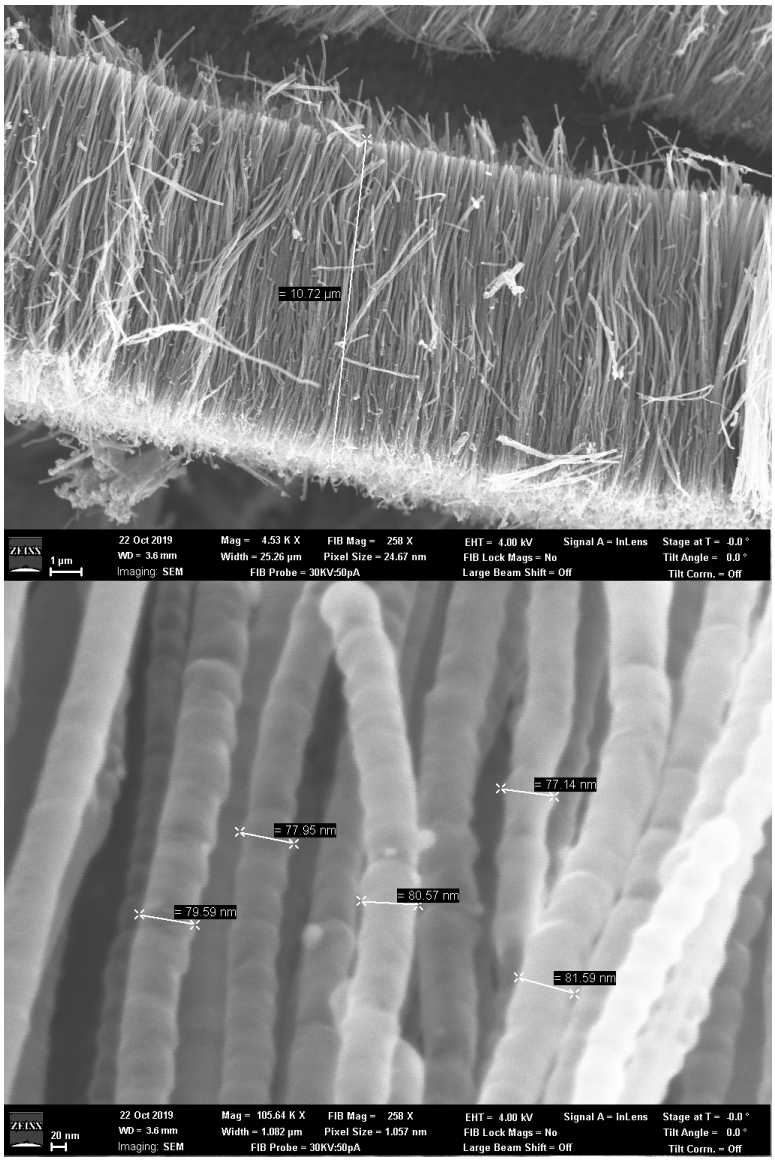

Figure A.10 SEM of lengths and diameters of NCNTs after 15 minutes at 775°C

After 15 minutes of synthesis time at 775°C, shows bulbous bamboo structured NCNTs without iron decoration. The NCNTs have a median length of 9 microns and a median diameter of 74 nm.

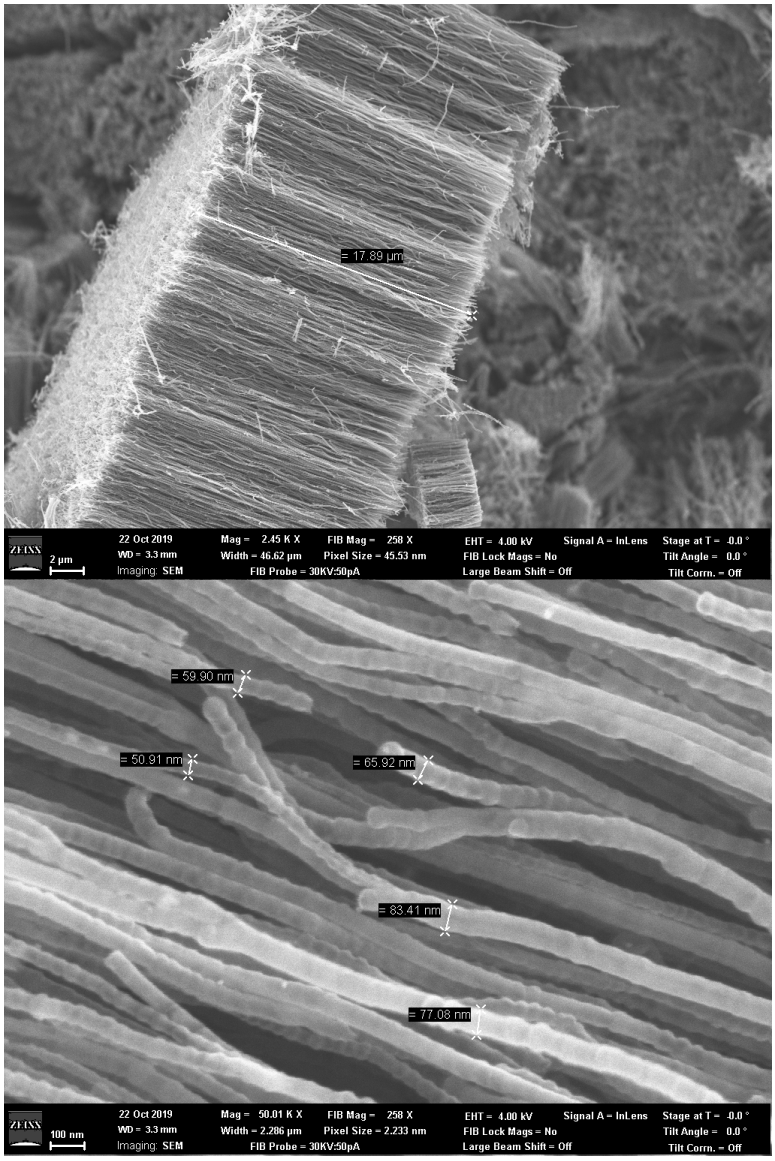

Figure A.11 SEM of lengths and diameters of NCNTs after 30 minutes at 775°C

After 30 minutes of synthesis time at 775°C, the NCNTs have a bulbous, bamboo structure with clean iron free sidewalls. The NCNTs have a median length of 15 microns and a median diameter of 69 nm.

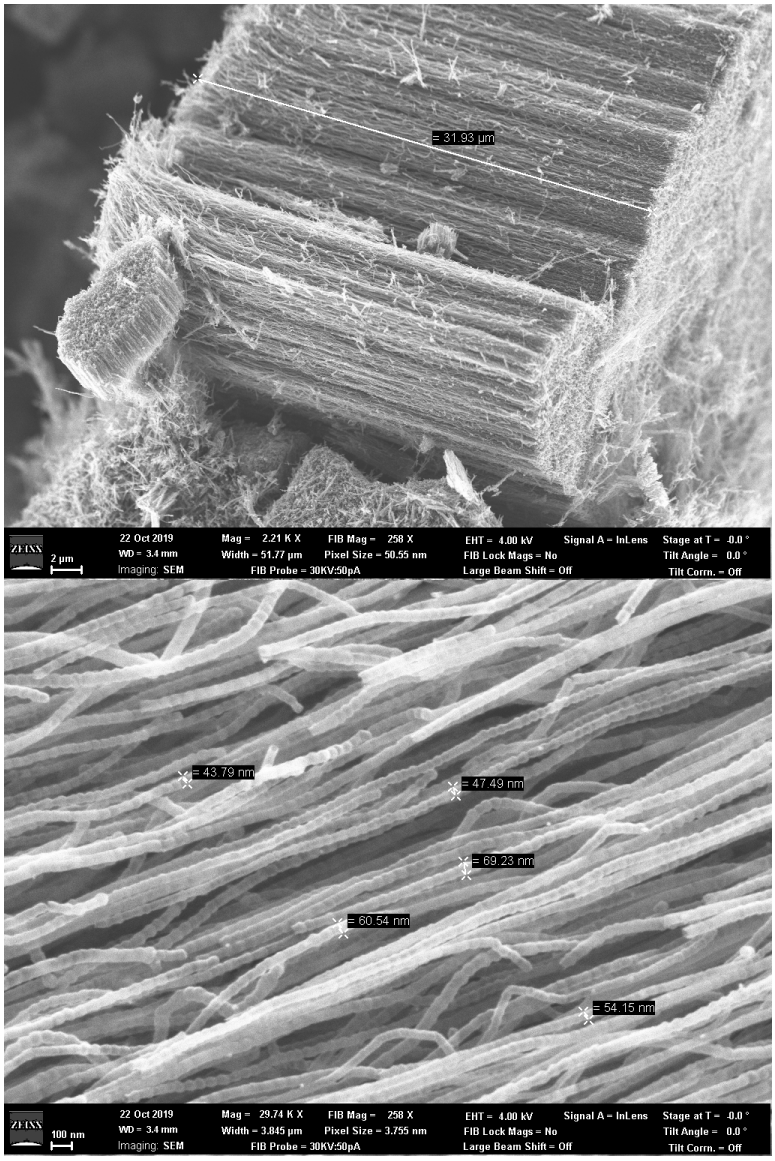

Figure A.12 SEM of lengths and diameters of NCNTs after 60 minutes at 775°C

After 60 minutes of synthesis at 775°C, the NCNTs have relatively clean sidewalls free from iron and maintain the bulbous, bamboo structure. The NCNTs have a median length of 33 microns and a median diameter of 60 nm.

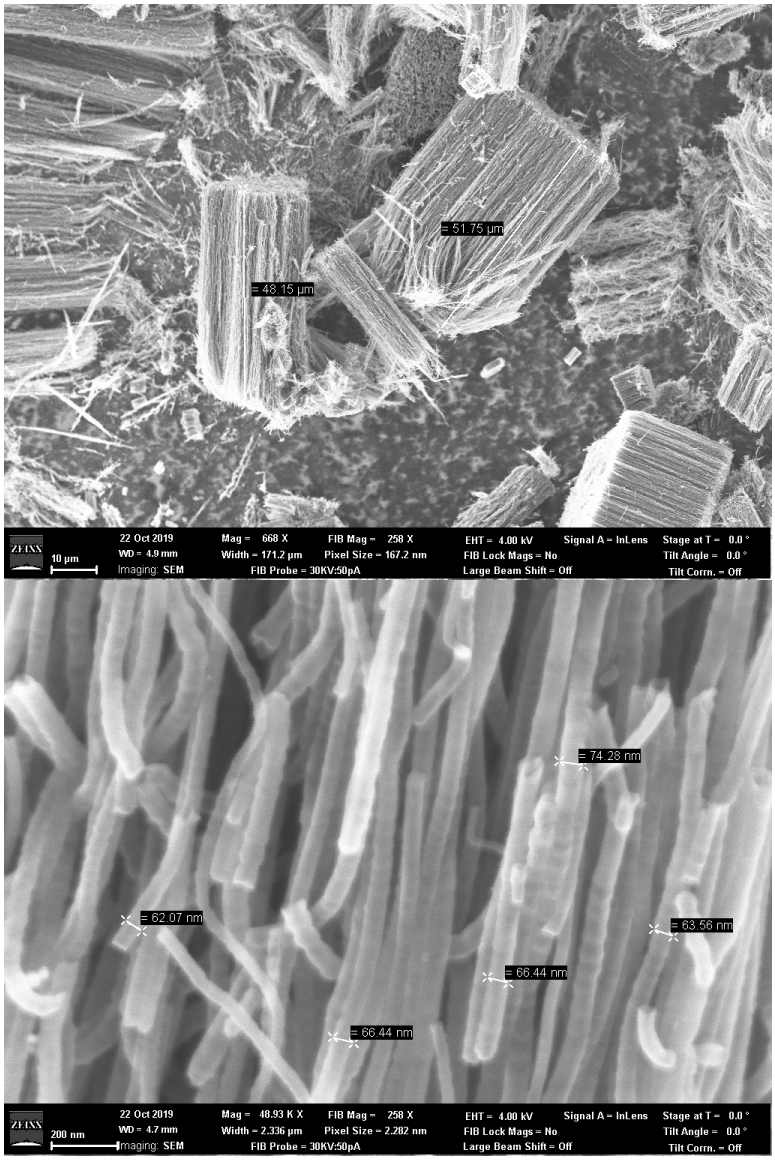

Figure A.13 SEM of lengths and diameters of NCNTs after 120 minutes at 775°C

After 120 minutes synthesis time at 775°C, the NCNTs synthesized remain somewhat free of iron in the sidewalls. The NCNTs still retain their bulbous, bamboo shape with a median length of 50 microns, and a median diameter of 62 nm.

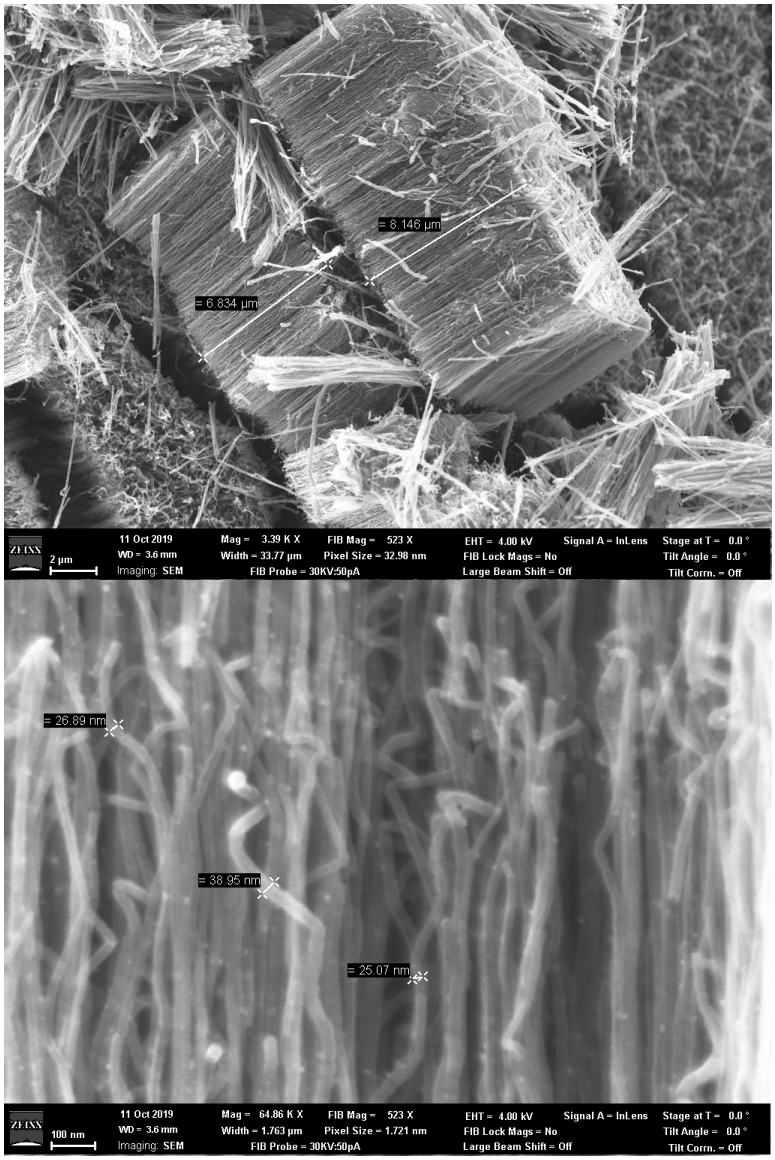

Figure A.14 SEM of lengths and diameters of NCNTs after 15 minutes at 800°C

After 15 minutes synthesis at 800°C, the NCNTs are less bulbous and have slightly smaller diameters with very light iron decoration. The NCNTs have a median length of 7 microns and a median diameter of 22 nm.

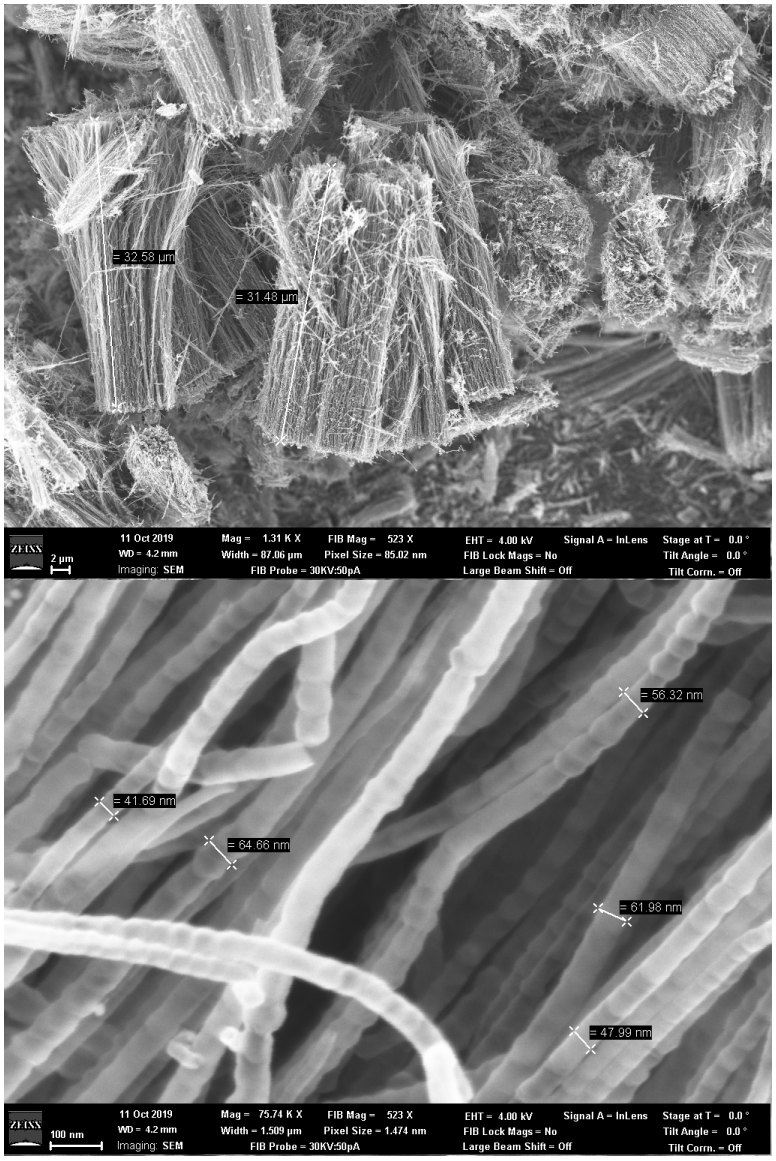

Figure A.15 SEM of lengths and diameters of NCNTs after 30 minutes at 800°C

After 30 minutes synthesis of NCNTs at 800°C, a bulbous structure is noted but no iron decoration. The NCNTs have a median length of 33 microns, and a median diameter of 59 nm.

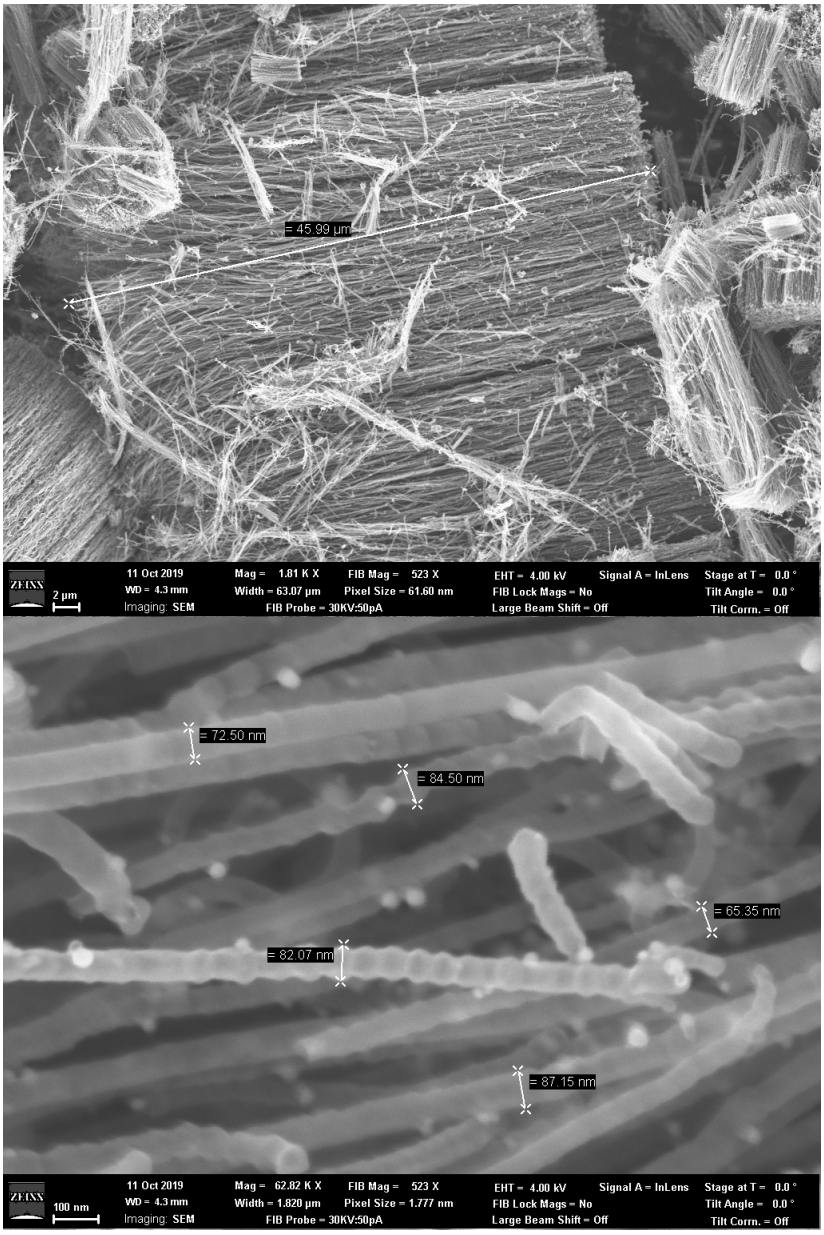

Figure A.16 SEM of lengths and diameters of NCNTs after 60 minutes at 800°C

After 60 minutes synthesis at 800°C, the NCNTs have a very bulbous structure and light iron decoration on the sidewalls. The NCNTs have a median length 49 microns and a median length of 82 nm.

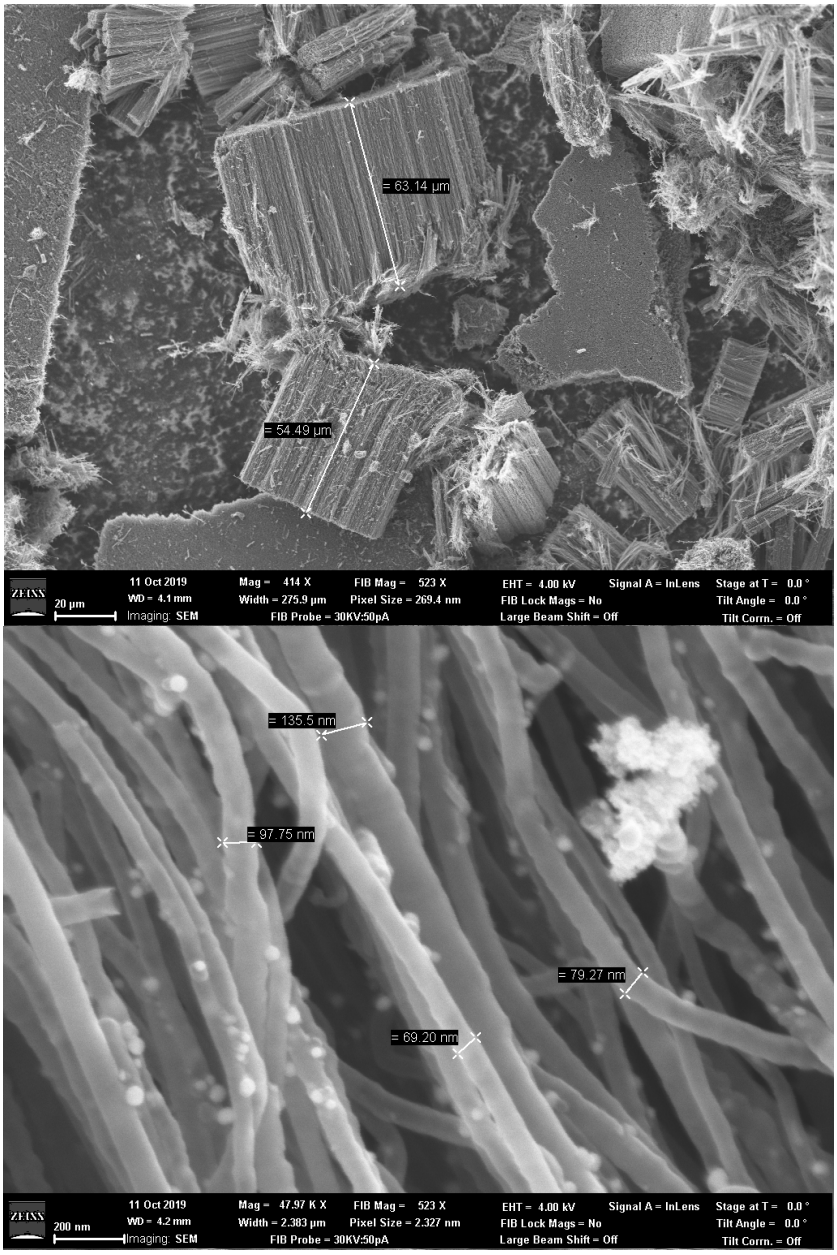

Figure A.17 SEM of lengths and diameters of NCNTs after 120 minutes at 800°C

After 120 minutes at 800°C, there is some iron decoration on the sidewalls, with a median length of 63 microns and a median diameter of 89 nm.

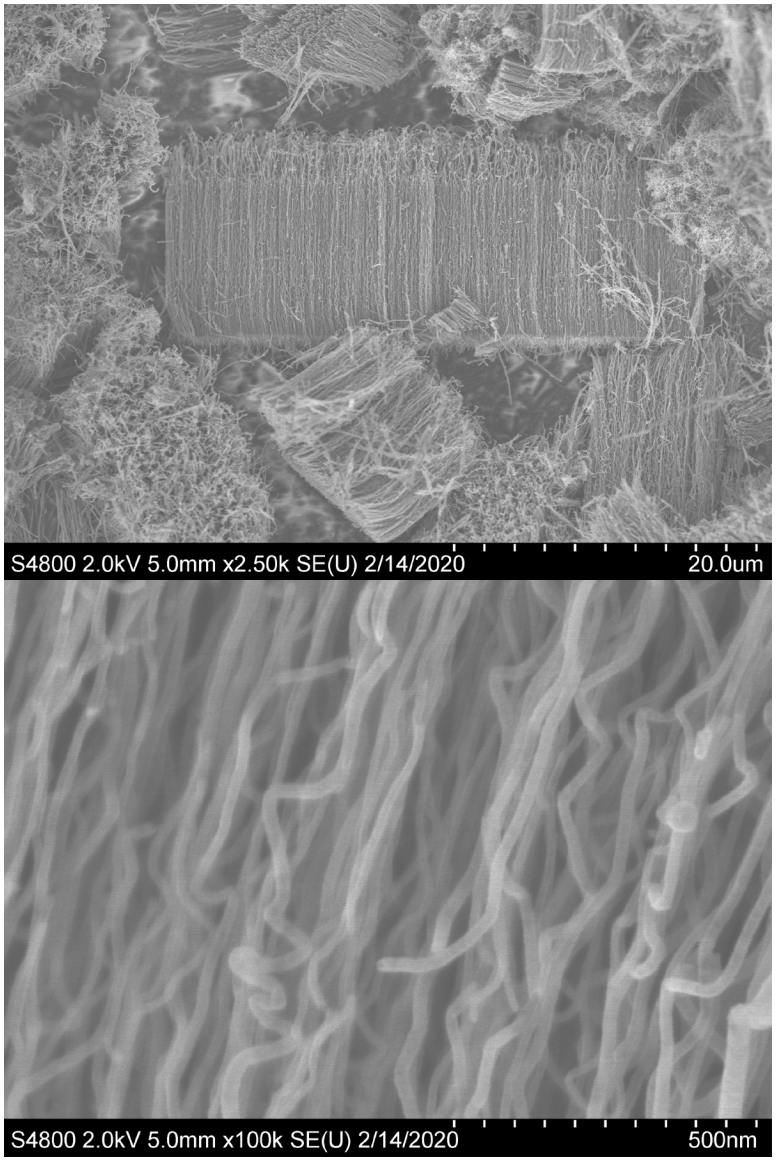

Figure A.18 SEM of lengths and diameters of NCNTs after 15 minutes at 825°C

After 15 minutes of NCNT synthesis at 825°C, the median length is 10 microns and the median diameter is 28 nanometers. The nanotubes are fairly clean from decoration at this time point.

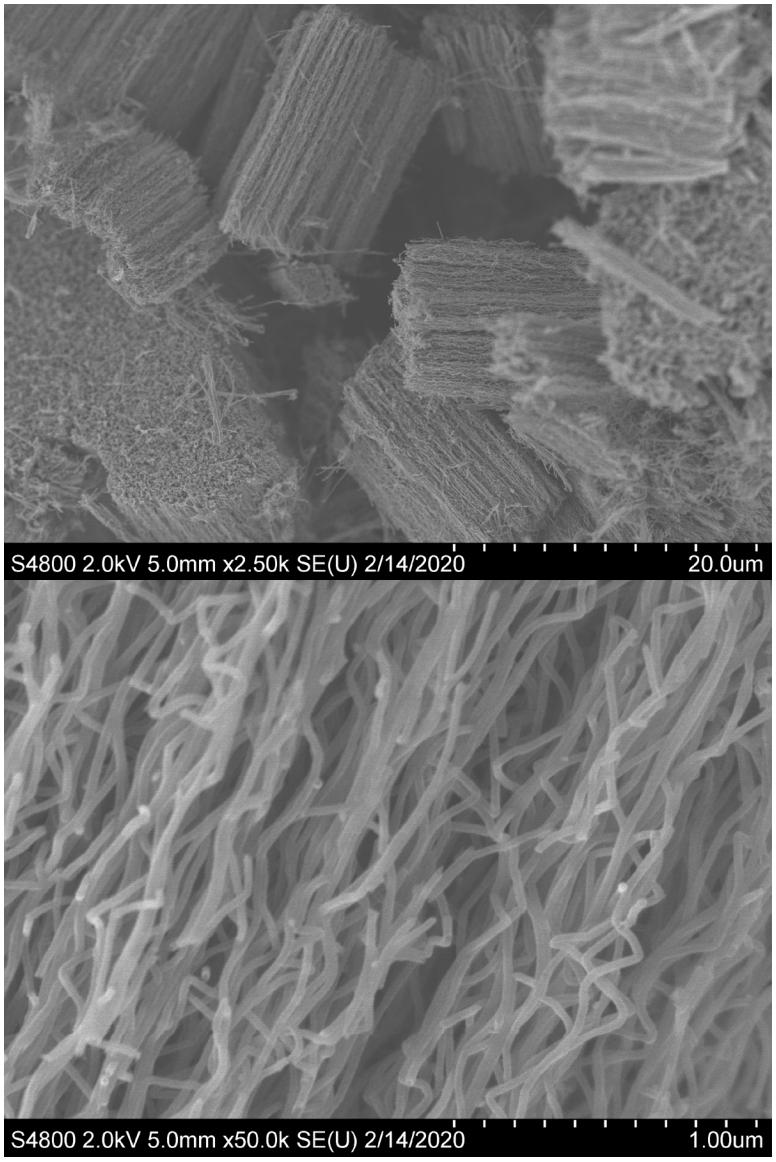

Figure A.19 SEM of lengths and diameters of NCNTs after 30 minutes of synthesis at 825°C

At 30 minutes of NCNT synthesis at 825°C, the median length is 12 microns and the median diameter is 38 nanometers. The nanotubes are still relatively clean at this time.

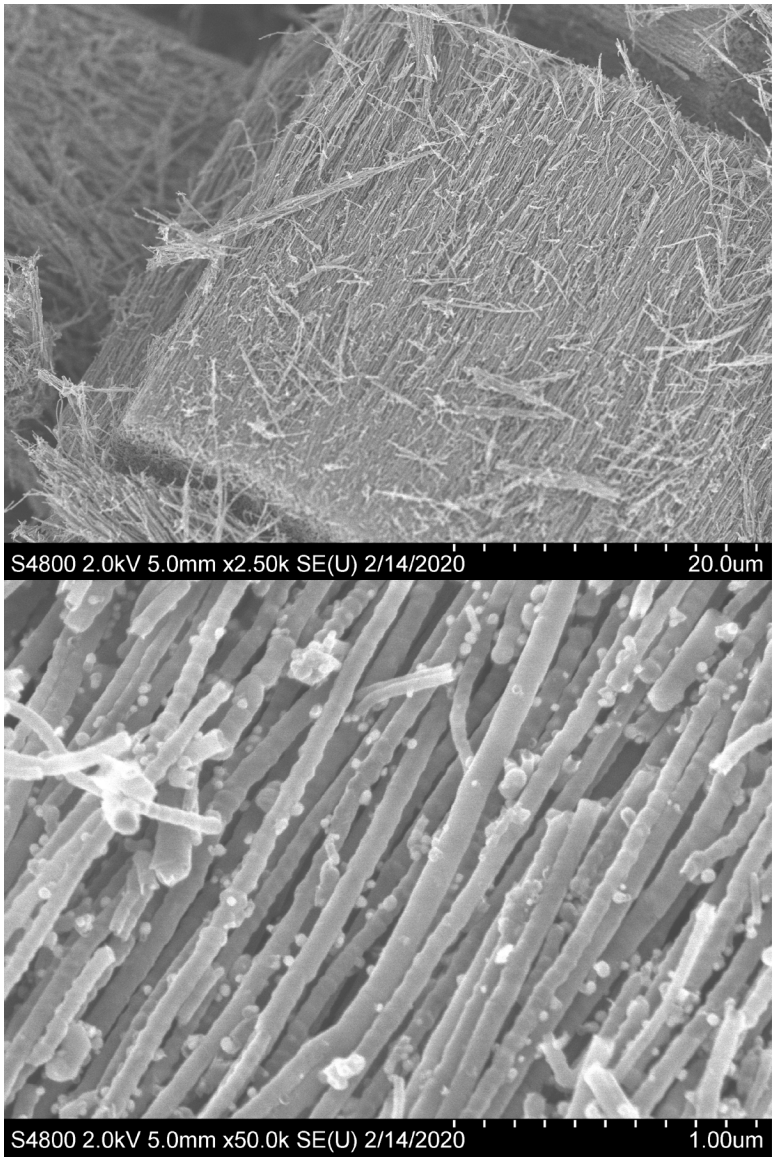

Figure A.20 SEM of lengths and diameters of NCNTs after 60 minutes at 825°C

After 60 minutes NCNT synthesis at 825°C, the median length is 48 microns and a median diameter of 72 nanometers. At this synthesis time, there is considerable iron nanoparticle decoration of the sidewalls.

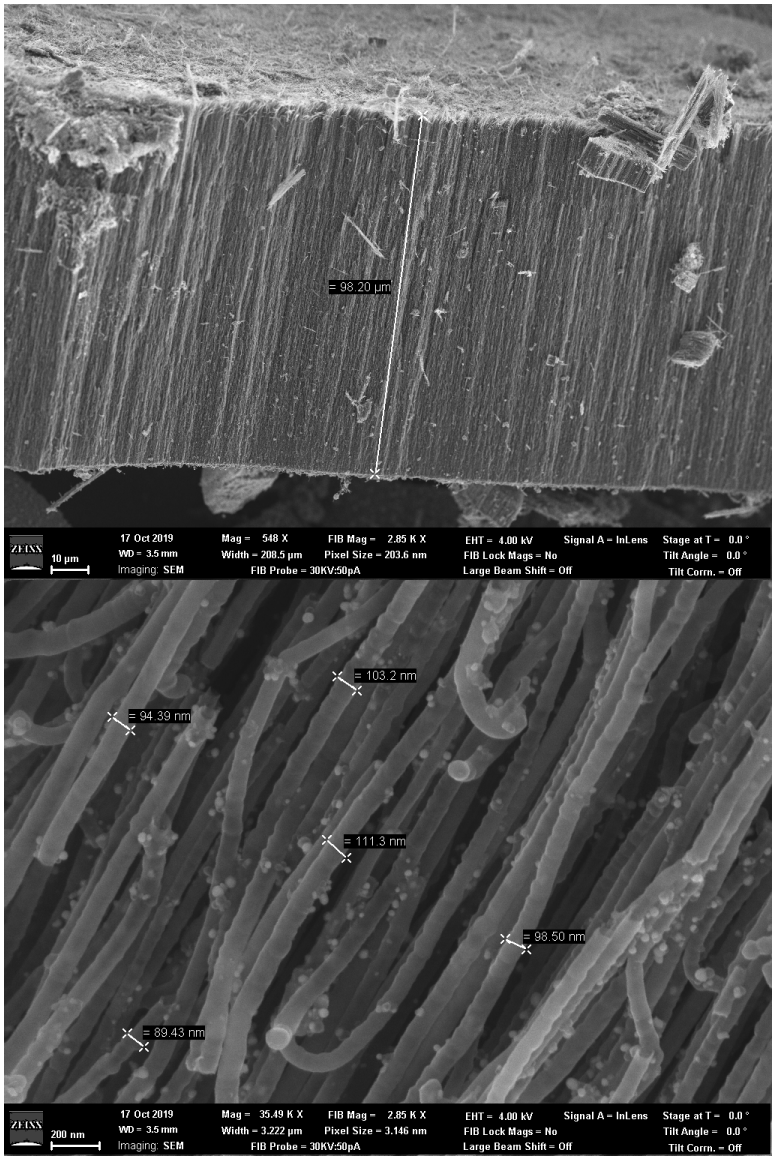

Figure A.21 SEM of lengths and diameters of NCNTs after 120 minutes of synthesis at 825°C

After 120 minutes of NCNT synthesis at 825°C, the median length is 91 microns and a median diameter of 92 nanometers. There is significant iron nanoparticle decoration on the bulbous NCNT sidewalls.

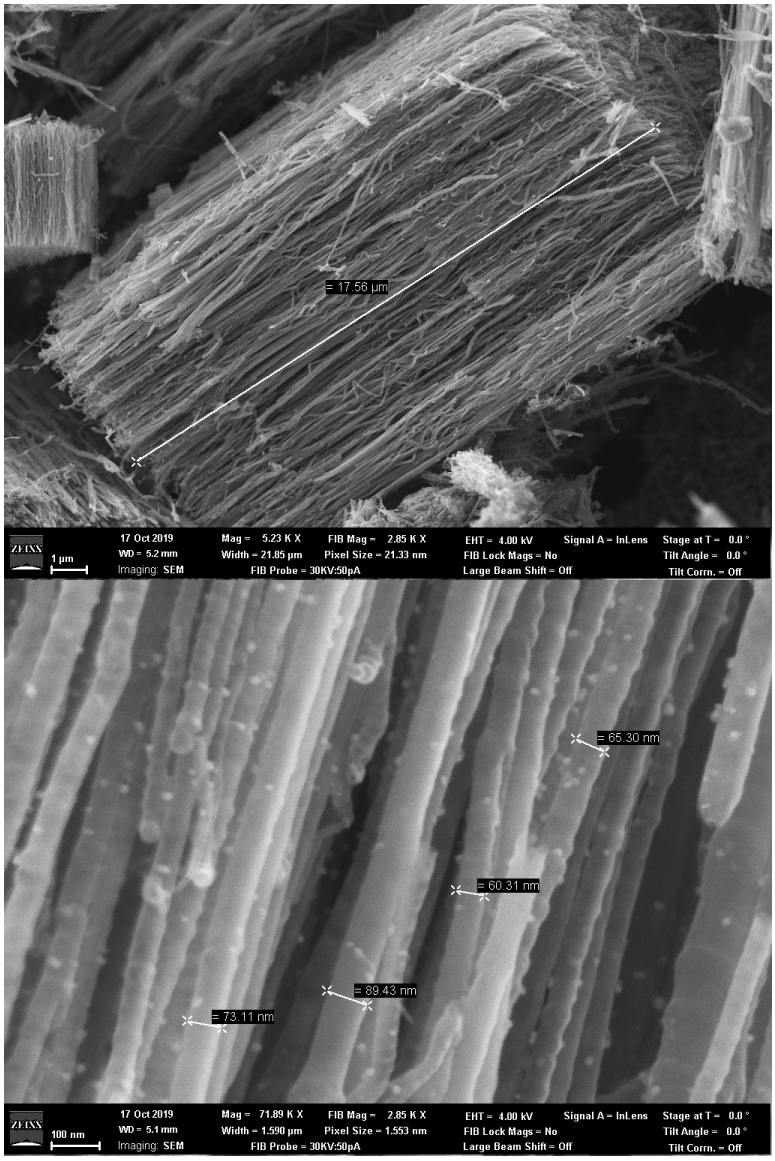

Figure A.22 SEM of lengths and diameters of NCNTs after 15 minutes at 850°C

There is some iron particle decoration after 15 minutes at 850°C with a median length of 26 microns and a median diameter of 65 nm.

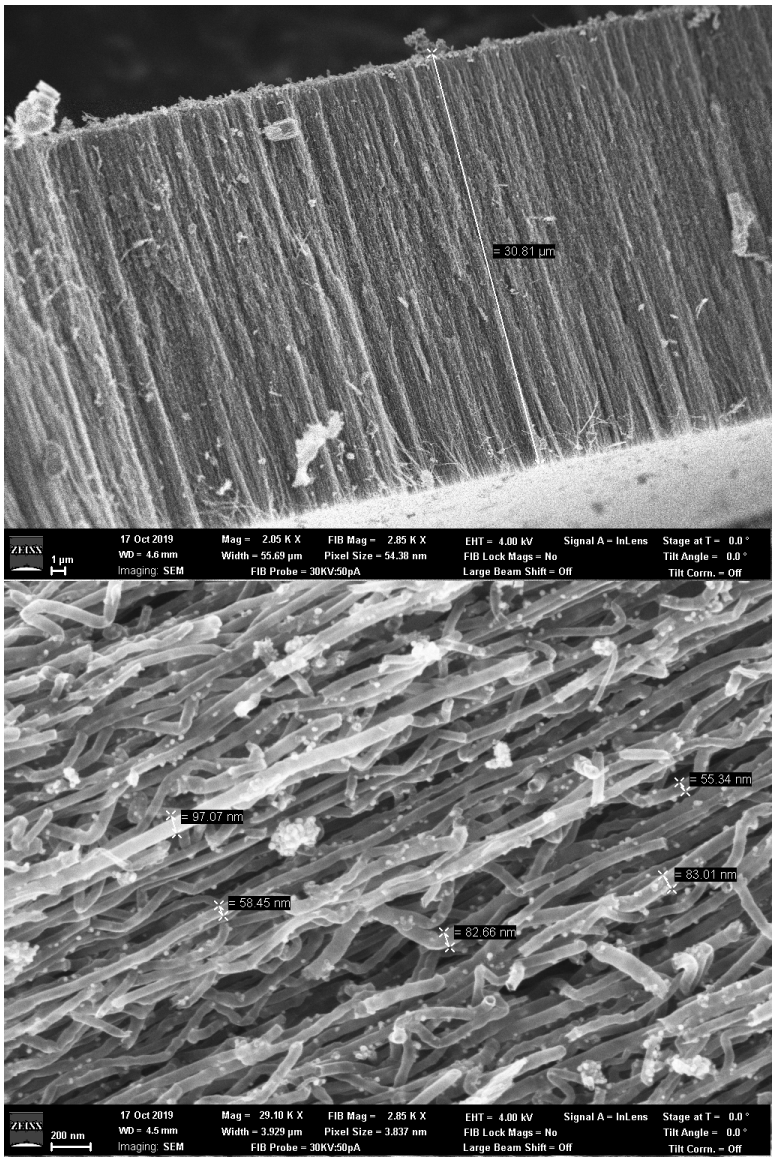

Figure A.23 SEM of lengths and diameters of NCNTs after 30 minutes at 850°C

Even after 30 minutes at 850°C there is iron decoration with a median length of 26 microns and a median diameter of 50 nm.

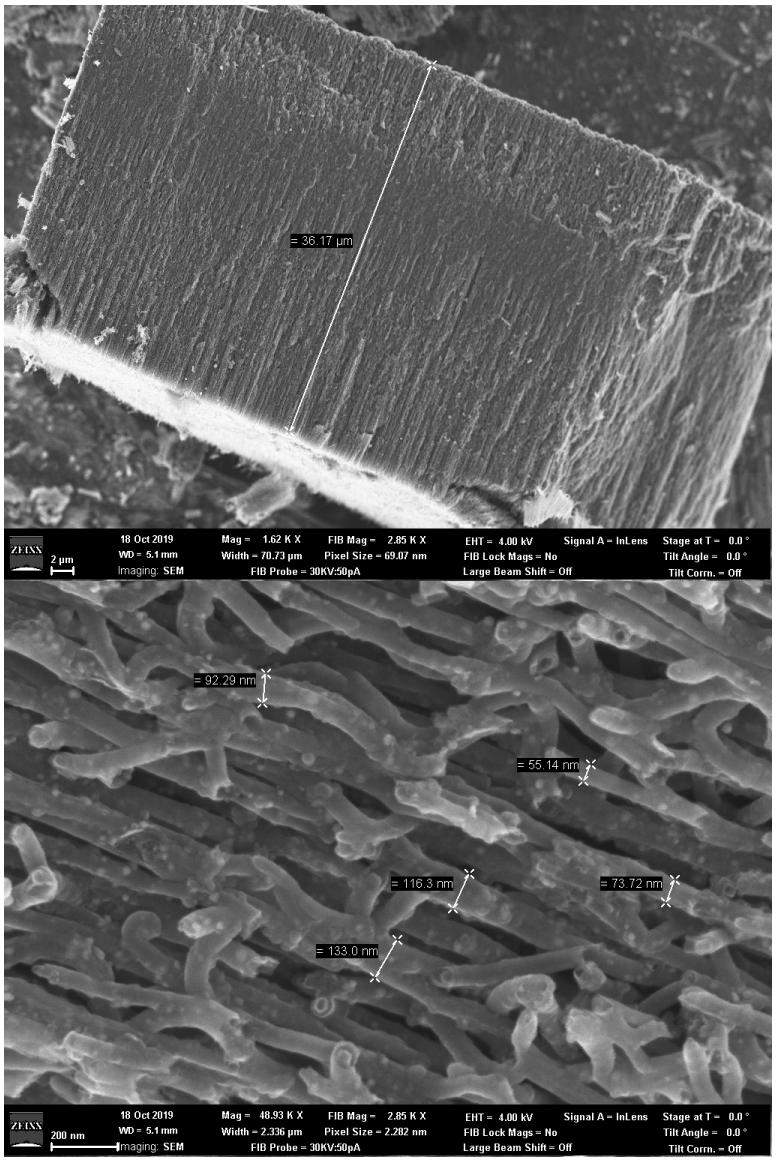

Figure A.24 SEM of lengths and diameters of NCNT after 60 minutes at 850°C

After 60 minutes at 850°C, significant sidewall degradation and branching starts occurring. The NCNTs have a median length of 28.5 microns and a median diameter of 73 nm.

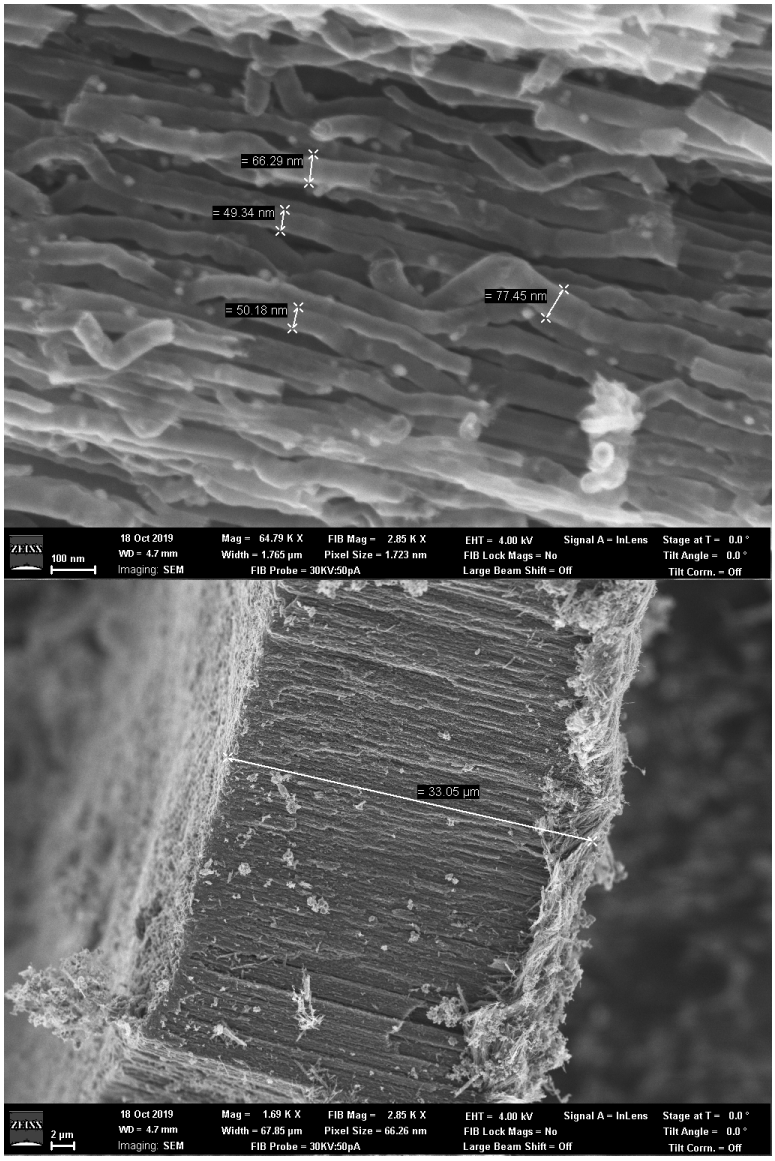

Figure A.25 SEM of lengths and diameters of NCNTs after 120 minutes at 850°C

After 120 minutes at 850°C, there is significant sidewall degradation and branching with iron particle decoration. The NCNTs have a median length of 33 microns with a median diameter of 60 nm.

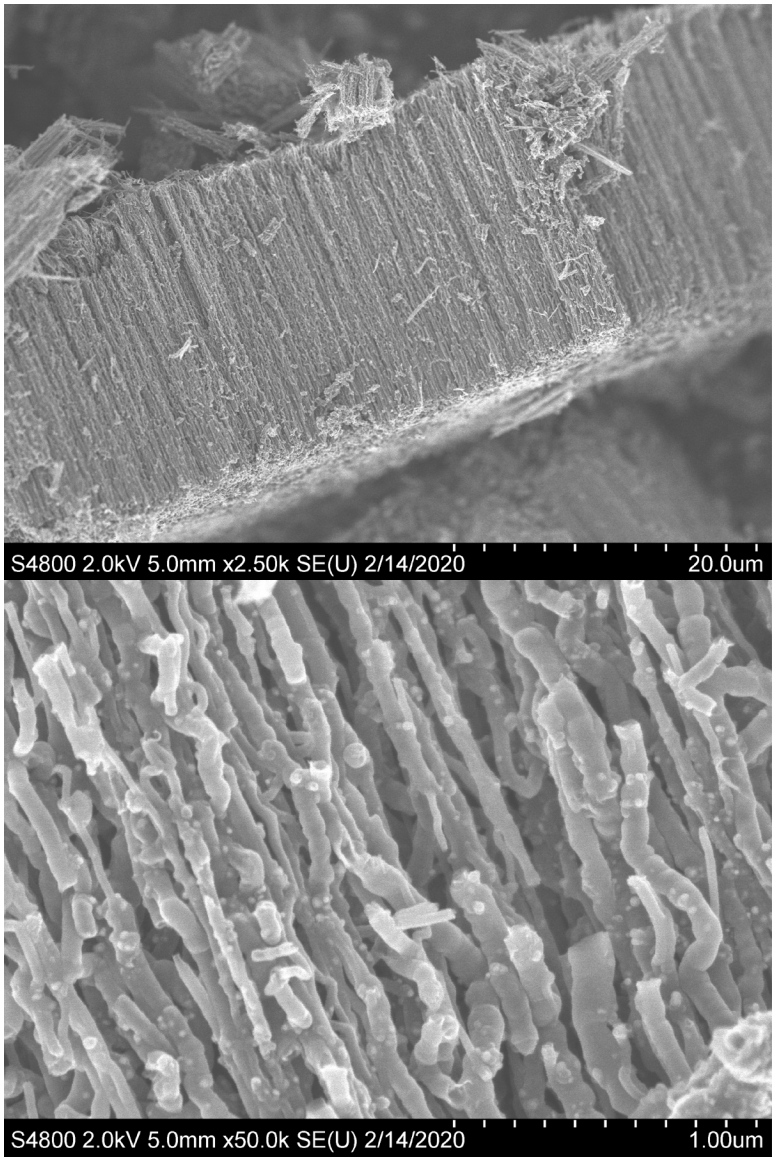

Figure A.26 SEM of lengths and diameters of NCNTs synthesized at 900°C for 30 minutes

In the initial study at 120 minutes no NCNT product was formed at 900°C. However after 30 minutes of synthesis there are NCNTs formed but there is extreme sidewall damage, branching, and sidewall to sidewall linking of nanotubes.

APPENDIX B XPS DATA

XPS data

sample no	time	Carbon	Nitrogen	temp	ln kN
3185-1	15	91.13	7.4	725	-15.952
3185-2	15	90.32	8.13	725	-15.858
3185-3	15	91.77	7.22	725	-15.981
3183-1	30	90.07	8.62	725	-15.819
3183-2	30	89.79	8.89	725	-15.566
3183-3	30	90.43	8.52	725	-15.610
3183-4	60	89.47	8.96	725	-15.495
3183-5	60	89.34	9.44	725	-15.447
3183-6	60	89.68	9.05	725	-15.321
mc3139-4	120	88.31	10.1	725	-15.295
mc3139-5	120	88.13	10.53	725	-15.180
mc3139-6	120	89.14	9.37	725	-15.370
mc3161-1	120	89.34	9.5	725	-15.443
mc3160-8	120	89.85	8.88	725	-15.466
mc3179-4	120	88.29	10.47	725	-15.304

sample no	time	Carbon	Nitrogen	temp	ln kN
3156-1	5	92.21	6.68	750	-15.629
3156-2	5	90.47	8.66	750	-15.375
3156-3	5	91.42	7.55	750	-15.508
3180-1	5	90.72	8.08	750	-15.440
3180-2	5	91.93	7.62	750	-15.505
3156-4	15	91	7.73	750	-15.911
3156-5	15	90.26	8.81	750	-15.786
3156-6	15	90.24	8.4	750	-15.828
3180-3	15	90.81	7.79	750	-15.902

3180-4	15	88.84	9.66	750	-15.689
3144-5	30	89.91	8.77	750	-15.109
3150-10	30	89.8	8.85	750	-15.388
3151-1	30	89.99	8.65	750	-15.123
3146-1	30	90.4	8.3	750	-15.297
3148-1	30	89.5	9.5	750	-15.322
3146-2	60	89.86	8.59	750	-15.450
3146-3	60	88.56	10.02	750	-15.300
3148-2	60	86.82	10.23	750	-15.264
3151-2	60	87.18	9.44	750	-15.185
3151-3	60	86.97	9.59	750	-15.168
3144-6	90	88.31	10.29	750	-15.241
3146-4	90	89.28	9.51	750	-15.374
3148-3	90	89.09	9.55	750	-15.426
3151-4	90	88.53	10.15	750	-15.155
3151-5	90	87.62	11.17	750	-15.162
mc3127-3	120	87.49	11.14	750	-15.125
mc3127-4	120	87.16	10.8	750	-15.266
mc3164-3	120	88.46	10.03	750	-15.227
mc3151-6	120	88.23	10.15	750	-15.291
mc3151-7	120	87.89	10.6	750	-15.210

sample no	time	Carbon	Nitrogen	temp	ln kN
3177-1	5	90.93	7.78	775	-15.476
3177-2	5	90.43	8.55	775	-15.385
3177-3	5	91.1	7.8	775	-15.475
3179-10	5	91.03	7.52	775	-15.508
3179-11	5	91.36	7.83	775	-15.474
3179-12	15	88.75	9.62	775	-15.286
3179-13	15	90.31	8.41	775	-15.422
3172-4	15	89.88	8.88	775	-15.774
3173-1	15	89.58	8.85	775	-15.369

3173-2	15	89.22	9.53	775	-15.705
3172-5	30	88.79	9.65	775	-15.146
3173-3	30	89.58	8.9	775	-15.226
3173-4	30	88.38	10.17	775	-15.095
3177-4	30	89.56	8.89	775	-15.093
3177-5	30	89.16	9.16	775	-15.196
3172-6	60	88.56	10.22	775	-15.128
3173-5	60	87.88	10.76	775	-15.150
3173-6	60	88.58	10.15	775	-15.134
3177-6	60	88.39	10.14	775	-15.287
3177-7	60	87.98	10.58	775	-15.166
3172-7	90	87.74	10.98	775	-15.178
3173-7	90	86.68	11.52	775	-15.126
3173-8	90	87.12	11.19	775	-15.209
3177-9	90	86.42	11.79	775	-15.052
3177-8	90	87.28	11.48	775	-15.189
mc3139-1	120	87.28	11.31	775	-15.038
mc3177-10	120	86.14	12.55	775	-14.972
mc3139-3	120	87.45	10.87	775	-15.145
mc3173-9	120	87.15	11.45	775	-15.061
mc3160-7	120	87.98	10.91	775	-15.042

sample no	time	Carbon	Nitrogen	temp	ln kN
3154-1	5	91.69	7.23	800	-15.550
3160-1	5	90.61	8.18	800	-15.427
3160-2	5	91.94	7.05	800	-15.576
3181-1	5	90.12	8.83	800	-15.353
3181-2	5	90.39	8.33	800	-15.408
3154-2	15	90.61	8.26	800	-15.441

3160-3	15	90.89	8.3	800	-15.440
3160-4	15	89.56	9.26	800	-15.328
3181-3	15	90.04	8.82	800	-15.376
3181-4	15	90.29	8.51	800	-15.411
3145-1	30	89.15	9.34	800	-15.333
3147-1	30	91.07	7.91	800	-15.347
3147-2	30	89.02	9.52	800	-15.027
3150-1	30	89.32	9.36	800	-15.178
3150-2	30	89.27	9.53	800	-15.162
3179-2	30	88.36	10.04	800	-15.107
3146-5	60	88.27	9.93	800	-15.081
3147-3	60	90.38	8.51	800	-15.309
3150-3	60	90.5	8.39	800	-15.323
3151-8	60	88.19	10.31	800	-15.116
3154-3	60	88.47	10.02	800	-15.299
3179-3	60	88.32	10.49	800	-15.177
3179-5	60	87.72	10.73	800	-15.151
3146-6	90	87.56	10.8	800	-15.139
3160-5	90	87.58	10.71	800	-15.252
3164-1	90	88.13	10.64	800	-15.209
3145-2	90	88.27	10.52	800	-15.121
3150-5	90	87.92	10.52	800	-15.271
mc3150-4	90	87.12	10.91	800	-15.231
mc3163-3	120	87.53	10.6	800	-15.373
mc3125-1	120	86.84	11.62	800	-15.487
mc3125-2	120	86.75	11.58	800	-15.288
mc3119-2	120	86.91	11.3	800	-15.267
mc3150-9	120	87.35	11.36	800	-15.224

sample no	time	Carbon	Nitrogen	Temp	ln kN
3184-1	15	90.82	8.14	825	-15.457
3184-2	15	90.45	8.38	825	-15.427
3184-3	15	89.32	9.07	825	-15.750
3184-4	30	88.86	9.69	825	-15.479
3184-5	30	88.89	9.53	825	-15.495
3184-6	30	88.05	10.75	825	-15.198
3184-7	60	87.7	10.82	825	-15.310
3184-8	60	87.33	11.18	825	-15.191
3184-9	60	88.84	10	825	-15.391
mc3138-1	120	89.26	9.32	825	-15.599
mc3138-2	120	89.42	9.17	825	-15.615
mc3163-4	120	88.65	9.9	825	-15.316
mc3161-2	120	88.8	9.5	825	-15.395
mc3161-3	120	89.01	9.36	825	-15.593

sample no	Time	Carbon	Nitrogen	temp	ln kN
3156-7	5	92.47	6.66	850	-15.645
3156-8	5	90.73	7.35	850	-15.537
3156-9	5	92.75	6.1	850	-15.729
3181-5	5	91.25	7.68	850	-15.503
3181-6	5	90.92	7.92	850	-15.471
3172-1	10	90.91	7.58	850	-15.523
3172-2	10	90.94	7.7	850	-15.509
3172-3	10	91.26	7.39	850	-15.549
3156-10	15	89.96	8.96	850	-15.767
3156-11	15	89.3	9.61	850	-15.698
3156-12	15	90.25	8.58	850	-15.404
3179-1	15	90.98	8.12	850	-15.461

3181-7	15	90.9	7.7	850	-15.914
3146-7	30	90.08	8.69	850	-15.589
3144-3	30	90.35	8.7	850	-15.591
3152-2	30	90.04	8.22	850	-15.862
3147-4	30	90.71	8.39	850	-15.850
3152-1	30	89.29	9.32	850	-15.742
3140-5	60	88.61	10.05	850	-15.385
3152-4	60	89.69	8.61	850	-15.852
3152-3	60	90.04	8.5	850	-15.548
3150-6	60	89.87	8.73	850	-15.975
3140-6	60	88.29	10.39	850	-15.671
3144-4	90	90.08	8.66	850	-15.872
3146-8	90	91	7.47	850	-16.197
3147-5	90	89.79	9.04	850	-16.236
3151-9	90	90.05	8.79	850	-16.040
3150-7	90	90.13	8.79	850	-16.146
mc3127-6	120	90.24	8.53	850	-16.046
mc3150-8	120	90.87	8.31	850	-16.230
mc3151-10	120	90.51	8.6	850	-15.907
mc3127-5	120	90.79	8.23	850	-16.325
mc3092-1	120	90.16	8.71	850	-16.100

sample no	time	temp	Pyridinic	Graphitic	Fe-N	Pyr-Ox	Nox
3185-1	15	725	46.96	28.2	7.11	11.33	6.4
3185-2	15	725	45.03	27.37	10.54	10.94	6.12
3185-3	15	725	46.43	28.55	9.29	8.95	6.78
3183-1	30	725	50.74	27.55	5.33	9.63	6.75
3183-2	30	725	49.64	28.28	7.15	8.89	6.05
3183-3	30	725	46	27.9	10.88	9.1	6.12
3183-4	60	725	49.18	27.06	7.48	9.69	6.6
3183-5	60	725	46.59	29.48	7.88	10.11	5.93
3183-6	60	725	46.87	29.08	9.63	9.9	4.52

mc3139-4	120	725	41.29	30.12	11.93	10.42	6.24
mc3139-5	120	725	45	30.19	8.08	10.41	6.32
mc3139-6	120	725	43.64	29.98	8.5	11.64	6.24
mc3161-1	120	725	44.29	30.39	9.41	11.46	4.45
mc3160-8	120	725	44.56	30.54	7.24	10.69	6.96
mc3179-4	120	725	46.78	30.95	8.16	9.23	4.87

sample no	time	temp	Pyridinic	Graphitic	Fe-N	Pyr-Ox	Nox
3156-1	5	750	45.16	29.08	7	11.87	6.89
3156-2	5	750	45.33	29.23	9.88	10.04	5.52
3156-3	5	750	44.61	28.68	7.62	11.48	7.61
3180-1	5	750	44.48	32.82	10.6	6.59	5.51
3180-2	5	750	45.13	28.16	10.11	10.12	6.49
3156-4	15	750	45.45	28.63	9.59	10.58	5.75
3156-5	15	750	45.41	29	9.92	10.87	4.8
3156-6	15	750	44.47	27.39	9.63	12.23	6.28
3180-3	15	750	47.5	24.85	9.67	10.76	7.23
3180-4	15	750	47.13	25.33	9.3	11.34	6.89
3144-5	30	750	46.45	27.99	8.24	11.21	6.11
3150-10	30	750	48.37	29.43	6.49	8.63	7.08
3151-1	30	750	45.85	29.5	6.5	11.06	7.09
3146-1	30	750	45.85	29.23	7.22	10.97	6.74
3148-1	30	750	47.4	27.59	9.05	9.93	6.04
3146-2	60	750	44.74	31.58	6.07	11.21	6.41
3146-3	60	750	46.64	31.29	4.87	10.53	6.69
3148-2	60	750	48.7	31.07	5.68	9.43	5.11
3151-2	60	750	46.75	29.72	5.94	10.56	7.02

3151-3	60	750	48.28	31.35	4.76	9.59	6.02
mc3127-3	120	750	46.4	28.65	8.68	11.45	4.81
mc3127-4	120	750	44.72	31.46	8.47	10.64	4.71
mc3164-3	120	750	48.86	32.45	5.06	8.26	5.37
mc3151-6	120	750	47.76	31.85	6.78	6	7.61
mc3151-7	120	750	47.57	32.32	6.2	8.52	5.39

sample no	time	temp	Pyridinic	Graphitic	Fe-N	Pyr-Ox	Nox
3177-1	5	775	45.44	29.3	9.9	9.4	5.96
3177-2	5	775	44.67	27.22	11.5	11.05	5.56
3177-3	5	775	45.26	29.56	9.93	10.29	4.96
3179-10	5	775	44.04	27.69	7.99	11.53	8.75
3180-5	5	775	46.12	28.68	7.67	9.97	7.57
3180-7	15	775	48.92	27.71	8.72	9.24	5.41
3180-8	15	775	45.97	27.63	10.22	10.35	5.84
3172-4	15	775	47.25	27.51	8.83	9.62	6.79
3173-1	15	775	44.97	28.42	7.75	11.12	7.75
3173-2	15	775	48.43	28.25	6.82	11.52	4.98
3172-5	30	775	46.79	35.55	5.52	8.02	4.13
3173-3	30	775	46.5	29.28	8.55	9.39	6.28
3173-4	30	775	47.08	26.74	9.05	9.79	7.34
3177-4	30	775	45.61	29.38	8.34	10.07	6.61
3177-5	30	775	47.78	28.57	7	11.18	5.46
3172-6	60	775	47.44	30.49	8.2	9.71	4.16
3173-5	60	775	45.04	32.23	8.03	9.47	5.23
3173-6	60	775	48.57	30.82	6.74	8.77	5.1
3177-6	60	775	46.46	30.65	7.2	10.87	4.82
3177-7	60	775	47.18	30.93	7.64	9.68	4.57
3172-7	90	775	49.17	33.21	5.52	6.67	5.43
3173-7	90	775	46.73	31.21	7.48	9.39	5.19
3173-8	90	775	47.91	32.19	6.17	8.87	4.86
3177-9	90	775	49.84	32.4	5.45	7.24	5.07
3177-8	90	775	48.22	30.41	7.23	10.44	3.69

mc3139-1	120	775	46.16	29.86	8.33	10.43	5.22
mc3177-10	120	775	48.52	31.83	6.84	8.88	3.93
mc3139-3	120	775	46.23	29.04	8.36	10.2	6.18
mc3173-9	120	775	46.69	30.32	5.05	11.27	6.68
mc3160-7	120	775	48.06	30.54	7.3	8.97	5.13

sample no	time	temp	Pyridinic	Graphitic	Fe-N	Pyr-Ox	Nox
3154-1	5	800	43.08	28.92	7.48	11.71	8.8
3160-1	5	800	44.21	29.39	7.61	12.1	6.67
3160-2	5	800	40.53	28.09	8.71	10.81	11.86
3181-1	5	800	47.03	26.79	8	10.73	7.44
3181-2	5	800	45.8	29.15	7.42	10.67	6.95
3154-2	15	800	42.99	30.78	6.41	11.13	8.69
3160-3	15	800	42.93	30.54	7.4	12.27	6.86
3160-4	15	800	46.14	30.22	7	9.42	7.21
3181-3	15	800	43.71	28.93	7.53	11.58	8.25
3181-4	15	800	45.23	27.81	7.67	11.57	7.72
3145-1	30	800	46.33	30.03	7.46	10.18	6
3147-1	30	800	41.87	31.98	8.1	9.56	8.49
3147-2	30	800	48.18	30.16	6.64	9.41	5.61
3150-1	30	800	46.69	30.72	8.92	9.38	4.29
3150-2	30	800	47.1	30.58	5.26	10.22	6.84
3179-2	30	800	45.3	30.51	7.84	9.16	7.19
3146-5	60	800	48.26	31.47	5.15	10.01	5.12
3147-3	60	800	45.2	31.15	6.82	10.15	6.66
3150-3	60	800	46.01	32.38	6	10.12	5.49
3151-8	60	800	47.73	28.69	8.53	9.4	5.65
3154-3	60	800	49.12	30.28	5.2	9.29	6.1
3179-3	60	800	48.02	32.1	6.25	8.45	5.18
3179-5	60	800	49.83	31.37	5.37	7.88	5.54

mc3163-3	120	800	49.03	33.12	6.46	7.75	3.63
mc3125-1	120	800	47.57	30.17	6.03	10.76	5.47
mc3125-2	120	800	48.26	29.26	6.26	11.15	5.07
mc3119-2	120	800	45.78	31.69	8.18	9	5.35
mc3150-9	120	800	48.28	31.53	5.54	9.96	4.69

sample no o2	time	temp	Pyridinic	Graphitic	Fe-N	Pyr-Ox	Nox
3184-1	15	825	46.3	27.88	7.05	10.46	8.31
3184-2	15	825	45.51	28.43	8.11	12.45	5.49
3184-3	15	825	46.82	28.91	6.47	10.81	7
3184-4	30	825	49.11	30.51	5.47	8.41	6.5
3184-5	30	825	48.18	30.82	5.74	7.82	7.43
3184-6	30	825	45.16	32.6	6.74	9.36	6.13
3184-7	60	825	47.04	32.55	6.03	8.47	5.9
3184-8	60	825	49.68	30.44	4.97	7.99	6.92
3184-9	60	825	49.13	30.85	4.76	8.67	6.59
mc3138-1	120	825	44.71	32.11	6.38	9.7	7.1
mc3138-2	120	825	42.58	32.21	6.94	11.52	6.74
mc3163-4	120	825	47.23	32.6	5.96	7.87	6.34
mc3161-2	120	825	47.05	32.63	5.1	9.44	5.77
mc3161-3	120	825	47.22	30.33	5.79	9.38	7.28

sample no	time	temp	Pyridinic	Graphitic	Fe-N	Pyr-Ox	Nox
3156-7	5	850	34.86	30.14	6.99	11.36	16.65
3156-8	5	850	43.87	30.37	5.41	10.4	9.94
3156-9	5	850	37.17	29.28	9.12	10.74	13.69
3181-5	5	850	40.25	27.98	9.37	9.45	12.95
3181-6	5	850	44.67	29.24	8.34	9.3	8.45
3156-10	15	850	44.26	33.33	7.2	8.34	6.87
3156-11	15	850	48.12	33.71	2.93	9.44	5.78
3156-12	15	850	45.23	32.23	5.78	10.2	6.57

mc3179-1	15	850	40.02	32.78	10.29	10.64	6.27
3181-7	15	850	43.38	32.89	7.57	9.51	6.64
3146-7	30	850	43.86	35.19	7.55	8.51	4.88
3144-3	30	850	43.57	33.32	6.56	10.53	6.03
3152-2	30	850	44.74	32.44	5.5	10.46	6.86
3147-4	30	850	46.79	31.79	7.21	8.1	6.11
3152-1	30	850	44.42	32.96	5.5	9.98	7.14
3140-5	60	850	50.2	30.44	5.97	7.97	5.41
3152-4	60	850	44.73	33.48	5.57	10.51	5.71
3152-3	60	850	45.85	31.04	5.55	9.63	7.92
3150-6	60	850	45.89	33.34	7.41	7.4	5.96
3140-6	60	850	46.32	28.69	9.76	9.88	5.36
mc3127-6	120	850	42.59	32.21	7.79	12.23	5.17
mc3150-8	120	850	44.84	30.16	10.47	9.64	4.9
mc3151-10	120	850	39.52	32.01	12.39	10	6.08
mc3127-5	120	850	43.46	35.59	8.96	7.24	4.74
mc3092-1	120	850	43.07	33.64	7.89	9.43	5.97

De-doping study

sample	time min	Temp C	Temp K	1/t (1/k)	N at. %	ln kN
mc3163-3	0	700	973	0.001028	10.6	-16.01
700-15	15	700	973	0.001028	10.09	-16.4128
700-30	30	700	973	0.001028	10.37	-17.0802
700-60	60	700	973	0.001028	9.58	-17.8532
700-120	120	700	973	0.001028	8.4	-18.6852
700-180	180	700	973	0.001028	9.8	-18.9453
700-15b	15	700	973	0.001028	10.71	-16.3516
700-30b	30	700	973	0.001028	9.79	-17.1448
700-60b	60	700	973	0.001028	10.57	-17.7591
700-120b	120	700	973	0.001028	9.74	-18.5399
700-180b	180	700	973	0.001028	9.45	-18.9771
700-15c	15	700	973	0.001028	10.54	-16.3737

700-30c	30	700	973	0.001028	9.89	-17.1322
700-60c	60	700	973	0.001028	9.51	-17.865
700-120c	120	700	973	0.001028	9.42	-18.5729
700-180c	180	700	973	0.001028	9.08	-19.0199
700-15d	15	700	973	0.001028	10.54	-16.3737
700-30d	30	700	973	0.001028	10.13	-17.1098
700-60d	60	700	973	0.001028	9.84	-17.8327
700-120d	120	700	973	0.001028	9.31	-18.5842
700-180d	180	700	973	0.001028	8.15	-19.1277
3173-7	0	750	1023	0.000978	11.52	
750-15a	15	750	1023	0.000978	10.46	-16.3827
750-30a	30	750	1023	0.000978	10.7	-17.0542
750-60a	60	750	1023	0.000978	9.82	-17.8377
750-120a	120	750	1023	0.000978	9.04	-18.6167
750-180a	180	750	1023	0.000978	9.07	-19.0226
750-15b	15	750	1023	0.000978	10.33	-16.3958
750-30b	30	750	1023	0.000978	10.23	-17.1033
750-60b	60	750	1023	0.000978	9.8	-17.8409
750-120b	120	750	1023	0.000978	8.57	-18.6675
750-180b	180	750	1023	0.000978	8.23	-19.1159
750-15c	15	750	1023	0.000978	9.81	-16.4456
750-30c	30	750	1023	0.000978	10.13	-17.1128
750-60c	60	750	1023	0.000978	8.82	-17.948
750-120c	120	750	1023	0.000978	9.32	-18.5839
750-180c	180	750	1023	0.000978	9.15	-19.0107
mc3173-9	0	775	1048	0.000954	11.45	
775-15a	15	775	1048	0.000954	10.15	-16.4152
775-30a	30	775	1048	0.000954	10.1	-17.118
775-60a	60	775	1048	0.000954	9.92	-17.8343
775-120a	120	775	1048	0.000954	9.44	-18.5747
775-180a	180	775	1048	0.000954	8.1	-19.1343
775-15b	15	775	1048	0.000954	9.9	-16.4404
775-30b	30	775	1048	0.000954	10.67	-17.0629
775-60b	60	775	1048	0.000954	9.87	-17.8302
775-120b	120	775	1048	0.000954	8.53	-18.6754
775-180b	180	775	1048	0.000954	9.52	-18.9752
775-15c	15	775	1048	0.000954	10.67	-16.3645
775-30c	30	775	1048	0.000954	9.93	-17.1331

775-60c	60	775	1048	0.000954	9.61	-17.8601
775-120c	120	775	1048	0.000954	8.07	-18.7273
775-180c	180	775	1048	0.000954	8.65	-19.0678
3177-9	0	800	1073	0.000932	11.79	
800-15a	15	800	1073	0.000932	9.25	-16.5134
800-30a	30	800	1073	0.000932	9.02	-17.2298
800-60a	60	800	1073	0.000932	8.43	-17.9933
800-120a	120	800	1073	0.000932	8.37	-18.6975
800-180a	180	800	1073	0.000932	8.12	-19.139
800-15b	15	800	1073	0.000932	9.63	-16.4706
800-30b	30	800	1073	0.000932	8.72	-17.2649
800-60b	60	800	1073	0.000932	8.54	-17.98
800-120b	120	800	1073	0.000932	8.2	-18.7186
800-180b	180	800	1073	0.000932	7.53	-19.2109
800-15c	15	800	1073	0.000932	9.32	-16.5013
800-30c	30	800	1073	0.000932	9.07	-17.225
800-60c	60	800	1073	0.000932	8.79	-17.9539
800-120c	120	800	1073	0.000932	6.81	-18.904
800-180c	180	800	1073	0.000932	7.99	-19.1519
mc3163-3	0	850	1123	0.00089	10.6	-16.18
850-15	15	850	1123	0.00089	9.73	-16.4572
850-30	30	850	1123	0.00089	8.05	-17.3452
850-60	60	850	1123	0.00089	8.21	-18.0207
850-120	120	850	1123	0.00089	6.95	-18.8864
850-180	180	850	1123	0.00089	7.17	-19.2661
850-15b	15	850	1123	0.00089	8.47	-16.595
850-30b	30	850	1123	0.00089	8.93	-17.2401
850-60b	60	850	1123	0.00089	7.84	-18.0655
850-120b	120	850	1123	0.00089	7.4	-18.8237
850-180b	180	850	1123	0.00089	6.83	-19.316
850-15c	15	850	1123	0.00089	8.54	-16.5891
850-30c	30	850	1123	0.00089	8.15	-17.3306
850-60c	60	850	1123	0.00089	7.65	-18.0906
850-120c	120	850	1123	0.00089	6.76	-18.9157
850-180c	180	850	1123	0.00089	6.04	-19.4364
850-15d	15	850	1123	0.00089	8.2	-16.6298
850-30d	30	850	1123	0.00089	8.09	-17.3406

850-60d	60	850	1123	0.00089	7.15	-18.1618
850-120d	120	850	1123	0.00089	7.05	-18.8759
850-180d	180	850	1123	0.00089	5.92	-19.4545

sample	Graphitic rel %	Pyridinic rel %	Fe-N rel %	Pyr Ox rel %	Nox rel %
mc3163-3	33.12	49.03	6.46	7.75	3.63
700-15	32.67	49.57	5.02	8.09	4.74
700-30	32.12	45.32	6.57	11.46	4.53
700-60	31.24	48.65	5.13	9.01	5.97
700-120	35.54	47.98	4.5	7.4	4.57
700-180	35.11	47.7	3.15	8.5	5.54
700-15b	32.58	47.27	5.04	9.72	5.39
700-30b	32.31	46.54	6.66	9.13	5.35
700-60b	31.79	48.98	5.66	9.1	4.48
700-120b	32.23	43.74	9.62	10.23	4.18
700-180b	33.86	49.8	2.97	8.52	4.85
700-15c	30.65	46.91	6.66	9.91	5.87
700-30c	33.76	46.5	5.5	8.83	5.36
700-60c	32.89	44.12	5.63	9.99	7.37
700-120c	33.06	47.01	2.97	12.36	4.6
700-180c	33.52	44.74	4.79	10.87	6.08
700-15d	30.21	47.38	5	10.45	6.96
700-30d	31.65	44.19	6.56	10.37	7.24
700-60d	30.62	44.72	6.1	10.78	7.77
700-120d	32.51	44.18	6.46	10.13	6.72
700-180d	33.33	44.85	7.78	9.56	4.48
3173-7	31.21	46.73	7.48	9.39	5.19
750-15a	33.41	48.84	4.22	9.48	4.06
750-30a	32.65	50.61	3.14	8.79	4.81
750-60a	34.96	45.6	5.75	9.23	4.46
750-120a	34.15	45.11	2.36	11.66	6.72
750-180a	37.04	44.78	4.35	9.19	4.64
750-15b	33.82	47.77	4.68	8.67	5.05
750-30b	32.14	48.18	5.25	8.89	5.54
750-60b	34.64	46.31	3.94	10.49	4.62
750-120b	35.2	44.6	3.33	10.79	6.07

750-180b	35.97	44.58	3.51	9.9	6.04
750-15c	32.77	47.53	3.62	10.48	5.61
750-30c	33.28	48.53	2.1	9.65	6.44
750-60c	33.01	49.38	2.55	9.57	5.48
750-120c	33.85	46.62	2.64	10.28	6.61
750-180c	35.67	45.01	3.11	9.91	6.3
mc3173-9	30.32	46.69	5.05	11.27	6.68
775-15a	33	47.22	5.06	9.47	5.25
775-30a	33.52	46.2	5.66	9.66	4.95
775-60a	32.65	48.12	4.19	10.03	5.01
775-120a	35.27	46.35	3.71	9.98	4.7
775-180a	35.81	43.29	5.91	9.63	5.35
775-15b	33.09	48.57	5.25	8.3	4.8
775-30b	32.18	48.61	5.1	8.9	5.21
775-60b	33.34	47.43	5.22	8.55	5.45
775-120b	34.89	46.2	4.87	9.08	4.96
775-180b	34.29	47.58	3.41	9.25	5.48
775-15c	32.27	48.64	4.4	9.48	5.21
775-30c	32.95	46.76	4.43	10.5	5.36
775-60c	32.59	47.46	5.09	9.66	5.19
775-120c	34.02	45.3	4.21	11.42	5.04
775-180c	36.81	43.33	3.55	11.46	4.85
3177-9	32.4	49.84	5.45	7.24	5.07
800-15a	32.31	46.19	4.9	9.96	6.64
800-30a	33.53	48.7	3.34	9.54	4.88
800-60a	34.23	44.27	4.63	9.52	7.35
800-120a	35.31	43.7	2.89	11.78	6.32
800-180a	35.17	43.4	3.19	12.72	5.52
800-15b	32.56	46.71	4.88	10.88	4.97
800-30b	34.08	47.48	3.52	10.33	4.6
800-60b	34.69	44.32	4.99	10.74	5.26
800-120b	34.51	44.7	4.16	9.85	6.78
800-180b	34.64	46.2	2.94	10.91	5.31
800-15c	32.14	47.87	5.11	9.9	4.97
800-30c	32.37	47.06	4.38	10.08	6.1
800-60c	34.22	44.33	4.21	11.1	6.14
800-120c	34.59	47.1	3.3	10.05	4.96
800-180c	33.95	47.8	4.04	9.31	4.91

	Graphitic rel %	Pyridinic rel %	Fe-N rel %	Pyr Ox rel %	Nox rel %
mc3163-3	33.12	49.03	6.46	7.75	3.63
850-15	36.57	45.31	3.27	10.31	4.54
850-30	35.05	42.71	4.73	11.4	6.12
850-60	35.89	42.49	6.42	8.28	6.92
850-120	38.93	41.1	3.64	10.03	6.28
850-180	40.24	41.91	2.75	8.99	6.1
850-15b	33.52	43	5.88	11.7	5.9
850-30b	35.46	46.92	3.71	10.61	3.3
850-60b	36.59	41.23	5.69	10.75	5.74
850-120b	37.73	40.38	5.56	11.2	5.13
850-180b	39.1	41.68	3.37	9.7	6.15
850-15c	34.9	43.72	7.45	9.12	4.8
850-30c	35.92	42.67	4.23	12.22	4.96
850-60c	37.09	42.27	5.05	11.12	4.47
850-120c	34.53	40.22	3.6	11.94	9.7
850-180c	38.6	39.78	4.18	11.2	6.24
850-15d	35.52	41.66	7.79	9.95	5.08
850-30d	35.43	42.47	5.1	10.77	6.24
850-60d	36.89	41.77	4.09	12.37	4.88
850-120d	36.5	41.03	3.8	11.8	6.87
850-180d	40.1	40.6	4.38	10.05	4.87